Polymerase Engineering to Expand Access to Nucleic Acid Diagnostics and Technologies

Ian Hull

A dissertation

submitted in partial fulfillment of the

requirements for the degree of

Doctor of Philosophy

University of Washington

2023

Reading Committee:

Barry Lutz, Chair

Douglas Fowler

Paul Yager

Program Authorized to Offer Degree:

Bioengineering

University of Washington

Abstract

Polymerase Engineering to Expand Access to Nucleic Acid Diagnostics and Technologies

Ian Hull

Chair of the Supervisory Committee:

Barry Lutz

Department of Bioengineering

Diagnostic and molecular biology workflows are often complex when first developed, and simplifying them is a key step in expanding their use from high-resource labs to low-resource settings such as clinics and developing countries. While dedicated devices can go about this task by automating steps and increasing throughput, an alternative and powerful approach is to employ dedicated *biomolecular* devices – proteins and enzymes such as DNA polymerases – to automate and streamline processes at the molecular scale. In this thesis, I describe methods and platforms that exemplify this "biology-first" mindset, its advantages, and its limitations. I cover two main projects that employ this approach. The first project synthesizes existing biomolecular technologies to demonstrate a novel format for HIV viral load testing with drastically reduced requirements for instrumentation and user handling. I show that this novel format can quantify HIV nucleic acids with accuracy comparable to clinically used assays, but does not require a thermal cycler instrument and can be interpreted by cell phone photography or naked eye. The second project demonstrates a platform for high-throughput screening and evolution of DNA polymerases. I propose that this platform can be used to rapidly develop novel polymerases for applications such as direct nucleic acid diagnostics with minimal or no sample preparation.

1 Contents

2 Acknowledgments 11

3 Preface 15

4 Isothermal Amplification with a Target-Mimicking Internal Control and Quantitative Lateral Flow Readout for Rapid HIV Viral Load Testing in Low-Resource Settings 19

4.1 Abstract 19

4.2 Introduction 20

4.3 Experimental Section 23

4.3.1 RPA Primer, Probe, and Synthetic Template Designs 23

4.3.2 Synthetic Template Preparation and Quality Control 24

4.3.3 RPA nfo Reactions 25

4.3.4 Lateral Flow Detection of RPA nfo Amplicons 26

4.3.5 Analysis of Lateral Flow Capture Line Intensities 26

4.4 Results and Discussion 29

4.4.1 Designed Competitive IAC Mimics HIV Target by using Identical Primer Sites and Shuffled Probe Sequence 29

4.4.2 Competitive RPA Enables Software and Cell-Phone Quantification of HIV DNA Inputs That Vary ≥0.2-Fold (~0.1 $\log_{10}$) from IAC DNA Threshold 31

4.4.3 Competitive RPA Enables Naked-Eye Quantification of HIV DNA Relative to Threshold 35

4.4.4 Competitive RPA Maintains Quantitative Behavior Regardless of IAC Threshold, Inhibitory Conditions, or Common HIV Mutations 36

4.4.5 One-Pot Competitive RT-RPA Enables Quantification of HIV RNA Relative to Threshold .. 40

4.5 Conclusions 41

4.6 Author Contributions 43

4.7 Acknowledgments 44

4.8 Addition 44

5 High-Resolution Polymerase Screening via Compartmentalized Self-Replication, Deep Mutational Scanning, and Molecular Dynamics Simulations 46

5.1 Abstract 46

5.2 Introduction 47

5.2.1 Protein Engineering Motivation 47

5.2.2 Chaotrope-Resistant (“Chaostable”) Polymerase Motivation 50

5.3 Experimental Section 54

5.3.1 Wild-Type Polymerase Characterization 54

5.3.2 CSR Primer Design and Screening 55

5.3.3 Mock Barcoded Library Construction 56

5.3.4 Barcoded Library Construction 59

5.3.5 CSR-DMS Selections 63

5.3.6 CSR Library Sequencing 65

5.3.7 Variant Scoring 68

5.3.8 Variant Polymerase Characterization 69

5.4 Results and Discussion 72

5.4.1 Wild-Type Thin Fingers Polymerase Exhibits Sufficient Resistance to Heat and Guanidinium to Enable Screening 72
5.4.2 CSR-DMS Design Uses Barcodes to Identify Polymerase Variants 74
5.4.3 Mock CSR-DMS Exhibits Strong Enrichment of Wild-Type Polymerase Over Inactive Variant 77
5.4.4 Differences in Variant Growth Prior to CSR-DMS Reveal Toxic Polymerase Domains 78
5.4.5 CSR-DMS Produces Sequence-to-Function Map of Polymerase Activity 80
5.4.6 CSR-DMS Tolerates Additional Selective Pressures to Identify Stabilized Variants 82
5.4.7 Activity Assays of High-Scoring Variants Validate CSR-DMS Predictions 88
5.5 Conclusions 93
5.6 Acknowledgments 95
5.6.1 Author Contributions 95
5.6.2 Funding 96
5.6.3 Competing Interests 96
6 Conclusions and Future Directions 97
6.1 Efficacy of CSR-DMS 97
6.2 Important Parameters for Validation, Maintenance, and Improvement of CSR-DMS Accuracy 99
6.3 Adaptability of CSR-DMS 103
6.4 Incorporating Novel Selective Pressures into CSR-DMS 104
6.4.1 Inhibitors (Beyond Guanidinium) 104
6.4.2 Reverse Transcription 105

6.4.3 Strand Displacement 106
6.4.4 Lesion Bypass 107
6.5 Expanding CSR-DMS to Study Other Enzymes 108
6.5.1 Multi-Enzyme Amplification Systems 108
6.5.2 Self-Replicating Biomolecules 110
7 List of Publications and Presentations 112
7.1 Journal Articles Included in This Dissertation 112
7.2 Other Journal Articles 112
7.3 Patent Applications 113
7.4 Conference Presentations 113
8 Appendix A: Supporting Information for Isothermal Amplification with a Target-Mimicking Internal Control and Quantitative Lateral Flow Readout for Rapid HIV Viral Load Testing in Low-Resource Settings 114
8.1 RPA Primer, Probe, and Template Sequences 114
8.2 Non-Linear Regression Analysis Results 115
8.3 IAC Exhibits Similar Sensitivity and Signal to HIV 117
8.4 Justification for Use of 1µL RPA Reaction in Lateral Flow 118
8.5 Survey Design 119
8.6 IAC Input is Tunable to Represent Various Clinical Thresholds, Sample Volumes, or Sample Preparation Yields 120
8.7 Competitive IAC Controls for Amplification Inhibition 123

8.8 High-Probability Mutations in HIV Sequence Do Not Affect Thresholding 125

8.9 Competitive RPA is Compatible with Genomic HIV RNA from Clinical Samples 127

8.10 MATLAB Script for Analysis of Cell Phone Photos of Lateral Flow Strips 128

9 Appendix B: Supporting Information for High-Resolution Polymerase Screening via Compartmentalized Self-Replication, Deep Mutational Scanning, and Molecular Dynamics Simulations 133

9.1 Sequences 133

9.1.1 Primer Sequences 133

9.1.2 Thin Fingers Codon-Optimized (TFO) DNA Sequence 133

9.1.3 Thin Fingers Polymerase Sequence 134

9.2 Preliminary Mock Selection (T7 Primers) 134

9.2.1 Plasmid Construction 134

9.2.2 Inactive Mutant Design 134

9.2.3 Culture and Expression 135

9.2.4 Emulsion PCR 135

9.2.5 Emulsion Breaking and DNA Purification 136

9.2.6 Amplicon Sequencing 136

9.3 Preliminary Mock Selection Demonstrated Insufficient Enrichment of Wild-Type Against Inactive Variant 137

9.4 Emulsion Validation 139

9.4.1 Plasmid Construction 139

9.4.2 Culture and Expression 139
9.4.3 Emulsion Thermal Cycling 140
9.4.4 Emulsion Microscopy 140
9.5 Microscopy Validates Emulsion Stability and Compartmentalization of Cells 140
9.6 Molecular Dynamics Simulations 142
9.7 Molecular Dynamics Simulation Results 144
9.8 Use of TF-WT in Molecular Assays for SARS-CoV-2 145
10 References 147

2 Acknowledgments

I would like to thank my advisor, Barry Lutz, for his guidance and support over the course of my doctoral work. Biological systems are incredibly complex, even in cases with seemingly minimal moving parts such as DNA binding; where I occasionally tend to chalk up unexpected results to noise and chaos, Barry's engineering mindset shines through, and he encourages me to deeply investigate a system to reach true understanding of the phenomena at play. I do not always succeed – sometimes the world of biomolecules truly is too intricate and convoluted to reduce to simple principles – but the cases where I have succeeded have strengthened my intuition for the workings of molecular systems and for the proper design of experiments to probe them. Barry's support is not just limited to advice, however. He has advocated for me in the development of my polymerase project, which relies on knowledge and skills that neither of us initially possessed. His support in that endeavor has imbued me with confidence that I sorely lacked at the beginning of my PhD, and for that I thank him.

I also thank all members of the Lutz Lab, past and present, for their support and camaraderie. Everyone in the lab has helped me in one way or another. Qin Wang, in particular, has always been a good friend and colleague. Qin and I began in the Lutz Lab at the same time, have worked together on many projects, and have followed similar paths and timelines in many ways. In some ways, Qin feels like my scientific twin, and I am glad that our similar trajectories have yielded such strong mutual support. Enos Kline has also been pivotal in my scientific development. Enos is an extremely knowledgeable molecular biologist (I could swap in a lot of scientific "-ist" words there and that statement would still be true), and without him I'm not sure my protein work would ever have gotten off the ground. He created the "Thin Fingers" polymerase on which many Lutz Lab projects are based, including my own. We worked together to build the infrastructure for protein work in our lab, but while I think he could have done that without me, I'm not so sure I could have done it without him. I thank Daniel Leon and Garima Thakur, whose

skillful and efficient management of our lab (plus their kind and welcoming spirits) have contributed immensely to productivity and morale. I also thank Amy Oreskovic and Nuttada Panpradist, who shared or preceded me in what Amy artfully describes as a “sunless, closet-sized office”. Implicit in that example is a sense of the trials and tribulations of the graduate student experience, which normalizes humility and toil far more than I think anyone deserves, but as my predecessors Amy and Nuttada exemplified a different sort of graduate student: the dignified, accomplished scientist who sets their own priorities and shapes their environment accordingly. Our office still has no window, but it has a nice poster of the Sun, which is far more reliable than the real thing in Seattle anyway.

I owe a lot to Valerie Daggett and Doug Fowler, whose knowledge of protein biophysics and experimentation has been essential to the success of my polymerase project. Valerie supported me in the writing and review of my R21 proposal (which funded the polymerase work) and taught me >90% of what I know about protein biophysics thanks to her excellent protein design class (for which I later became a teaching assistant). Matthew Childers (a Daggett Lab alum) also taught me how to run molecular dynamics simulations for that class and for my research, for which I am grateful. Doug similarly introduced me to next-generation sequencing and high-throughput screening, two incredibly impactful fields that (combined in the form of deep mutational scanning) have been an integral part of my work. I also thank Nicholas Popp, Rachel Powell, and Melinda Wheelock, all from the Fowler Lab, who were helpful and gracious collaborators in the sequencing and analysis of my polymerase screens.

I thank the Molecular Biophysics Training Program at the University of Washington, particularly Ning Zheng and Justin Kollman, who awarded me a traineeship that helped support the first two years of my polymerase project, including a critical period in which I was still generating preliminary data for an R21 grant proposal. The training program’s support is briefly mentioned in my publications, but they supported me in more ways than just funding, which deserves some elaboration here. I was not a typical candidate for the program, as our lab did not (yet) perform much protein engineering or biophysical

work, and I had much to learn in both of those fields. Nonetheless, they took a chance on me and welcomed our lab into the UW molecular biophysics community. I gained expertise and connections that proved critical in the intellectual development of my project (which is the main purpose of a training program after all!) and that nurtured my little side project into a career-defining research direction. I am extremely grateful for that support. UW has one more protein engineering group now, in large part thanks to them.

I thank my Supervisory Committee for their help in navigating the last few years of my work. Barry, Valerie, and Doug have already been mentioned. Paul Yager has been an excellent advisor, taking the time to read and comment on my documents not just for my Final and General Exams but also for my Qualifying Exam. Paul has also been a close collaborator with our lab for many projects, most recently HIV diagnostics work, and my HIV project benefited from his advice and that of others in his lab. Neil King, as my impartial Graduate School Representative, appropriately has no such strong ties to my research or mentorship, but I appreciate his time and expertise in the evaluation of my doctoral work.

I thank my friends and family. Most of my friends in Seattle are current or former UW graduate students (go figure), which makes them colleagues, but I have most valued them as companions for all sorts of (mostly outdoor) activities. I won't even try to sum up everything my parents have done for me, so I will focus specifically on their contribution to my interest in science. I'm privileged that my mom was my first scientific role model – as a marine biologist, she sparked my interest in the life sciences, and continues to offer me valuable career advice today. My dad is not formally a marine biologist, but nobody knows Sarasota Bay better than him, and many of my earliest experiences of scientific wonder began with him catching something with a rod or a net. My parents' influence is supported by statistics – 100% (N=2) of their kids have gone into science, now that my brother Dylan works across the courtyard from me in the Ocean Sciences Building at UW. Thanks for being a great running buddy, Dylan. I also have two grandmothers to thank. My late maternal grandmother, Granny Lu, honed my science communication

skills by asking me countless questions about science (including, eventually, my work). I miss her and I think about her whenever I try to communicate my work to non-scientists. My paternal grandmother, Grandma Hull, made this all possible by supporting each of her grandchildren with some of the cost of college (a privilege that she never experienced and resolved to make possible for her descendants). I cannot thank her enough for that support and that example.

Finally, I thank Meilyn Sylvestre, my wonderful partner. Her love and cheer are radiant, and I look forward to bright times ahead.

3 Preface

Nucleic acid diagnostics and sequencing technologies come in many forms and serve ever more purposes, but with few exceptions, rely on polymerases to process nucleic acids. It is not surprising that enzymes developed through billions of years of evolution to copy nucleic acids with extreme sensitivity, specificity, and speed have been our best tools for applications like biomarker detection, genome sequencing, and molecular cloning. However, polymerases have not evolved to flawlessly meet every requirement of the biotechnology industry, nor do they share many universal features. Their unifying functional definition, the ability to synthesize chains of nucleic acids (usually) based upon a template, belies an immense group of enzymes diverse in ability, stability, biological role, and evolutionary origin.

Polymerases are not simple tools to process genetic information; they are complex molecular machines, embodiments of the information encoded by their own genes, which can be mutated to suit different purposes. The primary sequence that defines a polymerase determines its preferred template molecules, nucleotide substrates, and operating environment. As a typical polymerase contains hundreds of amino acids, each of which can be varied to 19 other amino acids in the canonical genetic code, the astronomically vast sequence space of polymerases has barely been explored in billions of years of natural selection, let alone decades of human engineering.

To a protein biochemist, this is old news. The enormity of protein sequence space is discussed in introductory biochemistry courses and will forever eclipse our ability to explore it. But to a device engineer, this is an important point to remember when weighing priorities for assay development.

Whether designing a point-of-care diagnostic or a high-throughput DNA sequencer, device engineers are concerned with miniaturizing and automating processes as much as possible in machines of finite volume, content, and cost. These constraints are often addressed with clever microfluidics and robotics. Such approaches effectively bring a mindset akin to Moore's Law into device engineering ("How many

microfluidic channels can we fit on a flow cell?"). But this mindset has limits. Just as a modern integrated circuit can fit a large but finite number of transistors, a well-designed device can perform a large but finite number of operations – often at the expense of simplicity and reliability. At some point, in addition to increasing the ability of a device to perform complex tasks, it becomes equally important to seek ways to reduce the number or complexity of the tasks.

The diversity and information capacity of biological molecules like polymerases presents an opportunity to shift the complexity of an assay from intricate mechanical steps to well-suited biological machines. As an example, consider the role of *Taq* polymerase in polymerase chain reaction (PCR). When PCR was first developed, it used the Klenow fragment of *E. coli* DNA polymerase I[1,2], which is thermolabile and has to be re-added after the melting step of each PCR cycle. *Taq* polymerase, however, originates in a heat-tolerant organism and can withstand the thermal cycling of PCR[3]. It therefore does not need to be re-added after each cycle, and its use has greatly simplified the operation of PCR-based assays.

This "biology-first" mindset to assay engineering is not new (the *Taq* polymerase example dates to 1988), but it becomes more effective as our knowledge of natural proteins and our ability to study and modify them evolves. We now have techniques that are similar to PCR but avoid thermal cycling entirely by using polymerases naturally capable of processing through double-stranded DNA and displacing competing strands[4,5], as well as engineered polymerases that can use both RNA and DNA as templates and avoid the need for discrete reverse transcription steps for RNA diagnostics[6].

In my graduate work, I have conducted two main projects that employ this biology-first mindset to simplify diagnostic workflows. The first project is a synthesis of existing technologies to demonstrate a novel format for HIV viral load testing. It relies on a technique similar to PCR called recombinase polymerase amplification (RPA)[5], which operates at a single incubation temperature. RPA is one of many such "isothermal" mechanisms for nucleic acid amplification, but I consider it a particularly fitting example of a biology-first approach because it resembles PCR so strongly in form. Where PCR relies on heat to control DNA melting, primer binding, and strand synthesis, RPA instead uses recombinases, single-stranded-DNA-binding proteins, and a strand-displacing DNA polymerase to achieve the same end (**Figure I**), to great effect. It is as sensitive as PCR, but much faster and with lower instrumentation requirements, rendering it well-suited for use in point-of-care diagnostics. For quantitative use, however, proper controls and analysis are necessary to counteract uncertainties introduced by such rapid, unfettered amplification. We used a molecular approach to introduce those controls and analysis to develop an assay with much-simplified instrumentation for HIV viral load testing. This is the subject of the following chapter: "Isothermal Amplification with a Target-Mimicking Internal Control and Quantitative Lateral Flow Readout for Rapid HIV Viral Load Testing in Low-Resource Settings."

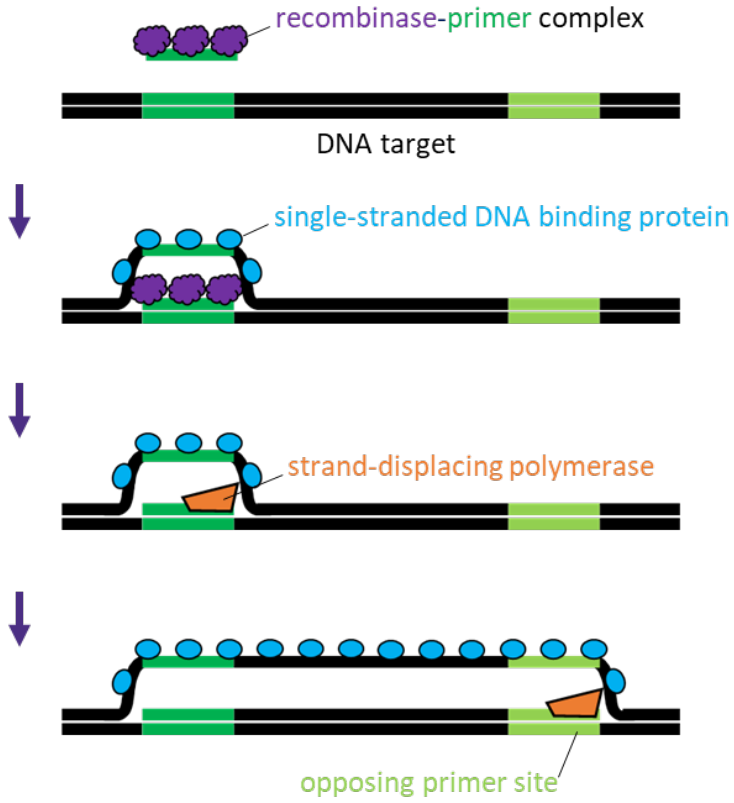

Figure I. *Recombinase polymerase amplification (RPA) mechanism. Recombinase complexes with primer and searches dsDNA for complementary sequence. At complementary site, recombinase initiates strand exchange, templating primer. Single-stranded DNA binding protein stabilizes displaced strand to prevent re-annealing. Strand-displacing polymerase extends from templated primer. Opposing primer site enables exponential amplification.*

My second project describes a platform for high-throughput screening and evolution of polymerases. It originates from an idea I had during my qualifying exam to develop a polymerase with activity in lysis buffers (thus avoiding some complex nucleic acid purification steps), but over time it has evolved into a more general platform for basic science research into the biophysics of polymerases with interesting capabilities, and for development of polymerases with novel capabilities for industrial applications. This is the subject of the chapter “High-Resolution Polymerase Screening via Compartmentalized Self-Replication, Deep Mutational Scanning, and Molecular Dynamics Simulations.”

It would be somewhat of a retcon to cast both of my projects as “inspired” by a biology-first mindset. After all, I joined the Lutz Lab because I wanted to devote my research to solving tangible global health problems. I was assigned the HIV project with well-defined goals but some freedom to choose the means, and I chose RPA as the amplification mechanism for practical (not philosophical) reasons. My polymerase project also arose from a concrete desire: the ability to lyse, amplify, and detect HIV in a single tube. It is more accurate to say that my biology-first mindset has been inspired *by* these practical experiences. Nevertheless, I find it a compelling guiding principle that has helped me frame my first publication, and it has informed the story I tell in the second publication.

4 Isothermal Amplification with a Target-Mimicking Internal Control and Quantitative Lateral Flow Readout for Rapid HIV Viral Load Testing in Low-Resource Settings

Ian T. Hull[1], Enos C. Kline[1], Gaurav K. Gulati[1], Jack Henry Kotnik[1], Nuttada Panpradist[1], Kamal G. Shah[1], Qin Wang[1], Lisa Frenkel[2-6], James Lai[1], Joanne Stekler[5], and Barry R. Lutz[1]*

[1]Department of Bioengineering, University of Washington, Seattle, WA 98195-5061, USA

[2]Department of Pediatrics, University of Washington, Seattle, WA 98195-9300, USA

[3]Department of Laboratory Medicine and Pathology, University of Washington, Seattle, WA 98195-7470, USA

[4]Department of Global Health, University of Washington, Seattle, WA 98195-1620, USA

[5]Department of Medicine, University of Washington, Seattle, WA 98195-6420, USA

[6]Center for Global Infectious Disease Research, Seattle Children's Research Institute, Seattle, WA 98145-5005, USA

*Send correspondence to blutz@uw.edu

This work[7] and an associated addition[8] have been published in *Analytical Chemistry*. The chapter below consists of the revised manuscript and does not include minor edits made by the publisher during the proofing stage. It has been lightly edited here for formatting. Most writing is mine, with the following exceptions: methods paragraphs on cell phone analysis (Qin Wang), naked-eye survey analysis (Jack Henry Kotnik), and RNA isolation from clinical samples (Gaurav K. Gulati); MATLAB script (Kamal Shah); and various minor edits (all authors).

4.1 Abstract

Point-of-care diagnostics often use isothermal nucleic acid amplification for qualitative detection of pathogens in low-resource healthcare settings, but lack sufficient precision for quantitative applications

such as HIV viral load monitoring. Although viral load monitoring is an essential component of HIV treatment, commercially available tests rely on relatively high-resource chemistries like real-time polymerase chain reaction and are thus used on an infrequent basis for millions of people living with HIV in low-income countries. To address the constraints of low-resource settings on nucleic acid quantification, we describe a recombinase polymerase amplification and lateral flow detection approach that quantifies HIV-1 DNA or RNA by comparison to a competitive internal amplification control (IAC) of known copy number, which may be set to any useful threshold (in our case, a clinically relevant threshold for HIV treatment failure). The IAC is designed to amplify alongside the HIV target with similar efficiency, allowing normalization of the assay to variation or inhibition, and enabling an endpoint readout that is compatible with commercially available kits for nucleic acid lateral flow detection and interpretable with minimal instrumentation or by naked eye. We find that this approach can reliably differentiate ≤600 or ≥1400 copies of HIV DNA from a 1000-copy threshold when lateral flow strips are imaged with a conventional office scanner and analyzed with free densitometry software. We further demonstrate a user-friendly adaptation of this analysis to process cell phone photos with an automated script. Alternatively, we show via survey that 21 minimally trained volunteers could reliably resolve ≥10-fold ($\log_{10}$) differences of HIV DNA or RNA by naked-eye interpretation of lateral flow results. This amplification and detection workflow requires minimal instrumentation, takes just 30 minutes to complete, and when combined with a suitable sample preparation method, may enable HIV viral load testing while the patient waits or a self-test, which has the potential to improve care. This approach may be adapted for other applications that require quantitative analysis of a nucleic acid target in low-resource settings.

4.2 Introduction

Isothermal nucleic acid tests (NATs) are useful for point-of-care (POC) diagnostics due to their minimal requirements for instrumentation and user expertise. Unlike polymerase chain reaction (PCR),

isothermal reactions amplify nucleic acids at a constant temperature and do not require a specialized thermal cycler, enabling POC detection of pathogens[9,10]. Quantitative applications of isothermal amplification, however, are difficult to implement at POC. Most quantitative NATs rely on real-time PCR to quantify a target based on number of cycles needed for the signal to exceed a certain threshold, as endpoint signal typically plateaus regardless of input copy number[11]. Real-time analysis requires fluorescence readers and external quantitative standards, which increase assay complexity. Isothermal techniques carry additional complications for real-time analysis, as the lack of thermal cycling to regulate amplification makes liftoff time highly sensitive to variations in reaction conditions such as incubation temperature[12], mixing[13], or interfering substances.

As a result, real-time PCR remains the standard technique for the most impactful quantitative NAT in global public health: HIV viral load (VL) monitoring. VL monitoring is integral to the management of antiretroviral therapy (ART). The VL of a person living with HIV (PWH), expressed as the number of HIV RNA copies per milliliter (c/mL) of plasma, is measured frequently during ART to monitor suppression of HIV replication. A VL that remains above 1000c/mL is defined as virologic failure by the World Health Organization (WHO) and is associated with HIV transmission and drug resistance. Persistent failure leads to depletion of CD4+ T cells and progression to AIDS[14]. Other public health authorities use lower VL thresholds (e.g. ≥200c/mL) to define virologic failure[15]. Virologic failure, or really any lack of virologic suppression, warrants clinicians to discuss medication adherence and potentially to evaluate virus for drug resistance.

Although roughly 32 of 37 million PWH globally reside in low- to middle-income countries (LMIC)[16], VL monitoring typically relies on high-resource tests that require expensive equipment and centralized laboratory facilities[17] such as real-time PCR by COBAS® Taqman® v2.0 (Roche) or the RealTi*m*e HIV-1 (Abbott). As a result, less than half of PWH on ART globally received routine (annual) VL tests in 2016[18]

(with access particularly low in sub-Saharan Africa, at 37% in Eastern and Southern Africa and 13% in Western and Central Africa[19]).

For quantitative NATs to have an impact in global public health, the constraints of POC settings must be addressed. An ideal POC HIV VL test, for example, requires minimal (ideally battery-powered) instrumentation, results within 30 minutes, resolution within 0.3 $\log_{10}$ (~2-fold) copies RNA, and sensitivity sufficient for fingerstick blood volumes (≤200µL)[20]. One assay developed by Crannell *et al.* uses real-time recombinase polymerase amplification (RPA)[21], which is an adaptation of a qualitative lateral flow RPA assay originally described by Boyle *et al.*[22]. This approach is isothermal, fast (< 30 minutes), and accurate to within 0.3 $\log_{10}$ copies of DNA for most inputs. However, it relies on real-time analysis, increasing assay complexity and vulnerability to errors due to reaction inhibition. Nycz *et al.* described a strand-displacement amplification (SDA) assay with a target-mimicking internal amplification control (IAC)[23]. This approach is endpoint-based and controls for reaction variability, saturation, and inhibition by comparing the HIV signal to that of the IAC, which co-amplifies at a fixed ratio dependent on the initial ratio of HIV and IAC input. This "competitive" approach is accurate and effective; in fact, competitive PCR predates real-time PCR and was the original technique used to establish the relationship between HIV VL and progression to AIDS early in the HIV/AIDS pandemic[24]. Nycz *et al.*[23] expanded this concept to an isothermal chemistry, but used radiolabeled probes and an electrophoresis readout that would be inaccessible in POC settings.

Here, we describe an isothermal quantitative or semi-quantitative NAT with features accessible in POC settings. We combine the HIV RPA assay described previously with the competitive IAC quantification approach previously used in PCR and SDA. By comparing amplification of the HIV target relative to the IAC, we establish that the resulting fractions in endpoint signal can be used semi-quantitatively to determine if the HIV input exceeds the IAC threshold (which should be sufficient for most POC VL tests), or quantitatively to estimate HIV input copy number with 95% confidence intervals (which may be used

for tracking of ART efficacy over time). This "competitive RPA" assay has several advantages. Analysis occurs at endpoint, minimizing instrumentation and enabling a lateral-flow-strip readout that can be interpreted by the naked eye or automated with a commercially available cell phone camera. The competitive IAC enhances the accuracy of the assay and accounts for inhibiting conditions by normalizing HIV amplification relative to that of the IAC. Finally, we show that the assay maintains accuracy when challenged with common HIV-1 genomic variants. Given these qualities, this competitive amplification approach should prove to be a useful template to develop various isothermal quantitative NATs, including but not limited to POC HIV VL tests.

4.3 Experimental Section

4.3.1 RPA Primer, Probe, and Synthetic Template Designs

We chose the HIV pol RPA assay described by Boyle et al.[22] for modification to include a competitive IAC and biplexed lateral flow detection of HIV and IAC targets. The primer designs and HIV probe sequence are unchanged from the original pol assay[22], but the HIV probe was given a 5' digoxigenin label for lateral flow detection. The IAC probe sequence was designed using Geneious 11.1.4 (https://www.geneious.com) to comprise the same base content as the HIV probe, but with a shuffled sequence. The Mutate & Shuffle plugin was used to randomize the positions of all bases in the IAC probe except the "TGC_CT" motif at positions 28-33. This motif was preserved so that the endonuclease IV probe system would have similar kinetics at the abasic site and so the flanking thymidines could be used as conjugation sites for alternative fluorescence-based probe chemistries (not shown). We used the DNA Fold tool in Geneious to screen 20 shuffled probe sequences *in silico* for predicted secondary structure at 39°C. We chose the sequence with minimal secondary structure for use in the IAC probe and gave this probe a 5' 6-FAM label for lateral flow detection. Synthetic templates were based on sequences from the Los Alamos National Laboratory (LANL) HIV Sequence Database[25]; all experiments used a majority

consensus sequence HIV-1 template (unless otherwise noted) and an IAC template identical to the HIV template except with IAC probe sequence substituted at the probe site. Finally, each template was given flanking PCR primer sites and a T7 promoter site to enable in-house DNA and RNA production. Full template design notes are included in the Supplementary Information. All primer, probe, and template DNA sequences were ordered from Integrated DNA Technologies (IDT) (Coralville, Iowa) and are listed in **Table A1**.

4.3.2 Synthetic Template Preparation and Quality Control

To better quantify DNA templates prior to use in our assay, we amplified our gBlocks using M13 PCR primers and Q5 HotStart High-Fidelity DNA Polymerase (New England BioLabs (NEB) M0493). Each 50µL PCR reaction contained 1x Q5 Reaction Buffer, 200µM each dNTPs, 500nM each M13 primer, 1U Q5 HotStart High-Fidelity DNA Polymerase, and 10ng gBlock template. PCR thermal cycling parameters were: 98°C for 30 seconds, 25 cycles of [98°C for 5 seconds, 57°C for 10 seconds, 72°C for 5 seconds], then 72°C for 2 minutes. PCR amplicons were purified using a QIAquick PCR Purification Kit (Qiagen 28104) or PureLink PCR Purification Kit (Invitrogen K310002). PCR amplicons were then quantified using a ThermoFisher NanoDrop 2000c and stored in aliquots of 10^9 copies dsDNA template per µL.

To prepare synthetic RNA templates, we transcribed the dsDNA PCR amplicons using T7 RNA Polymerase (NEB M0251S) using the manufacturer-recommended protocol and 100ng of template DNA. RNA transcripts were purified using a Monarch RNA Cleanup Kit (NEB T2030), checked for length and integrity using an RNA ScreenTape Assay (Agilent 5067-5576) on a TapeStation 2200, and quantified with a Qubit High-Sensitivity RNA Assay (ThermoFisher Q32852). The RNA was then diluted with nuclease-free water to 10^9 copies/µL and stored at -80°C in single-use 50µL aliquots.

4.3.3 RPA nfo Reactions

RPA nfo reactions[5] (TwistDx TANFO02KIT (temporarily discontinued)) were set up as recommended by the manufacturer. (These reactions contain endonuclease IV ("nfo") enzymes included in the lyophilized pellets; these enzymes cleave antigen-labeled probes when bound to a target amplicon and thereby enable polymerases to extend the cleaved probes to form a dual-labeled complex with biotinylated reverse primers.) Briefly, a master mix was prepared such that the 50µL reactions would have final concentrations of 1x primer-free rehydration buffer, 420nM each primer, and 60nM each probe. For reactions with RNA templates, the master mix was supplemented such that each 50µL reaction would contain 4U OmniScript Reverse Transcriptase (Qiagen 205111) and 50U human pancreatic ribonuclease inhibitor (NEB M0307). Lyophilized RPA nfo pellets were resuspended with 45.5µL of master mix. A 2.5µL droplet of 280mM magnesium acetate was added to the lid of each reaction tube. Finally, 2µL of template were added to each reaction tube.

Reactions were initiated by spinning the magnesium acetate droplets down into reactions using a microcentrifuge, vortexing briefly, and spinning down once more. Reactions were then immediately transferred to a preheated Bio-Rad T100 thermal cycler. All reactions were incubated at 39°C for 20 minutes unless otherwise noted. 5 minutes into incubation, the thermal cycler timer was paused and reactions were briefly mixed via vortex and spun down before being returned to the thermal cycler to resume incubation. At the end of incubation, reactions were rapidly cooled to 4°C on the thermal cycler, spiked with 5µL each of 0.5M EDTA to stop amplification, vortexed briefly, and spun down. The amplicons were then run immediately on lateral flow strips or stored overnight at 4°C before continuing with lateral flow detection.

4.3.4 Lateral Flow Detection of RPA nfo Amplicons

Lateral flow assays were performed using PCRD-FLEX strips (Pocket Diagnostics FD51676) in a 96-well plate on an open benchtop. Unless otherwise noted, 1µL of RPA nfo amplicons was mixed with 149µL of PCRD extraction buffer in a single well of the 96-well plate. (See **Figure A2** for our justification to use 1µL of amplicons instead of the recommended 10µL). One PCRD-FLEX strip was dipped into each well and allowed to wick for 10 minutes. These strips contain carbon particles that bind to biotin-labeled amplicons and produce black capture lines upon detection.

PCRD-FLEX strips were then removed from the wells and taped to a sheet of printer paper. The strips were scanned within 15 minutes using an Epson Perfection V700 photo scanner and SilverFast Software SE 8.5 (LaserSoft Imaging). All strips from each experiment were scanned as a single image. Raw images were saved in TIF format at a resolution of 600 pixels per inch.

For some experiments as noted, the strips were then allowed to dry completely (to reduce artifacts from refractive index dependent on membrane wetness) and individually photographed using an iPhone 11 camera using default settings and 1x zoom via the Camera application. Strips were photographed under weak ambient laboratory lighting, with care taken to avoid strong and/or directional lighting sources, as these may cause overexposure or lighting gradients in the photos.

4.3.5 Analysis of Lateral Flow Capture Line Intensities

4.3.5.1 Scanner-Based Imaging and Analysis

All software-based analyses of the strips were conducted with scanned images except those labeled as cell phone analysis. Scanned images of the lateral flow strips were processed in Image Studio Lite Version 5.2 (LI-COR, discontinued). Boxes of equal dimensions (within each experiment) were drawn around each capture line, excluding the edges of lateral flow strips to eliminate flow artifacts and shadows. The background for each box was specified as the median of all green-channel intensities 3

pixels above or below the box. The raw signal for each capture line was determined by subtracting the background of its box from the green-channel intensities of each pixel within the box and summing across all pixels within the box. The HIV and IAC signals for each strip were further normalized relative to each other, such that for each strip, the "HIV signal fraction" equals (DIG/(DIG+FAM)) and the "IAC signal fraction" equals (FAM/(DIG+FAM)).

The intended assay format, in which a known quantity of IAC target is co-amplified with an unknown quantity of HIV, should always produce a signal in one or both capture lines, as IAC is present even when HIV is undetectable. If neither line is observed, it should be interpreted clinically as a failed or inconclusive reaction, from which no information can be drawn. Such failed reactions could have multiple causes, including reagent expiry, inputs below the assay limit of detection, improper amplification conditions, or inhibition due to contaminants. These reactions should not be used for diagnosis or quantification because the capture line intensities are dominated by random noise. To identify such reactions, we chose a cutoff for minimum capture line intensity that indicates a successful amplification and can be used for quantification. Reactions were classified as "failed" if the raw DIG and FAM signals were both less than 12,000 units despite a positive HIV and/or IAC input. This cutoff was chosen retroactively, as we observed that the noise of raw DIG or FAM signals from reactions without their respective targets fell within a range of $\pm$8,000 across all experiments, but a cutoff of +12,000 was necessary to minimize divide-by-zero errors from strips with very faint (i.e. noisy) capture lines. All failed reactions are labeled with an 'X' in strip images and omitted from plots where noted. FC lines were visible (and well above the 12,000-unit cutoff) for all reactions; therefore, we attribute failed reactions to insufficiently sensitive amplification, rather than any problems with the lateral flow assays. Note that all "NTC" reactions (to which we added neither IAC nor HIV) also had raw DIG and FAM signals below the 12,000-unit cutoff and would be classified as "failed" in a real-world context (e.g. if sample preparation

failed and no HIV or IAC was added to the reaction), but for clarity, we distinguish here between NTCs and reactions that fail despite a positive input.

4.3.5.2 Cell-Phone-Based Imaging and Analysis

Images of the lateral flow strips taken by iPhone 11 camera were processed using an in-house automated script using MATLAB[26] (code provided in supplement). Briefly, this script imported cell phone images and cropped to nitrocellulose membranes of individual lateral flow strips (using blue regions of the PCRD FLEX strips as a reference). It then obtained a signal profile of each strip for the centermost 50% of the width and 90% of the length of the nitrocellulose membrane. This signal profile was first integrated across the width of the strip, then saved with respect to the length. The user manually designates certain positive strips as a reference for the location of the three capture lines in each strip. Finally, the script determines the area under the curve of signal at the three capture lines for each strip.

4.3.5.3 Non-Linear Regression Analysis

Where noted, mathematical curves describing the relationship between HIV input copy number and HIV signal fraction were determined using non-linear regression analysis in GraphPad Prism version 9.2.0 for Windows (GraphPad Software). We fit four-parameter logistic curves ("Sigmoidal, 4PL, X is concentration") to data using least squares regression (all default options). All analyses passed the D'Agostino-Pearson omnibus (K2) test[27] to verify that data was normally scattered around the curves. Curves and 95% prediction bands are included as plots in figures; parameters defining these curves and other results of non-linear regression analysis are available in **Table A2**.

4.3.5.4 Naked-Eye-Based Analysis

Scanned images of lateral flow strips were cropped to contain only the nitrocellulose membrane from one strip per image. They were then digitally annotated with a random, unique numerical identifier and three arrows, each indicating the position of an expected test line (typical lateral flow cartridges for

consumer use similarly indicate these positions). Images were assigned a random order and copied into a survey instrument (Google Forms, forms.google.com) (**Figure A3**). Volunteers were recruited from "non-lab" (N = 14) and "lab" personnel (N = 7) familiar with lateral flow assays but blinded to the inputs of each strip. Volunteers were given a short description of the test's purpose and function, and a schematic showing the different possible outcomes of the test, with a letter A-G and a short description (**Figure A3**). The answers in the survey corresponded to the A-G outcomes on the schema; volunteers completed the survey using the schematic as a guide. Images were annotated using ImageJ (https://imagej.nih.gov/ij/)[28]. This study was approved by the University of Washington Human Subjects Division (IRB STUDY00013312).

4.4 Results and Discussion

4.4.1 Designed Competitive IAC Mimics HIV Target by using Identical Primer Sites and Shuffled Probe Sequence

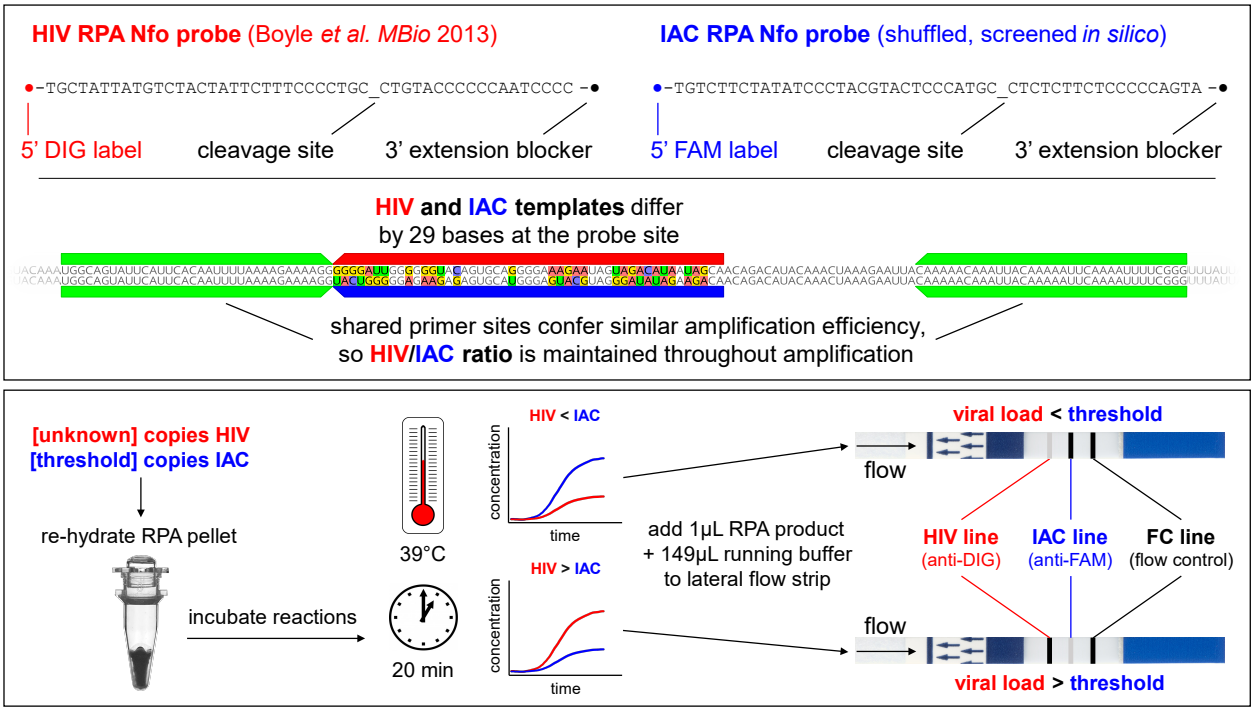

Figure 1. Competitive IAC design and concept. *(TOP) Sequences for HIV and IAC probes and synthetic templates. HIV probe sequence is unchanged from Boyle et al.[22] but has been modified to use digoxigenin (DIG) as an antigenic label. IAC probe sequence contains same base content as HIV probe but with shuffled sequence and a FAM antigenic label. (BOTTOM) Conceptual workflow for competitive RPA assay, with mock data demonstrating outcomes with HIV input below or above the VL threshold represented by the IAC. Because the HIV and IAC targets should amplify with similar efficiency, the endpoint HIV/IAC signal ratio should correspond to the input HIV/IAC ratio. (Note that RPA products flow from left to right in this depiction; the blue arrows on strips are physical stickers to indicate correct end down for placement of strips in sample wells).*

We designed a competitive IAC (**Figure 1**) to incorporate into the HIV-1 RPA assay described by Boyle et al.[22]. Design of the IAC to mimic the HIV target as closely as possible was essential, as the quantitative nature of the competitive amplification depends on identical amplification efficiency for both targets. Isothermal amplification of a target can be roughly modeled as exponential growth:

$$HIV(t) = HIV_{t=0} \cdot 2^{\frac{t}{\tau_{HIV}}} \qquad IAC(t) = IAC_{t=0} \cdot 2^{\frac{t}{\tau_{IAC}}}$$

where t represents time since reaction initiation and τ represents the doubling time (a representation of amplification efficiency) for a specific target. If both targets possess equal amplification efficiency, then $\tau_{HIV} = \tau_{IAC}$ and the endpoint ratio ($\frac{HIV(t)}{IAC(t)}$) will equal the input ratio ($\frac{HIV_{t=0}}{IAC_{t=0}}$). However, slight differences in amplification efficiency can lead to large deviations from the input ratio; for example, if $\tau_{HIV} = 60s$ and $\tau_{IAC} = 57s$, then the IAC yield will be roughly double the HIV yield after 20 minutes, and VL will be underestimated. This simplified model does not capture more complicated phenomena, such as reagent diffusion and depletion[29], but illustrates the importance of preserving amplification efficiency for this application, particularly because isothermal amplification lacks thermal cycling to synchronize doubling times.

Amplification efficiency is influenced by many factors, including primer sequence, target sequence, target length, and GC content[30]. To control these factors, we made the minimum modification necessary to achieve specific probe binding to the IAC, by shuffling bases at the probe site yet preserving overall target length, base content, and non-probe sequence. The competitive IAC is therefore composed of two parts: a synthetic nucleic acid template that mimics the HIV target sequence in every way, except

with a shuffled probe binding site, and a corresponding RPA nfo probe (probe chemistry is described in Piepenburg *et al.*[5]). To enable separate and specific detection of the HIV and IAC by lateral flow immunocapture, the HIV probe is labeled with digoxigenin while the IAC probe is labeled with 6-FAM.

We confirmed that the RPA assay sensitively detects as few as 10 copies of synthetic HIV or IAC DNA, with similar amplification efficiency and endpoint signal for each target, but virtually no cross-reactivity (**Figure A1**). In later experiments, we used synthetic DNA templates, where indicated, to demonstrate engineering concepts, as the assay is more sensitive to DNA. We also synthesized or extracted RNA templates to test the clinical viability of this assay, as HIV virions in plasma possess RNA genomes.

4.4.2 Competitive RPA Enables Software and Cell-Phone Quantification of HIV DNA Inputs That Vary ≥0.2-Fold (~0.1 $\log_{10}$) from IAC DNA Threshold

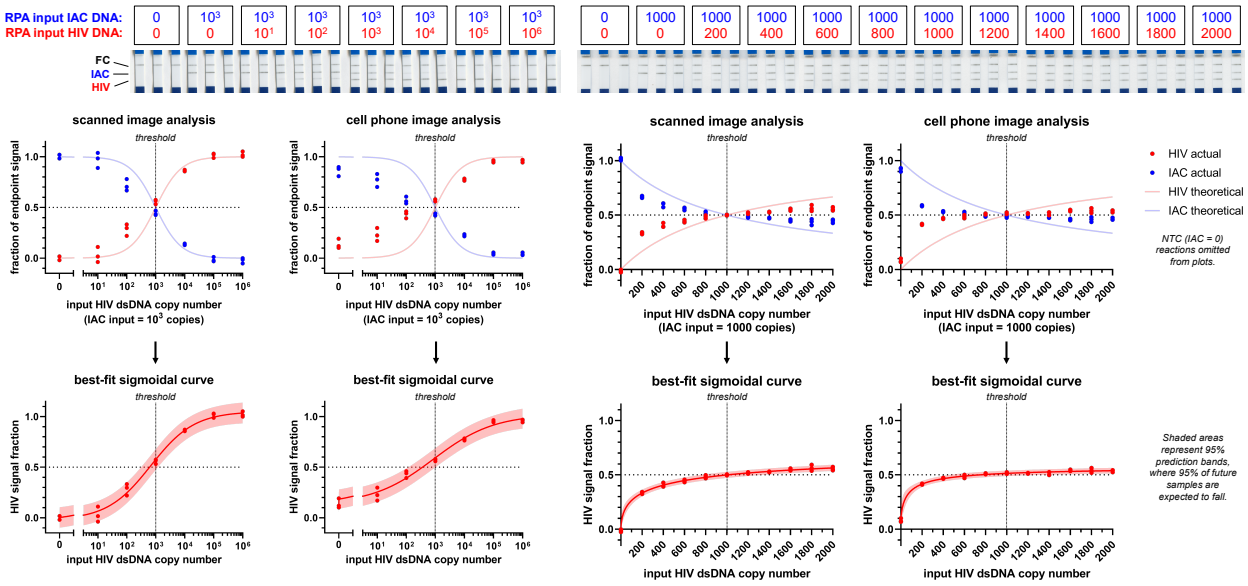

Figure 2. Competitive RPA results analyzed by software. *RPA reactions were run with 1000 copies IAC DNA and varying copy numbers of HIV DNA, then wicked through lateral flow strips for endpoint signal analysis. (TOP) Scanned images of lateral flow strips. (CENTER) Analysis of lateral flow strips using scanned images with ImageStudio Lite software or cell phone photos with a custom MATLAB script. Dots represent actual assay results (endpoint HIV or IAC signal divided by the sum of these signals) (N=3), while lines represent the theoretical or expected results (input HIV or IAC copy number divided by the sum of these copy numbers). (BOTTOM) Sigmoidal curve fit to assay results using non-linear regression analysis. Dots represent actual assay results (N=3). Lines represent a four-parameter logistic equation fit to the data in each plot. Shaded areas represent 95% prediction bands, where 95% of future samples are expected to fall.*

By co-amplifying a constant copy number of IAC with varying copy numbers of HIV, we found that the endpoint HIV signal fraction approximates the input HIV copy number fraction and can be used to identify the predominant target with high accuracy (**Figure 2**). 1000 copies of IAC DNA (representing the WHO VL threshold for a 1mL plasma sample) and varying copy numbers of HIV DNA (representing a sample with unknown VL) were added to RPA nfo reactions and run on lateral flow strips. We then quantified capture line signal intensities from scanned images and normalized them to the total (HIV + IAC) signal. For all HIV inputs tested, the target with more copies at reaction initiation (input fraction > 0.5) produced a more intense capture line at endpoint (signal fraction > 0.5), even when the HIV input differed from the 1000-copy IAC threshold by just 200 copies (20%, corresponding to a difference of less than 0.1 $\log_{10}$). This implies that competitive RPA can be used to compare an HIV input to a certain threshold (represented by the IAC) with resolution comparable or superior to qPCR, but with much simpler instrumentation.

A similar analysis approach was conducted using cell phone photos processed by a custom MATLAB script. We took photos of the strips on a laboratory benchtop using an iPhone 11 camera and processed the images using a custom MATLAB script (see supplement for code). While the cell phone analysis slightly overestimated HIV relative to IAC (the average HIV signal fraction exceeds IAC signal fraction when HIV input = 800 copies DNA), the dominant signal at endpoint generally corresponded to the more abundant target at initiation. The slight overestimation of HIV relative to IAC may have occurred in cell phone photos due to non-uniform ambient lighting that could not be fully negated via background subtraction. Further development of cell phone image analysis algorithms, coupled with optical guides on lateral flow cassettes and real-time feedback via phone app to improve camera lighting, exposure, and focus, could improve the accuracy of this method and enable user self-testing[31].

We also observed that despite the correlation between HIV and IAC input and signal fractions, both signal fractions exhibited a systematic bias towards a value of 0.5 (in other words, the more abundant

target was typically underestimated). We attribute this effect to the RPA nfo probe system, which does not directly produce signal upon binding to amplicons, but relies on enzymatic cleavage of bound probes. Any turnover in this process (i.e., ability of multiple probes to sequentially bind to one amplicon and get cleaved) to the point of saturation likely drives the endpoint HIV or IAC signal fractions to approximate the fraction of their respective probe concentrations (fixed to 0.5 for both probes), rather than the fraction of amplicons. Another potential reason for underestimation of the more abundant target is re-annealing of amplicons[32], which inhibits primer or probe binding and disproportionately affects the more abundant target. These effects have little impact on our goal to semi-quantitatively compare HIV to a clinical VL threshold, but would affect the accuracy of full quantification. While it should be possible to fully quantify a target using competitive RPA (as has been demonstrated using competitive SDA[23] or PCR[24]), additional development should be performed to counteract underestimation of the more abundant target. We suggest using an alternative probe chemistry that directly detects amplicons upon hybridization (e.g. molecular beacons[33] or Pleiades probes[34]), though care must be taken to ensure that the DNA-binding proteins used in RPA do not interfere with probe chemistry[35].

To improve quantification and determine statistical confidence in the assay results, we performed non-linear regression analysis on the data from each experiment to define the relationship between HIV input copy number and HIV signal fraction. The resulting sigmoidal curves resemble the plots of theoretical results, but essentially correct for systematic underestimation of the more abundant target by finding best-fit parameters for the baselines, slopes, and midpoints of each curve (see **Table A2** for these parameters). Scatter of the data around each curve can then be used to generate a 95% prediction band, which is the area around the curve that is expected to encompass 95% of future samples. For semi-quantitative applications, this analysis can effectively be used to estimate whether 95% of samples at a given HIV copy number will consistently produce an HIV signal fraction above or below a semi-

quantitative diagnostic threshold. For example, the prediction bands for scanned image analysis of HIV inputs of 800 or 1200 copies slightly overlap the 0.5 signal fraction threshold (**Figure 2**, second plot from right), implying these inputs may occasionally be misdiagnosed with >5% frequency, but inputs of 600 or 1400 copies have prediction bands that do not overlap the 0.5 signal fraction threshold and should therefore be misdiagnosed with <5% frequency. For quantitative applications, this analysis may be used to interpolate unknown samples (the curve estimates the HIV copy number that produced a given HIV signal fraction, while a horizontal line that is drawn across the 95% prediction band at that signal fraction defines a 95% confidence interval for the input copy number). We believe this analysis is a powerful and convenient way to predict the performance of an assay and analyze its results, provided that it is validated across experiments and conditions in which the assay will be used.

4.4.3 Competitive RPA Enables Naked-Eye Quantification of HIV DNA Relative to Threshold

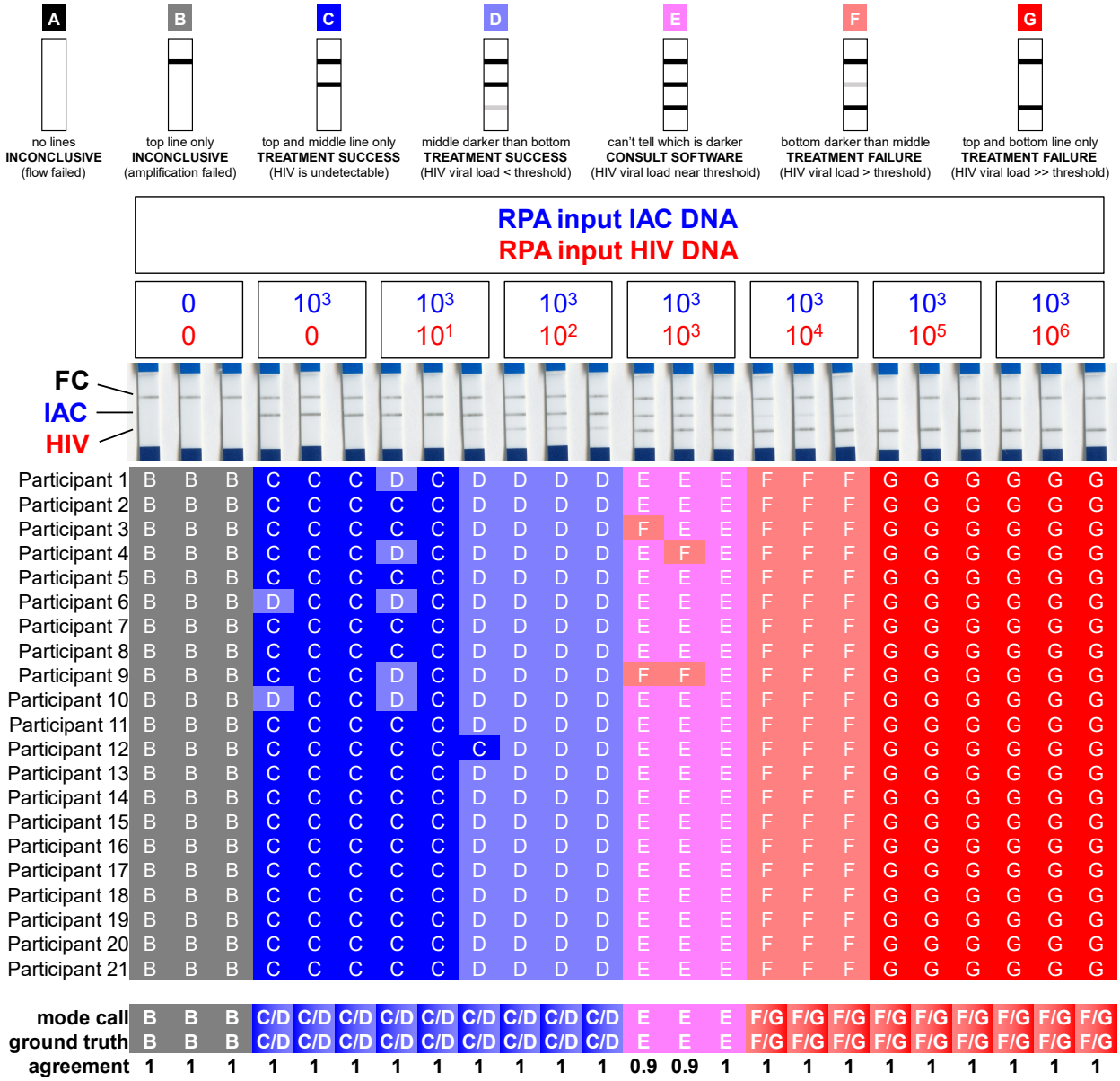

Figure 3. Competitive RPA results analyzed by naked eye survey. *Survey participants classified lateral flow strip results according to options in the schematic (TOP) for RPA reactions run with DNA targets. Individual and mode responses for each strip are displayed below strip images (CENTER) in a table (BOTTOM). Options C and D suggest successful HIV treatment under current WHO guidance and are thus combined in calculations, as are options F and G, which both represent treatment failure.*

To demonstrate the feasibility of naked-eye analysis of these strips, we had 21 minimally trained volunteers interpret scanned strip images (**Figure 3**) that were previously analyzed *via* software. The volunteers' judgment agreed well with the ground truth (true input copy numbers of HIV and IAC) and with software analysis despite being blinded to both. They were able to identify a dominant capture line

(HIV or IAC) for all HIV DNA inputs that deviated from the IAC threshold by an order of magnitude or more, and correctly identified the dominant capture line as that of the target with a higher input copy number. They therefore correctly classified all DNA reactions as representative of treatment success or treatment failure, except for the reactions with no HIV or IAC DNA (which they correctly classified as "inconclusive") or the strips with 1000 copies each of HIV and IAC DNA (which were too close to call for most volunteers). Only 4/504 calls (0.8%) in this experiment differed from the ground truth, all of which judged the HIV signal to be higher than the IAC for two reactions with 1000 copies each of HIV and IAC. While this "HIV=IAC" condition is a somewhat indeterminate case (it is possible through random sampling that these reactions did have a higher HIV input than IAC, or *vice versa*), these "incorrect" calls agreed with the software analysis in **Figure 2**, which found a slightly higher HIV signal than IAC for the strips in question. The volunteers who made these "incorrect" calls may therefore have been *more* sensitive to minute differences in signal than the other volunteers. Altogether, these results show that naked-eye-determined comparison of lateral flow line intensities agrees with software quantification and may be sufficient for test analysis at the point of care.

4.4.4 Competitive RPA Maintains Quantitative Behavior Regardless of IAC Threshold, Inhibitory Conditions, or Common HIV Mutations

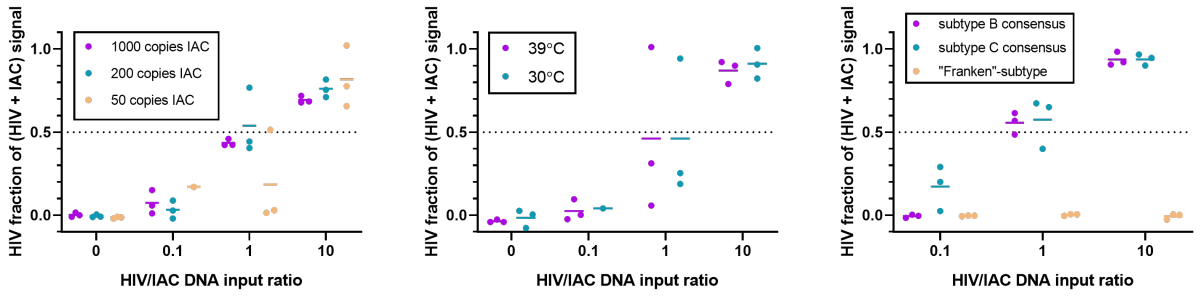

Figure 4. Competitive RPA assay results in response to changes in IAC copy number, incubation temperature, or HIV sequence. *RPA reactions were run with 1000 copies IAC DNA (unless otherwise specified) and varying ratios of HIV DNA relative to IAC, then wicked through lateral flow strips for endpoint signal analysis via scanner and ImageStudio Lite. Dots represent replicate assays while horizontal lines represent sample means (N=3). Failed reactions are omitted from analysis; see* ***Figure S4*** *and* ***Figure S5*** *for discussion. (LEFT) Competitive RPA assay with lower IAC thresholds (and proportional changes in HIV input) to simulate sample loss, lower sample volume, or lower thresholds for treatment failure. (CENTER) Competitive RPA assay at lower*

temperature to simulate reaction inhibition. (RIGHT) Competitive RPA with HIV template sequences based on subtypes of HIV-1 Group M to simulate mutations relative to primer and probe designs.

We tested the limitations of the assay (**Figure 4**) with lower IAC thresholds (to simulate lower sample yield or volume, or a different choice of treatment failure threshold), a lower incubation temperature (to simulate amplification inhibition), or HIV templates with mutations relative to the primer and probe designs (to simulate the HIV genetic diversity expected in clinical samples). More detailed information on the justification for and effects of changing these parameters can be found in the supplement (**Figures A4-A6**).

Lower IAC thresholds may occur when some yield is lost during sample preparation (assuming the IAC is added prior to sample preparation as an extraction control), when lower volumes of sample are collected, or may intentionally be built into the assay to meet a different definition of treatment failure (e.g. the 200c/mL threshold used by the CDC[15]). Although sensitivity was reduced with low IAC inputs (2/3 reactions with 50 copies IAC and 5 copies HIV failed) (**Figure A4**) the assay either maintained accurate quantification of HIV relative to IAC or failed to detect both targets (an inconclusive result, which is preferable to a false negative) (**Figure 4**, left). This demonstrates that the IAC input need not be a specific quantity for a given assay, but may be set to any threshold that is useful for the desired application.

The IAC further serves to protect the assay against amplification inhibition that may otherwise affect quantification. Temperature is a significant determinant of RPA reaction speed and sensitivity[5,12], and quantification methods that estimate input copy numbers based on liftoff time may be sensitive to temperature variations without proper controls. Also, while RPA is robust to many inhibitors, it can be adversely affected by background DNA at concentrations typical of fingerstick blood samples (though serum, which contains HIV virions and is commonly used in viral load tests, does not significantly inhibit RPA)[36,37]. While the optimal incubation temperature for this assay is 39°C[22], a POC test with minimal

instrumentation may lack tight control of incubation temperature. We tested the function of this assay at 30°C to simulate a POC scenario with an imprecise heater, which also serves as a useful model system for any kind of reaction inhibition, such as that caused by background DNA. Although reactions at 30°C took longer to qualitatively detect 1000 copies of HIV DNA than at 39°C (**Figure A5**), the competitive assay (**Figure 4**, center) maintained accurate quantification of HIV relative to IAC due to the normalizing effect of the IAC. This demonstrates that errors in quantification are less likely to occur when a competitive IAC is used rather than a non-competitive IAC or external standards (which are commonly used for real-time PCR), as long as the cause of inhibition affects HIV and IAC amplification equally. However, we have noted the large variation of reactions with an HIV/IAC DNA input ratio of 1 in this experiment. We believe this variation is due to delayed mixing. Briefly, mixing ensures that amplification initiation and efficiency are consistent for HIV and IAC, but imperfect or delayed mixing may randomly favor one target over another. For this reason, a competitive assay procedure must ensure that proper mixing is achieved, particularly in low-resource settings. Further discussion on this point is in the Supporting Information (**Figure A5**).

However, mutations in the HIV template are a unique scenario in which HIV amplification could be adversely affected relative to that of the IAC and lead to an underestimate of VL, especially when variant HIV sequences exhibit mismatches to the primers or probe. We note that the qualitative version of this RPA assay has been shown to detect 51/56 sequences from a diverse panel of HIV variants in 3/3 replicate reactions, including one variant with 9 total mismatches to the primers and probe, although 1-4 mismatches are more common and the effect of any mismatch appears to depend on its location[22]. To assess the risk that HIV mutations could affect the accuracy of quantification even if qualitative detection is maintained, we ran the competitive RPA assay using HIV templates with a subtype B consensus sequence (1 mismatch to the forward primer), subtype C consensus sequence (1 mismatch each to the reverse primer and probe), and a “Franken”-subtype sequence that we created to represent

the combined mutations of all HIV-1 Group M subtype consensus sequences relative to the primers and probe (9 total mismatches to the primers and probe) (see **Figure A6** for a sequence alignment). The assay maintained accuracy with the subtype B and C sequences, but in the case of the "Franken"-subtype, we observed no detection of HIV (unlike the aforementioned 9-mismatch variant[22]; we believe that differing locations of mutations caused this discrepancy), while the IAC was unaffected (**Figure 4**, right). We conclude that the competitive RPA assay is robust to common HIV mutations to a certain extent, but in rare cases with abundant mutations or mutations in locations that are critical to primer or probe function, a false negative for HIV treatment failure may result. We therefore urge careful *in silico* or clinical evaluation before using this assay in PWH cohorts who are expected to have high HIV sequence diversity, but we note that similar validation is needed for most HIV NATs regardless of the assay format. Fortunately, the geographical distribution of HIV-1 genomic diversity is well-documented, with hundreds of thousands of PWH sample sequences available from 116 countries from 1990 to 2015 (in general, diversity is low in India, Ethiopia, Southern Africa, and the United States, while diversity is high in Western Europe and Central Africa)[38]. With this knowledge, *in silico* screening of this assay against HIV genome alignments by country can be a useful tool to identify mutations to validate the assay against, or to confirm that the HIV genomic diversity of a PWH cohort meets a minimum desired prevalence of pre-validated sequences for assay compatibility.

4.4.5 One-Pot Competitive RT-RPA Enables Quantification of HIV RNA Relative to Threshold

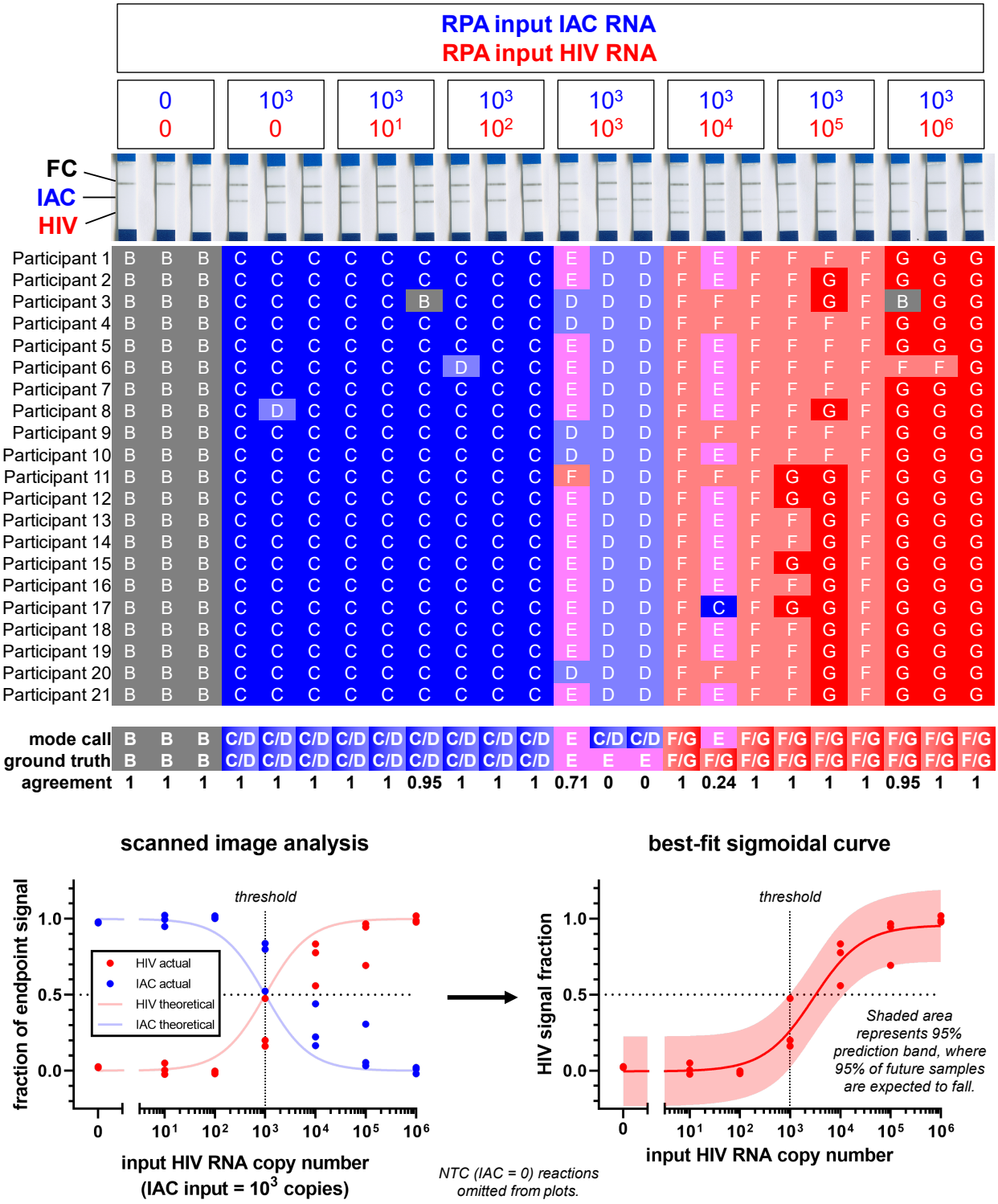

Figure 5. Competitive RT-RPA results analyzed by naked eye survey and by software. *RT-RPA reactions were run with 1000 copies IAC RNA and varying copy numbers of HIV RNA, then wicked through lateral flow strips for endpoint signal analysis. (TOP) Images of lateral flow strips. (CENTER) Survey responses for naked-eye analysis of each strip. (BOTTOM LEFT) Software analysis of strips via scanner and ImageStudio Lite. Dots represent actual assay results (endpoint HIV or IAC signal divided by the sum of these signals) (N=3), while lines represent the theoretical or expected results. (BOTTOM RIGHT) Sigmoidal curve fit to assay*

results using non-linear regression analysis. Dots represent actual assay results (N=3). Lines represent a four-parameter logistic equation fit to the data in each plot. Shaded areas represent 95% prediction bands.

To demonstrate the ability of this assay to quantify HIV RNA, as needed in a clinical VL test, we ran reactions with synthetic RNA targets (**Figure 5**) and analyzed them with the same survey or software approaches previously performed on DNA targets. Overall, the survey and software analyses agreed well with each other and with the ground truth. While the survey and software analysis both appeared to slightly underestimate HIV RNA relative to IAC RNA in the HIV=IAC condition (see the abundant 'D' responses in the survey where HIV=10^3, or the HIV signal fractions substantially lower than 0.5 in software analysis of the same strips), the agreement between the two analyses indicates that this underestimation is not due to errors in either analysis method. Given the tight accuracy of quantification previously observed with DNA targets, we believe that the HIV RNA target may have degraded slightly more than the IAC prior to RPA, although it is also possible that reverse transcription of the IAC target is more efficient (perhaps due to loss of secondary structure). We observed similar behavior when we tested the assay against HIV RNA extracted from clinical samples (**Figure A7**). Nevertheless, it appears that naked-eye and software analysis are both capable of distinguishing ≥10-fold ($\log_{10}$-scale) differences in HIV RNA copy number from the WHO treatment failure threshold. This may be sufficient for most VL tests, as PWH who discontinue ART typically experience a viral rebound with VL exceeding thresholds for treatment failure by an order of magnitude or more (in a prospective study, mean VL for 18 PWH exceeded 10^4 copies RNA/mL within 4 weeks of stopping ART[39]).

4.5 Conclusions

Competitive isothermal amplification is a powerful tool for quantification of nucleic acids and is useful for semi-quantitative HIV VL testing. The endpoint-measured lateral flow system enables naked-eye interpretation for most tests, while software and/or cell-phone mediated analysis can make a diagnosis when VL is too close to the treatment failure threshold for visual interpretation to be definitive.

Furthermore, the competitive IAC controls for the variability of isothermal reactions and confers robustness to several potential complications, including low sample preparation yield, reaction inhibition, and common HIV mutants. Competitive IACs have been used for HIV VL quantification before[23,24], and a semi-quantitative lateral-flow-based VL test (SAMBA semi-Q) has been described[40], but the competitive RPA assay described herein is the first (to our knowledge) to combine these technologies into a low-resource workflow.

A clinical adaptation of this assay should focus on development of a kit to address other POC priorities, such as ready-to-use shelf-stable reagents, low-resource sample preparation, and prevention of amplicon contamination. Although lyophilized RPA reaction pellets are recommended to be stored at -20°C, one study suggests that they remain viable at 25°C for three months or at 45°C for three weeks[13], which simplifies distribution and storage in low-resource settings (furthermore, the IAC could indicate reaction failure due to expired reagents). A more important concern for reagent storage is ease of use; ideally, all oligos should be stored with the lyophilized pellet to reduce assay setup complexity[41,42], and any liquid reagents should be combined into a single, small volume that is easy to add to the pellet (e.g. with a single-use exact volume transfer pipette). We have observed favorable performance and user feedback with a similar workflow conducted by non-trained 1st-time users or healthcare workers for HIV[41,43] or SARS-CoV-2 assays[44]. These changes have the added benefit of minimizing reagent volume, which allows for a larger sample input volume. Sample preparation must also be addressed in a clinical implementation; a blood sample for VL testing must first be collected, filtered or otherwise processed to remove cellular components, and purified to remove ribonucleases and other inhibitors and concentrate viral RNA[20]. We did not address sample preparation in this work, but paper-based methods for processing viral RNA from human specimens have been described[45,46]. A more sensitive RT-RPA assay[47,48] may also be desired if a PWH cohort is expected to have lower VLs or if the desired sampling method is a fingerstick. Finally, containment of amplicons is essential to prevent contamination of future tests

carried out in the same location. This can be achieved procedurally through separation of pre- and post-amplification workspaces in clinics, for example, but for self-testing, a sealed lateral flow cartridge (e.g., U-Star Disposable Nucleic Acid Lateral Flow Detection Units) may be ideal.

The assay chemistry described here is aimed at a specific application for HIV VL testing, but the concept and utility of a competitive IAC may be generalized to many isothermal amplification systems and applications. Indeed, although RPA nfo is a discontinued product at the time of writing, we have developed a fluorescence-based version of this assay using the RPA exo kit with similar semi-quantitative behavior (not shown). We also suggest that the nfo kit chemistry could be replicated by adding *E. coli* endonuclease IV to the basic RPA chemistry, as described in Piepenburg *et al.*[5]. Competitive amplification may be used in practically any chemistry with multiplexable detection methods[23,49]. Loop-mediated isothermal amplification (LAMP), for example, is another multiplexable chemistry used for POC diagnostics[50], and a direct RT-LAMP assay for HIV RNA detection in whole blood has been described[51]. Adaptation of such assays with demonstrated robustness to include a competitive IAC and a lateral flow readout should be relatively straightforward, although the barriers to POC implementation described previously still apply to virtually any NAT. Further innovations in the assay chemistry, such as direct measurement of amplicons with a hybridization-based probe system, may enable full quantification when desired for HIV VL testing or other POC applications.

4.6 Author Contributions

I.T.H. designed the competitive RPA workflow, conducted all assays, and analyzed lateral flow results. E.C.K. contributed to competitive isothermal assay design. G.K.G. prepared RNA from HIV-positive plasma samples. J.H.K. and N.P. conducted the survey for naked-eye analysis of lateral flow strips. K.G.S. developed the MATLAB script for analysis of cell phone photos of lateral flow strips and Q.W. conducted

the cell phone analysis. L.F. and J.S. contributed analysis of the clinical utility of this work. J.L. and B.R.L. oversaw the study. All authors contributed to writing and/or review of this manuscript.

4.7 Acknowledgments

We thank other Lutz Lab members (Amy Oreskovic, Daniel Leon, Shane Gilligan-Steinberg, and Robert Atkinson), members of the Frenkel Lab (Ingrid Beck, Ceejay Boyce, and Jackson Wallner), and members of the Yager Lab (Paul Yager, Sujatha Kumar, and Erin Heiniger) for their technical advice and helpful discussion. We thank Rongyu Zhang for preliminary development of lateral flow assays. We thank Paul Drain for advice pertaining to the clinical applications of this assay in HIV viral load monitoring. This work was supported by NIH/NIAID research grants R61AI140460 and R01AI145486. I.T.H. was supported in part by the National Institute of General Medical Sciences of the National Institutes of Health under Award Number T32GM008268.

4.8 Addition

We wish to acknowledge and direct readers to the article entitled "A Semi-Quantitative Isothermal Diagnostic Assay Utilizing Competitive Amplification"[52] by the Springer Lab at Harvard Medical School. Their article describes a similar competitive recombinase polymerase amplification (RPA) assay for semi-quantitative detection of HIV-1 and SARS-CoV-2 targets and was published in *Analytical Chemistry* just two and half months before we submitted our manuscript to the same journal, after our literature search was complete. Regretfully, we did not discover their work until after our own article was published, thus we did not discuss it. The Springer Lab's work is not only comparable to ours, but complementary and commendable for overcoming several shortcomings of our assay. We note that their RPA primers are extremely sensitive, in some cases detecting HIV RNA at titers below 10 copies per reaction. They also screened and sequenced a primer mutational library to characterize their assay's tolerance to primer mismatches, an approach that strikes us as extremely effective and worth

reproducing for many nucleic acid diagnostics. While their assay uses the same concept of competitive amplification, their detection and analysis methods differ in meaningful ways. Notably, their lateral flow assay uses a post-amplification heat denaturation and probe hybridization step that does not rely on the (discontinued) RPA Nfo probe chemistry described in our work. Finally, their supporting information describes several experiments to evaluate the robustness of competitive RPA to chemical perturbations and temperature variation, the importance of choosing an RNA competitor molecule when quantifying RNA targets, and other important considerations for this assay format. We strongly recommend that any readers interested in our work also read the Springer Lab's article for more discussion of and alternative approaches to competitive isothermal nucleic acid amplification.

5 High-Resolution Polymerase Screening via Compartmentalized Self-Replication, Deep Mutational Scanning, and Molecular Dynamics Simulations

Ian T. Hull[1], Nicholas A. Popp[2,3], Enos C. Kline[1], Rachel L. Powell[2], Melinda K. Wheelock[2,4], Matthew C. Childers[1], Qin Wang[1], Valerie Daggett[1], Douglas M. Fowler[1,2,4], and Barry R. Lutz[1,4*]

[1]Department of Bioengineering, University of Washington, Seattle, WA 98195-5061, USA

[2]Department of Genome Sciences, University of Washington, Seattle, WA 98195-5065, USA

[3]Medical Scientist Training Program, University of Washington School of Medicine, Seattle, WA 98195-5065, USA

[4]Brotman Baty Institute for Precision Medicine, Seattle, WA 98195-5065, USA

*Send correspondence to blutz@uw.edu

5.1 Abstract

We present a novel platform for high-resolution mapping of DNA polymerase activity and stability under the effects of harsh chemistries that are incompatible with most other mutational scanning methods. This approach pairs compartmentalized self-replication (CSR), a high-throughput method for polymerase directed evolution, with deep mutational scanning (DMS), a method of quantifying variant effect via next-generation sequencing of libraries that are subjected to a functional selection. We demonstrate the validity of this "CSR-DMS" platform by showing that it identifies loss-of-function variants at sites with known DNA binding or catalytic activity in the wild-type protein. We further explore the efficacy of this method by imposing denaturing selective pressures (heat or guanidinium thiocyanate) during screening and showing that variants with high positive enrichment under these selective pressures possess novel

resistance to denaturation in activity assays. These variants may be useful for "direct" diagnostic workflows that detect biomarkers from crude sample matrices with little to no sample purification. Furthermore, the mechanisms of stabilizing mutations can be inferred from trends in the scores of similar mutations in sequence-to-function heatmaps and corroborated by the behavior of residues of interest in molecular dynamics simulations of the wild-type protein. These mechanisms, uncovered by CSR-DMS, inform future approaches to rational design of extremely stable DNA polymerases. Overall, we anticipate that CSR-DMS could be used both for the study of the biophysical mechanisms of selective pressures and for the engineering of polymerases with novel capabilities.

5.2 Introduction

5.2.1 Protein Engineering Motivation

Polymerases are central to many workflows for amplifying, detecting, or sequencing nucleic acids. The biotechnology industry has repurposed naturally occurring polymerases, such as DNA polymerase I variants from *Thermus aquaticus* (*Taq*) and *Bacillus stearothermophilus* (*Bst*), for use in reactions such as polymerase chain reaction (PCR)[3] and loop-mediated isothermal amplification (LAMP)[4] due to traits such as thermostability and strand displacement activity. Furthermore, variants have been engineered for capabilities such as reverse transcription activity[6] and high sequence fidelity[53].

The importance of polymerases in molecular biology workflows has inspired the development of platforms for high-throughput polymerase evolution and screening[54]. One such method that has proven particularly useful is compartmentalized self-replication (CSR)[55]. CSR is a powerful technique for directed evolution of polymerases (**Figure 6**). It relies on the coupling of polymerase genotype to phenotype by isolating polymerase variants into separate compartments and forcing polymerase proteins to copy their own coding sequences from their plasmids. Mutants with better activity under selective conditions will create more copies of their coding sequence, enriching themselves amongst the population of

amplicons. CSR was originally developed to select for thermostable polymerases[55] and has since been adapted to select for various activities, including reverse transcription[56], strand displacement[57], and fast DNA binding/extension[58].

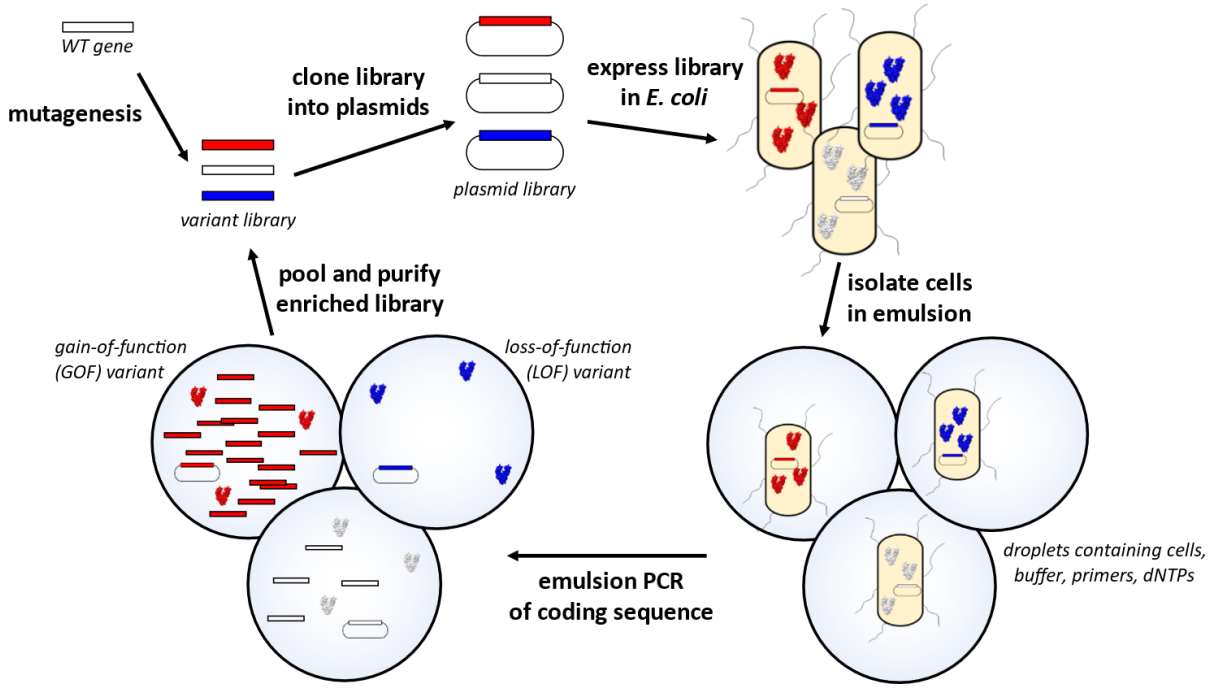

Figure 6. CSR for directed evolution of polymerases. *Polymerase libraries are expressed in E. coli. Cells are compartmentalized in an emulsion and heat-lysed. Polymerases copy their own plasmids via PCR under selection criteria; polymerases with higher activity or stability (shown here in red) create more copies of their genes. Amplicons are then pooled, amplified by PCR, and characterized or propagated into the next round of selection.*

While CSR has a long track record of producing functional polymerase variants, it is rarely used for high-resolution studies of polymerase activity and stability. CSR is typically used in a conventional "directed evolution" approach, in which multiple successive rounds of selection are conducted until a few high-performing variants dominate a library, at which point individual variants are characterized and their mutations retroactively interpreted in the context of the selective pressure. While this conventional approach may be effective for rapid development of variants for a single application, it is less effective at resolving the biophysical effects of the selective pressure and the mechanism by which fitter variants adapt to the pressure. This is because subjecting the library to several rounds of selection and characterizing a sample of the enriched variants deliberately reduces library diversity and discards

information from the variants that do not persist through selection. Such information is valuable because the less fit mutations are more susceptible to the selective pressure, and knowledge of their identities and distribution can uncover a much richer understanding of the mechanism of the selective pressure and inform future approaches to protein design. A notable example is a study performed by the Ellington Lab that used CSR to evolve reverse transcription activity in a DNA polymerase that previously lacked this capability[56]. In this study, the authors deep-sequenced the library as it evolved, allowing a high-resolution structural view of residues involved in RNA binding and reverse transcription to emerge. This study demonstrates the power of such mutational scanning, but was limited in scope because the library was not saturated with mutations and the deep-sequencing approach could not discern single mutants from variants containing multiple (potentially epistatic) mutations.

In contrast to conventional directed evolution, deep mutational scanning (DMS) is a technique used for extremely high-resolution studies of protein function. DMS interrogates protein sequence-function relationships by coupling high-throughput sequencing to a functional selection[59,60]. Unlike conventional directed evolution, which uses multiple rounds of selection to enrich functional variants until they dominate a library, DMS uses high-throughput sequencing to count variants pre- and post-selection, assigning functional scores to variants based on how much they enrich themselves in the library. With sufficient library size, screening throughput, and sequencing coverage, DMS can quantify the function of every single-residue mutant (and potentially many higher-order mutants) of a protein, often after a single round of selection. DMS has previously been performed on polymerase variant libraries to identify residues in polymerase catalytic sites that define substrate specificity in droplet-based microfluidic approaches[61,62], but has not been demonstrated for CSR (which requires little to no specialized instrumentation) or on entire polymerase coding sequences (which may contain stability-defining residues outside of catalytic sites).

We hypothesize that CSR can be paired with DMS (a technique we will call CSR-DMS) to quantify the function of every single-residue mutant of a polymerase. In this work, we demonstrate this approach to probe polymerase baseline activity and tolerance to thermal cycling (via CSR alone), extreme thermostability (via CSR preceded by a heat spike), and tolerance to chemical denaturation (via CSR with added guanidinium thiocyanate (GuSCN), a potential inhibitor that is commonly encountered in diagnostic workflows). CSR is well-suited for DMS; its maximum reported throughput is 10^8 variants per round of selection and it can produce variant DNA sequences as a direct output of selection[63]. Furthermore, we will perform molecular dynamics (MD) simulations on the polymerase to cross-validate DMS results, as MD simulations produce a similar high-resolution (in this case, atomic-scale) map of protein responses to pressures such as heat and chemical denaturants.

For this work, we will use a polymerase previously developed by our lab for applications in point-of-care (POC) diagnostics[44,64]. It is a chimera of DNA Pol I from *Thermus thermophilus* with a synthetic "fingers" domain from *Thermodesulfatator indicus*. We have named this chimera "Thin Fingers" (TF) polymerase. TF polymerase possesses several features amenable to CSR and POC use, as demonstrated in the results section and previous work[44,64].

5.2.2 Chaotrope-Resistant ("Chaostable") Polymerase Motivation

Nucleic acid amplification tests (NAATs) are established diagnostics for highly sensitive and specific detection of pathogen genomes. NAATs involve three main steps: sample preparation, amplification, and detection. While isothermal amplification and lateral flow detection methods are promising low-complexity methods for implementation at the point-of-care (POC), sample preparation remains a bottleneck[9,65]. Nucleic acid purification often requires precise fluid handling steps and instrumentation incompatible with low-resource settings. Direct amplification methods, in which a sample is added

directly to an amplification master mix, have been explored[66–68], but these require polymerases resistant to inhibitors and risk degradation of nucleic acid targets by endogenous nucleases.

Sample preparation is particularly strenuous for RNA targets, despite the importance of RNA in infectious disease diagnostics. Several diseases of global public health importance are caused by RNA viruses. These include HIV, influenza, coronaviruses, polio, Ebola, measles, rabies, and the hepatitis viruses (excluding hepatitis B)[69]. NAATs that target these pathogens must lyse virions to extract RNA, but this may expose RNA to ribonucleases (RNases) in the sample. For example, free RNA added to human plasma degrades to <1% of its original concentration within 15 seconds[70]. Heating does not completely inactivate RNases[71] (and RNA itself degrades upon heating[72]). RNA therefore requires rapid stabilization in buffers that denature RNases. RNase inhibitors, while frequently used in amplification buffers to prevent trace RNase activity, are expensive, specific to mammalian RNases, and unstable above 50°C. RNase inhibitors therefore are not a sufficient replacement for chemical denaturants in lysis buffers.

A major reason why sample preparation for RNA targets is strenuous is that lysis buffers used for RNA purification are usually not compatible with amplification buffers that employ polymerases to detect biomarkers. Many procedures for RNA purification are derived from the Boom method[65,73]. This method employs a sample lysis step in a buffer with chaotropic agents, commonly guanidinium hydrochloride (GuHCl) or guanidinium thiocyanate (GuSCN). Chaotropic agents, or “chaotropes”, facilitate protein unfolding through a variety of direct and indirect effects[74–76]. Chaotropes lyse target virions or cells, denature proteins that may interfere with the assay (e.g. RNases), and create favorable conditions for nucleic acids to bind to silica. Lysed samples are thus applied to silica columns and washed to remove inhibitors (including the chaotrope itself), then nucleic acids are eluted for amplification.

The protein-denaturing activity of chaotropes used in the Boom method is useful for sample processing, but it potently inhibits downstream amplification if not properly removed. Typical lysis buffers contain

high concentrations (3-6M) of GuSCN to ensure rapid lysis and nuclease denaturation[73,77,78], but *Taq* polymerase loses 50% of its activity in just 63.5mM guanidinium thiocyanate[79], necessitating stringent wash steps prior to addition of RNA to an amplification mixture. While chaotrope concentrations in lysis buffers could possibly be decreased for some applications, RNases are very stable enzymes with disulfide-bonded tertiary structures, and they retain activity in up to 3M GuHCl[80,81], well beyond the tolerance of natural polymerases.

The development of a chaotrope-resistant ("chaostable") polymerase could enable a new class of sample-preparation-free RNA diagnostics. A polymerase developed for chaostability can be used in a simplified POC NAAT format (**Figure 7**), in which a patient sample is mixed with a chaotropic buffer and then diluted into a larger-volume reaction mix containing polymerase and amplification reagents for an isothermal method such as reverse transcription loop-mediated amplification (RT-LAMP)[4]. If the polymerase tolerates chaotrope concentrations in the hundreds of millimolar range, then denatured samples with chaotrope in the molar range would require a relatively minimal dilution (roughly tenfold) to enable amplification directly in one tube without any further processing, excessive reaction volumes, or exorbitant reagent costs. The amplification products could then be detected by a variety of POC detection methods (e.g. color change, fluorescence, or lateral flow).

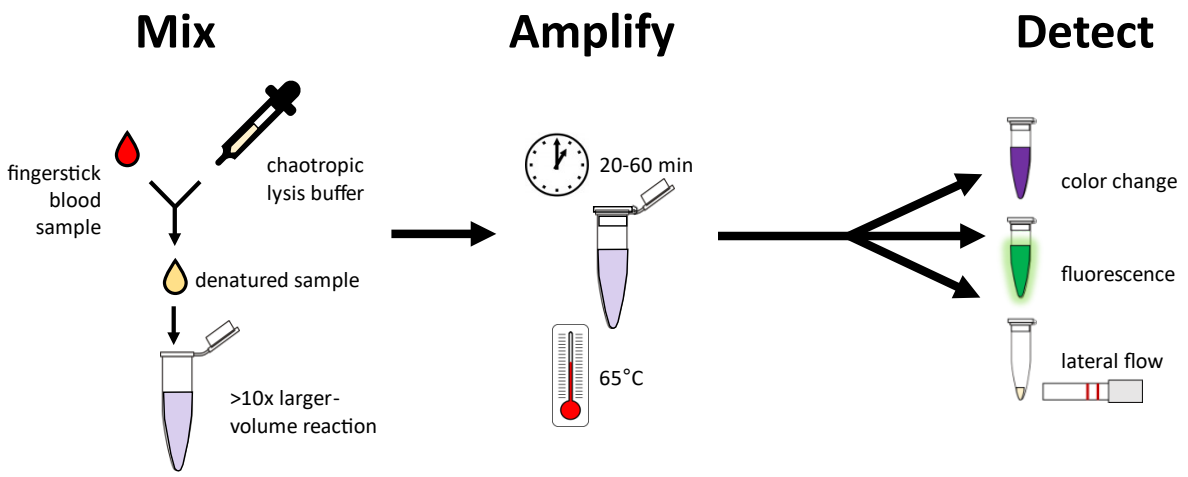

Figure 7. Example format for direct RT-LAMP from a patient blood sample. *Patient sample and a chaotropic buffer are mixed to lyse virions and denature nucleases, then added directly to a larger-volume reaction to dilute the chaotrope. Amplification is enabled using a "chaostable" polymerase that tolerates moderate concentrations of the chaotrope. Amplification can be detected by color change[82], fluorescence[83], or lateral flow[84].*

A deeper understanding of protein chaostability would also enable development of novel chaostable proteins for various applications. Biophysical insights from proteins resistant to a specific chaotrope may be applied to design other proteins with enhanced resistance to the same chaotrope. For example, most isothermal amplification systems require more than just a polymerase; isothermal strand displacement amplification requires a nicking enzyme[85], while recombinase polymerase amplification (RPA) requires recombinase, single-stranded DNA binding protein, and various co-factors[5]. Knowledge of protein properties necessary for enhanced stability in chaotropic conditions may be applied to develop other chaostable proteins for these multi-enzyme systems. Further, a deep understanding of the specific effects of a chaotrope may help predict whether a protein that resists these effects is likely to be universally tolerant to various chaotropes or whether it should only tolerate a specific chaotrope or category of chaotropes.

We hypothesize that a polymerase can be evolved to exhibit higher chaostability than target virions or RNases. Proteins vary in their ability to resist denaturation under chaotropic conditions, with some exhibiting long half-lives of unfolding in 6.6M GuHCl[86]. Notably, streptavidin retains the ability to bind biotin in 6M urea, and unfolds slowly in 6M GuHCl with a half-life of ~50 days[87]. Furthermore, T7 RNA polymerase activity increases with small concentrations of GuHCl, peaking around 50mM GuHCl[88]. These examples imply that a polymerase may be engineered to resist denaturation under chaotropic conditions; however, protein stability engineering efforts have largely focused on other measures of stability, such as thermostability. In this work, we will use CSR-DMS to screen for polymerase variants that exhibit higher activity in PCR conditions containing GuSCN.

5.3 Experimental Section

5.3.1 Wild-Type Polymerase Characterization

5.3.1.1 Plasmid Construction and Protein Production

Polymerase cloning, expression, and purification were performed as previously described[44] for non-codon-optimized wild-type Thin Fingers polymerase ("TF-WT") in a pET His6 TEV LIC cloning and expression vector (2B-T) (this vector was a gift from Scott Gradia (Addgene plasmid #29666; http://n2t.net/addgene:29666; RRID:Addgene_29666)).

5.3.1.2 PCR Activity Assays

25µL reactions were prepared each containing 1x OneTaq buffer (New England Biolabs B9022SVIAL), 0.2mM each dNTPs, 200nM each forward and reverse primer, 0.5x EvaGreen intercalating dye (Biotium 31000), 0.1112pmol TF-WT polymerase, varying concentrations of GuSCN (Sigma-Aldrich 50983), and varying copy numbers of a DNA template. Master mix containing all reagents except GuSCN and DNA template was first prepared on ice and added to individual reaction tubes on ice. 2µL of DNA template was then added to each tube. In order to minimize and control the amount of time each reaction was exposed to GuSCN before incubation, 4.17µL of 6x GuSCN solution was added to the inside lid of each tube, then tubes were closed and simultaneously spun on a minicentrifuge and vortexed before quickly being transferred to a pre-heated Bio-Rad CFX96 real-time PCR thermal cycler. Reactions were incubated at 94°C for 30 seconds followed by 38 cycles of (94°C for 10 seconds, 53°C or 54°C as indicated for 20 seconds, 72°C for 20 seconds, plate read) and a final extension at 72°C for 2 minutes.

5.3.1.3 LAMP Activity Assays

25µL reactions were prepared each containing 1x Thermopol buffer (New England Biolabs B9004SVIAL), 2mM supplemental MgSO4 (New England Biolabs B1003SVIAL), 0.4mM each dNTPs, 1x GAPDH LAMP primer mix (prepared as described[57]), 1M betaine (Sigma Aldrich B0300), 1x EvaGreen intercalating dye

(Biotium 31000), 0.116pmol TF-WT polymerase, varying concentrations of GuSCN (Sigma-Aldrich 50983), and varying copy numbers of GAPDH dsDNA template (Integrated DNA Technologies gBlock with sequence as described[57]). Master mix containing all reagents except GuSCN and DNA template was first prepared on ice and added to individual reaction tubes on ice. 2µL of DNA template was then added to each tube. In order to minimize and control the amount of time each reaction was exposed to GuSCN before incubation, 4.17µL of 6x GuSCN solution was added to the inside lid of each tube, then tubes were closed and simultaneously spun on a minicentrifuge and vortexed before quickly being transferred to a pre-heated Bio-Rad CFX96 real-time PCR thermal cycler. Reactions were incubated at 68°C for 1 hour with plate reads taken every 30 seconds.

For the LAMP experiment on SARS-CoV-2 templates, lyophilized reactions were set up as previously described[44], with GuHCl added to reactions in an identical manner to the previous paragraph.

5.3.2 CSR Primer Design and Screening

The Primer-BLAST[89] webtool was used to generate primers that bind to a TFO-WT (codon-optimized wild-type Thin Fingers polymerase; see Barcoded Library Construction section for discussion) in 2B-T plasmid template with the following key parameters: product size 100-250bp, primer T_m 62-68°C (optimum 65°C, maximum difference 1°C), specificity check on for *E. coli* (taxid:562), primer size 15-25 bases (optimum 20 bases), primer GC content 50-60%, thermodynamic oligo and template alignment on, 40mM monovalent cations, 2mM divalent cations, 1.04mM dNTPs. These parameters were chosen to closely match the thermal cycling parameters and buffer content of a published CSR protocol[63], but with newly designed primers that amplify a short stretch of the target plasmid and are unlikely to amplify off-target sites in the *E. coli* genome or form undesired primer dimers.

Out of 24 generated primer pairs, seven pairs targeted sites in the plasmid that had no known function and could likely tolerate the introduction of CSR-DMS barcodes. These seven primer pairs were ordered

as custom DNA oligos (Integrated DNA Technologies) with 5' tags for recovery PCR. The primers then underwent extensive *in vitro* screening in PCR conditions similar to CSR (1x ThermoPol buffer, 0.26mM each dNTPs, 1x EvaGreen intercalating dye (Biotium), 500nM each primer, varying copies TFO-WT plasmid template), but with Hot Start Taq Polymerase (New England Biolabs M0495S) instead of TFO polymerase, as we typically observe that TFO enzyme stocks are contaminated with low levels of their coding plasmid (likely co-purified while bound to TFO enzyme during our in-house production) which obfuscates analysis of PCR assays targeting the same plasmid. Note that we observed some room temperature activity of the Hot Start Taq Polymerase despite the advertised hot-start feature, so we set reactions up on ice and added primers last, to the undersides of tube lids, before spinning reactions down, mixing by vortex, and immediately transferring to a thermal cycler. PCR screens were run on a Bio-Rad CFX96 real-time PCR thermal cycler with the following protocol: 95°C for 3 minutes, 45 cycles of (95°C for 30 seconds, 62°C (or 58-68°C gradient) for 30 seconds, 68°C for 30 seconds), 68°C for 8 minutes, and a melt curve (60-95°C, 0.2°C per step, 5 seconds per step).

5.3.3 Mock Barcoded Library Construction

5.3.3.1 Plasmid Construction

TFO-WT (codon-optimized wild-type Thin Fingers polymerase; see Barcoded Library Construction section for discussion) was ordered as a HiFi gBlock dsDNA fragment (Integrated DNA Technologies) with tags for ligation-independent cloning (LIC), cloned into 2B-T plasmid (Addgene plasmid #29666) via LIC, and transformed into T7 Express LysY/Iq cells (New England Biolabs C3013I) as previously described[44].

TFO-WT in 2B-T plasmid was mutated to an inactive variant using a Q5 site-directed mutagenesis kit (New England Biolabs E0554) following the manufacturer-recommended protocol and transformed into T7 Express LysY/Iq cells. The mutation induced (D318A) is depicted in **Figure 8**. The missense D-to-A mutation was chosen to knock out polymerase activity, as the aspartic acid residue coordinates with two

magnesium ions that are essential for catalysis[90]. The resulting inactivated mutant, dubbed "TFO-XX", was verified by Sanger sequencing from the T7 promoter (forward) and T7 terminator (reverse).

Figure 8. Mutation induced in TFO-XX. *Immutable[90] aspartic acid D318 (corresponding to D610 in Taq polymerase) was mutated to alanine.*

Following generation of TFO-XX from TFO-WT, we submitted both constructs for nanopore sequencing to validate the plasmid backbones. We observed two unexpected backbone mutations (a trinucleotide deletion in the plasmid basis of mobility region and a synonymous mutation in a residual tetracycline resistance gene fragment) in both constructs but these were presumed harmless (as we had already used this backbone for several constructs that expressed functional protein). More concerning, however, was the presence of plasmid concatemers in the nanopore raw reads and read length histograms. Every plasmid DNA sample prepared from the T7 Express LysY/Iq cells contained dimers and trimers, with the TFO-XX concatemers possessing the desired D-to-A mutation in every copy of the TFO gene, suggesting that the concatemers likely were not formed during *in vitro* enzymatic reactions but rather originated from monomer transformants during cell growth and plasmid replication. We then subcloned the TFO-WT, TFO-XX, and original 2B-T plasmid into NEB Stable cells (New England Biolabs C3040H) following the manufacturer-recommended protocol. The resulting plasmid preparations all had the same backbone mutations (suggesting they are legacy mutations present in 2B-T and possibly the plasmids it was originally derived from) but were free of concatemers. We believe that recombinase A (which is present in T7 Express LysY/Iq but deficient in NEB Stable cells) may be responsible for the formation of concatemers.

The presence of plasmid concatemers in T7 Express LysY/Iq cells concerned us because they introduce multiple sites for mutagenesis and barcoding in a single molecule, potentially muddling barcode-variant

linkages. For this reason, we decided to use NEB Stable cells (and plasmids prepared from them) for all subsequent cloning and library preparation steps while reserving the use of T7 Express LysY/Iq cells solely for protein expression (including CSR).

5.3.3.2 Barcoding

Barcodes were designed to be inserted in the middle of the CSR target sequence (roughly equidistant from each CSR primer binding site) to minimize the chance that barcodes could form secondary structures with CSR primer binding sites. Barcode oligos consisted of 24 random nucleotides flanked by 25 bases on either side homologous to the desired site in the plasmid backbone. For the mock selection, a tag ("AAA" for TFO-WT and "TTT" for TFO-XX) was included immediately 5' to the random barcode to enable identification of variants without any prior subassembly (**Figure 9**).

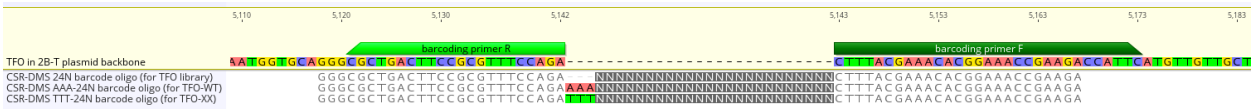

Figure 9. Method for barcoding TFO constructs in 2B-T plasmid backbone. Plasmid is linearized by PCR at the desired barcode insertion site. Barcode oligos consisting of 24 random bases (plus tags for mock selection) and 25-base homologous flanking sequences are cloned into the resulting PCR product using NEBuilder Assembly.

TFO-WT and TFO-XX plasmid constructs were linearized by PCR at the desired barcode insertion site using barcoding primers, 10pg TFO-WT or TFO-XX plasmid template, and Q5 HotStart High-Fidelity DNA Polymerase (New England Biolabs M0493S), following the manufacturer-recommended recipe for 50µL reactions with 1x Q5 High GC Enhancer. Thermal cycling parameters were 98°C for 30 seconds, 35 cycles of (98°C for 10 seconds, 72°C for 5 minutes), 72C for 2 minutes, 4°C hold. PCR products were purified using a Monarch PCR Cleanup Kit (New England Biolabs T1030S). Barcode oligos (ordered as Ultramer ssDNA oligos from Integrated DNA Technologies) were then cloned into the linearized plasmid PCR products using NEBuilder HiFi DNA Assembly Master Mix (New England Biolabs E2621S) following the manufacturer-recommended protocol for bridging double-stranded DNA with a single-stranded DNA oligo (1pmol oligo, 0.005 pmol vector, 1x NEBuilder master mix in 20µL reactions incubated at 50°C for

60 minutes followed by a 4°C hold). 2µL of the chilled NEBuilder products were then transformed into NEB Stable cells following the manufacturer-recommended high efficiency transformation protocol. Following outgrowth, varying dilutions of cells in NEB Stable outgrowth medium (100µL cells, 10µL cells plus 90µL outgrowth medium, or 1µL cells plus 99µL outgrowth medium) were plated on LB+carb agar plates and incubated at 30C overnight or added to 1.9mL LB+carb medium and incubated at 30C, 250rpm overnight. The following day, plasmid was purified from the liquid cultures using a Monarch Plasmid Miniprep Kit (New England BioLabs T1010). Colony counts from plates were estimated using OpenCFU[91]. Plates with 100µL or 10µL cells were too dense for quantification, so plates with 1µL cells were used for colony counts and the results were extrapolated to estimate library size for each plasmid preparation. We used the plasmid preparations from 100µL-cell cultures for mock selection (estimated library size of 2.5e4 barcodes for TFO-WT and 1e4 barcodes for TFO-XX). Nanopore sequencing of the purified barcoded TFO-WT and TFO-XX plasmids confirmed the presence of random barcodes with the appropriate tags.

5.3.4 Barcoded Library Construction

5.3.4.1 Library Design

We ordered a library saturated with all possible single-residue mutants of Thin Fingers polymerase from Twist Bioscience. To synthesize this library, the vendor needed to codon-optimize the wild-type sequence, and provided us with the optimized sequence (which we are calling “TFO”, for “Thin Fingers Optimized”). We validated that TFO-WT can be expressed and purified at yields comparable to TF-WT.

Table 1 includes information about the TFO library parameters.

Parameter	**Specification**
Codon optimization	*E. coli* strain B
GC content	<65%. TF-WT is 67% GC. TFO-WT is 56.7% GC.
Wild-type amino acids included?	Yes (synonymous codon if possible, otherwise WT codon)
STOP codons included?	Yes

Single codon deletions included?	Yes
Length (bp)	1620 (1690 with 35-base flanks for 2B-T cloning)
Length (codons)	540
Variants per codon	22 (each amino acid, STOP, deletion)
Number of total variants	11880

Table 1. Parameters for site-saturation variant library.

5.3.4.2 Plasmid Construction

The TFO library was delivered dry in 96-well plates, with each well containing 50ng of DNA saturated at a single codon, for total of 540 wells. We resuspended each well in 20uL of IDTE buffer (10mM Tris, 0.1mM EDTA, pH 8.0) (Integrated DNA Technologies) for a final concentration of 2.5ng/µL. 10µL of each well was sampled and pooled to mix all variants. The pooled library was cloned into 2B-T plasmid (Addgene plasmid #29666) using NEBuilder HiFi DNA Assembly Master Mix (New England Biolabs E2621S) following the manufacturer-recommended protocol for assembling two dsDNA fragments (2:1 molar ratio of TFO library insert to 2B-T vector, 0.03pmol total fragments, 1x NEBuilder master mix in 20µL reactions incubated at 50°C for 60 minutes followed by a 4°C hold). 2µL of the chilled NEBuilder products were then transformed into NEB Stable cells following the manufacturer-recommended high efficiency transformation protocol. Following outgrowth, varying dilutions of cells in NEB Stable outgrowth medium (1µL cells plus 99µL outgrowth medium, 1µL previous dilution plus 99µL outgrowth medium) were plated on LB+carb agar plates and incubated at 30C overnight while the remaining 999µL of cells were added to 9mL LB+carb medium and incubated at 30C, 250rpm overnight. The following day, plasmid was purified from the liquid culture using a Monarch Plasmid Miniprep Kit (New England BioLabs T1010) (culture was split into eight replicate plasmid preps). Colony counts from plates were estimated using OpenCFU[91] and the results were extrapolated to estimate a total transformation yield of roughly 7e5 colony-forming units in the liquid culture (well in excess of the total number of synthesized variants and therefore expected to maintain coverage for all but the least abundant variants).

5.3.4.3 Barcoding

The TFO saturated variant library was barcoded in a similar manner to the mock selection TFO-WT and TFO-XX constructs, but with additional care taken to minimize the number of PCR cycles and the fraction of unbarcoded variants.

The library was linearized by PCR at the desired barcode insertion site using barcoding primers, 10ng TFO library in 2B-T plasmid, and Q5 HotStart High-Fidelity DNA Polymerase (New England Biolabs M0493S), following the manufacturer-recommended recipe for 50µL reactions with 1x Q5 High GC Enhancer. The reaction was supplemented with 1x EvaGreen intercalating dye (Biotium), monitored during amplification on a Bio-Rad CFX96 real-time PCR thermal cycler, and stopped before the PCR plateau phase. Thermal cycling parameters were 98°C for 30 seconds, 18 cycles of (98°C for 10 seconds, 72°C for 5 minutes). PCR products were purified using an Invitrogen PureLink PCR Cleanup Kit (using B3 high-molecular-weight-cutoff binding buffer), digested with *DpnI* (New England Biolabs R0176S) in 1x rCutSmart buffer for 15 minutes at 37°C to remove carryover circular plasmid template, and purified once more with the PureLink PCR Cleanup Kit (B3 buffer).

Barcode oligos (ordered as Ultramer ssDNA oligos from Integrated DNA Technologies) were then cloned into the linearized plasmid PCR products using NEBuilder HiFi DNA Assembly Master Mix (New England Biolabs E2621S) following the manufacturer-recommended protocol for bridging double-stranded DNA with a single-stranded DNA oligo (1pmol oligo, 0.005 pmol vector, 1x NEBuilder master mix in 20µL reactions incubated at 50°C for 60 minutes followed by a 4°C hold). 2µL of the chilled NEBuilder products were then transformed into NEB Stable cells following the manufacturer-recommended high efficiency transformation protocol. Following outgrowth, varying dilutions of cells in NEB Stable outgrowth medium (1µL cells plus 99µL outgrowth medium, or 100µL of (1µL cells plus 999µL outgrowth medium)) were plated on LB+carb agar plates and incubated at 30C overnight while the remaining 998µL of cells were added to 9mL LB+carb medium and incubated at 30C, 250rpm overnight. The

following day, plasmid was purified from the liquid culture using a Monarch Plasmid Miniprep Kit (New England BioLabs T1010) (culture was split into eight replicate plasmid preps). Colony counts from plates were estimated using OpenCFU[91] and the results were extrapolated to estimate a total transformation yield of roughly 1.1e5 barcoded variants in the liquid culture.

5.3.4.4 PacBio Sequencing and Subassembly

To associate barcodes with variants, we sequenced entire plasmid molecules from the barcoded TFO library with high-fidelity long reads using PacBio sequencing (**Figure 10**).

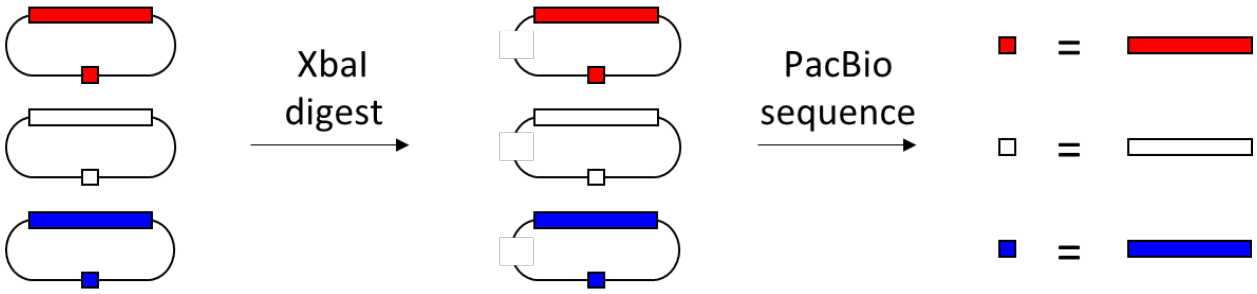

Figure 10. Subassembly of plasmid library to associate barcodes with polymerase variants. *Barcoded polymerase library is linearized by digestion with a single restriction enzyme (XbaI). Linearized plasmids are sequenced via PacBio sequencing, which sequences each individual molecule several times to generate a highly accurate consensus sequence of the full plasmid that can be used to link barcodes to variants.*

20µL (roughly 1140ng) of barcoded TFO library plasmid was digested with *XbaI* (New England Biolabs R0145S) in 1x rCutSmart buffer for 60 minutes at 37°C to linearize the library. Note that *XbaI* was specifically chosen because it had a single predicted cut site in the plasmid backbone and no predicted cut sites in the coding sequence of any TFO variant. The digested product was then purified using an Invitrogen PureLink PCR Cleanup Kit (using B3 binding buffer).

We submitted the linearized barcoded TFO library to University of Washington PacBio Sequencing Services, where it was prepared for sequencing using an Amplicon SMRTBell Prep Kit v3 and then sequenced on a Sequel II platform with Sequel II v3.2 chemistry, an SMRT Cell 8M, and a 30 hour movie.

The run produced roughly 1.65 million HiFi reads of the library, with a median HiFi read quality of Q53. These reads were processed with scripts to produce a barcode-variant map as follows.

"HiFi" PacBio reads were processed with a custom analysis pipeline, AssemblyByPacBio. Each circular consensus sequence (CCS) was aligned to the TFO-WT DNA sequence using BWA-MEM v0.7.10-r789[92], generating CIGAR and MD strings, which were then used to extract barcodes and TFO variant sequences. The output from AssemblyByPacBio was then processed with PacRAT[93], which creates a multiple sequence alignment of all variant sequences with the same barcode to improve variant calling. PacRAT was run with a variant agreement threshold of 0.6 and 3 independent CCS reads to call a barcode. A custom R script was then used to parse the PacRAT output and generate a final barcode-variant map.

5.3.5 CSR-DMS Selections

5.3.5.1 Culture and Expression

100ng of barcoded TFO library (or, for mock selection, 1ng of barcoded TFO-WT and 100ng of barcoded TFO-XX) was transformed into 50µL T7 Express LysY/Iq cells using the manufacturer's recommended high-efficiency protocol. The transformed cells were outgrown in 1mL SOC medium at 37C 250rpm for one hour, then inoculated into 10mL 2x YT broth with 100µg/mL carbenicillin in 50mL sterile conical tubes covered with AirPore sheets (Qiagen). Cultures were incubated overnight at 30°C, 200rpm. The following morning, 100µL of each culture was subcultured into 10mL fresh media and grown at 37°C 250rpm until exponential phase was reached (OD600 = 0.4-0.6). Cultures were induced with 0.4mM IPTG and allowed to express for 2 hours. Culture OD600 measurements were taken and an equivalent of 0.5mL of culture at OD600=1.0 was aliquoted to a new microcentrifuge tube for further processing.

To determine pre-CSR variant frequencies in this "grown" library, two 1mL samples of culture were also saved and pelleted at 16,000g for 1 minute, after which supernatant was removed and pellets were

stored at -20C. These pellets were later processed using a Monarch Plasmid Miniprep Kit (New England BioLabs T1010).

5.3.5.2 Emulsion PCR

1.2mL of oil phase was prepared fresh for each condition: 54µL Span 80, 4.8µL Tween 80, 0.6µL Triton X-100, and 1140.6µL light mineral oil (all from Sigma Aldrich). Oil phase was aliquoted into 2mL tubes, to each of which a rubber stopper from a 1mL syringe was added, vortexed, and chilled on ice.

0.3mL of aqueous phase was prepared fresh for each condition and chilled on ice: 30µL 10x ThermoPol buffer, 7.8µL of (10mM each) dNTPs, 15µL 10µM CSR-DMS forward primer, 15µL 10µM CSR-DMS reverse primer, 50µL 6x GuSCN (water for conditions with no GuSCN), and 182.2µL water.

The previously aliquoted cells were pelleted at 1500g for 15 min. Supernatant was removed and cells were resuspended in 1mL tris-buffered saline (TBS). Cells were then pelleted and resuspended in 0.3mL of ice-cold aqueous phase. The cell-aqueous phase mixtures were then added to the 1.2mL oil phase aliquots and emulsified on a Qiagen TissueLyser LT at 42 Hz for 4 min at 4°C. Following emulsification, 100µL aliquots of emulsions were distributed into 0.2mL PCR tubes (total twelve tubes per condition). Emulsions were placed onto a Bio-Rad T100 thermal cycler and incubated as follows: (CSR+heat condition only: 100°C for 10 minutes), 95°C for 3 minutes, 20 cycles of (95°C for 30 seconds, 62°C for 30 seconds, 68°C for 30 seconds), 68°C for 8 minutes. Emulsions were then kept at 4°C for up to one week before further processing.

5.3.5.3 Emulsion Breaking and DNA Purification

Emulsions were combined into a single 1.5mL tube per condition and centrifuged for 10 min at 12,000g. The top oil layer was removed and discarded. To the bottom emulsion layer, 300µL (approximately 1:1 v/v) of chloroform was added and vortexed for 10 to 20 seconds, until the bottom layer appeared dissolved. The entire mixture was added to a PhaseLock tube (VWR 10847-802) and centrifuged for 2

minutes at 16,000g. The top aqueous layer was transferred to a new 1.5mL tube and further purified using an Invitrogen PureLink PCR Purification Kit following the manufacturer's recommended instructions.

5.3.6 CSR Library Sequencing

5.3.6.1 Mock Library Sequencing

For the column-purified grown mock plasmid library, 50µL PCR reactions were prepared with 1x Q5 reaction buffer, 0.2mM each dNTPs, 500nM forward AmpliconEZ-CSR primer, 500nM reverse AmpliconEZ-CSR primer, 1U Q5 Hot-Start High-Fidelity polymerase (NEB M0493), 1x EvaGreen intercalating dye (Biotium), and 10ng plasmid library template. PCR duplicates were prepared for each sample. Reactions were incubated in a Bio-Rad CFX96 real-time thermal cycler with initial denaturation at 98°C for 30 seconds and cycled at (98°C for 10 seconds, 72°C for 30 seconds) repeatedly until sufficient yield was observed (roughly 2000 RFUs or more) (about 15 cycles), then stopped before reactions entered plateau phase. Reactions were purified using an Invitrogen PureLink PCR Purification Kit following the manufacturer's recommended instructions.

For the column-purified mock CSR product library, 50µL PCR reactions were prepared with 1x Q5 reaction buffer, 0.2mM each dNTPs, 500nM forward AmpliconEZ-recovery primer, 500nM reverse AmpliconEZ-recovery primer, 1U Q5 Hot-Start High-Fidelity polymerase (NEB M0493), 1x EvaGreen intercalating dye (Biotium), and 10µL column-purified CSR product template. PCR duplicates were prepared for each sample. Reactions were incubated in a Bio-Rad CFX96 real-time thermal cycler with initial denaturation at 98°C for 30 seconds and cycled at (98°C for 10 seconds, 66°C for 30 seconds, 72°C for 30 seconds) repeatedly until sufficient yield was observed (roughly 2000 RFUs or more) (about 15 cycles), then stopped before reactions entered plateau phase. Reactions were purified using an Invitrogen PureLink PCR Purification Kit following the manufacturer's recommended instructions.

Following PCR amplification with the AmpliconEZ-adapter-tagged primers, purified PCR products were submitted for Illumina sequencing via the AmpliconEZ service offered through Genewiz, which provides >50,000 (in our experience, roughly 200,000) 2x250bp reads. Paired reads from each sample were merged in Geneious Prime (Biomatters) and aligned to a reference barcoded plasmid sequence (barcode in reference represented as `WWWNNNNNNNNNNNNNNNNNNNNNNN`). Bases aligning to the reference barcode were extracted and filtered for length = 27 bases. The number of barcodes containing WT (`AAA`) or XX (`TTT`) tags were counted in Microsoft Excel.

5.3.6.2 Real Library Sequencing

For the column-purified original and grown plasmid libraries, 50µL PCR reactions were prepared with 1x Q5 reaction buffer, 0.2mM each dNTPs, 500nM forward adapter-recovery-CSR primer, 500nM reverse adapter-recovery-CSR primer, 1U Q5 Hot-Start High-Fidelity polymerase (NEB M0493), and 10ng plasmid library template. PCR duplicates were prepared for each sample. Reactions were incubated in a Bio-Rad T100 thermal cycler with initial denaturation at 98°C for 30 seconds, 5 cycles of (98°C for 10 seconds, 72°C for 40 seconds), final extension at 72°C for 2 minutes, then 4°C hold. Reactions were stored at -20°C before being purified with Ampure XP beads (Beckman Coulter) (1x beads:sample ratio, washed twice with 80% ethanol, and eluted in 10µL water).

For the column-purified CSR product library, 50µL PCR reactions were prepared with 1x Q5 reaction buffer, 0.2mM each dNTPs, 500nM forward adapter-recovery primer, 500nM reverse adapter-recovery primer, 1U Q5 Hot-Start High-Fidelity polymerase (NEB M0493), and 10µL column-purified CSR product template. PCR duplicates were prepared for each sample. Reactions were incubated in a Bio-Rad T100 thermal cycler with initial denaturation at 98°C for 30 seconds, 5 cycles of (98°C for 10 seconds, 66°C for 30 seconds, 72°C for 10 seconds), final extension at 72°C for 2 minutes, then 4°C hold. Reactions were

stored at -20°C before being purified with Ampure XP beads (Beckman Coulter) (1x beads:sample ratio, washed twice with 80% ethanol, and eluted in 10µL water).

Following the above PCR reactions to add adapters to the plasmid and CSR product libraries, a second PCR was performed to add Illumina cluster-generating sequences and indexes for multiplexing to each sample. 50µL PCR reactions were prepared with 1x Q5 High Fidelity master mix (NEB M0492), 500nM forward index-adapter primer, 500nM reverse index-adapter primer, 0.5x SYBR Green I, and 5µL of the above PCR products (note: original and grown plasmid libraries were first diluted 1:2, CSR product libraries were first diluted 1:20, CSR+heat and CSR+GuSCN product libraries were not diluted). Reactions were incubated in a Bio-Rad CFX96 real-time thermal cycler with initial denaturation at 98°C for 30 seconds and cycled at (98°C for 10 seconds, 70°C for 30 seconds, 72°C for 10 seconds) repeatedly until sufficient yield was observed (roughly 3000 RFUs or more) (10 cycles for original and grown plasmid libraries, 6 cycles for CSR product libraries, 15 cycles for CSR+heat and CSR+GuSCN product libraries), then stopped before reactions entered plateau phase.

PCR products were then mixed with 6x purple loading dye (NEB B7024A) and run on a 1% agarose in TBE gel for 60min at 100V. The 315bp product bands were excised and purified using Bio-Rad Freeze 'N Squeeze DNA Gel Extraction Spin Columns following the recommended instructions (note: for CSR+heat and CSR+GuSCN samples, the freeze step was accidentally skipped, but yields were still acceptable). The samples were further purified using Zymo Clean & Concentrator columns to remove the purple loading dye. Final product yields were quantified using a Qubit High Sensitivity (HS) dsDNA Assay kit and the products were immediately pooled at equimolar concentrations into a final sequencing library.

The sequencing library was prepared for sequencing with a NextSeq 1000/2000 P2 Reagents (100 Cycles) v3 kit (Illumina product number 20046811). The pooled library was prepared for sequencing following the recommended instructions, with a 12.5% PhiX DNA control spiked in. Custom read primers

for barcode and index sequences were used (**Figure 11**). Barcodes were sequenced with 26 cycles per read and indexes were sequenced with 9 cycles per read.

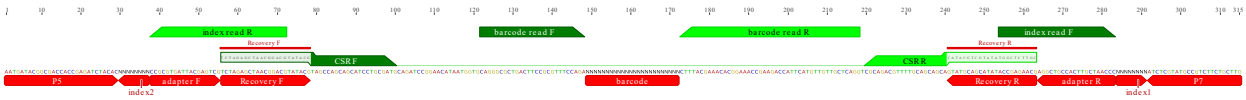

Figure 11. Amplicon design for Illumina sequencing. *Adapter sequences are added in initial PCR and serve as binding sites for secondary PCR. Secondary PCR adds index sequences (unique combinations of which are used to identify samples in the multiplexed pool) and P5/P7 cluster-generating sequences. Custom read primers for barcode and index sequences are used to begin sequencing directly at regions of interest, thereby minimizing the number of sequencing cycles required (which decreases kit cost and increases read accuracy).*

Following Illumina sequencing, custom scripts were used to count the number of occurrences per demultiplexed sample of every variant present in the previously subassembled barcode-variant map. First, barcode reads were converted to FASTQ format and demultiplexed using the bcl2fastq (v2.20) tool from Illumina. Then, forward and reverse barcode reads were paired and merged using PEAR[94] (v0.9.11) and the number of paired reads for each unique barcode was counted. Barcodes were then mapped to known variants based on the barcode-variant map from PacBio sequencing and pooled by variant. Barcodes associated with insertions or multiple mutations were excluded from analysis. To reduce counting noise error, we removed variants with a frequency lower than 10^{-6} and variants that were present in less than two experimental replicates.

5.3.7 Variant Scoring

Barcodes were pooled by variant to create a total read count for each variant in each library. Variants were then scored with the same formula used by Enrich2[95] for two-timepoint selections. A pseudo-count of 0.5 reads per variant was added to prevent divide-by-zero errors. Variants were then scored by dividing variant counts by wild-type counts to generate a WT-normalized variant frequency, calculating enrichment of this frequency by dividing the post-selection value by the pre-selection value, taking the

natural logarithm of this enrichment, and then averaging the resulting log-transformed enrichment across experimental replicates:

$$score = average_{replicates}(ln\left(\frac{count_{variant,post-selection} + 0.5}{count_{WT,post-selection} + 0.5} \div \frac{count_{variant,pre-selection} + 0.5}{count_{WT,pre-selection} + 0.5}\right))$$

The samples used to represent "pre-selection" and "post-selection" frequencies depend on the selection being discussed; as noted in Results, we observed that library growth and expression prior to CSR imposed a large selective pressure that enriched certain nonsense and missense variants relative to the original library. Thus, when discussing this growth effect, we represent the "pre-selection" sample as the original library and the "post-selection" sample as the grown library. Furthermore (to account for this growth effect), when discussing CSR selections, we represent the "pre-selection" sample as the grown library and the "post-selection" sample as the CSR products produced by a particular CSR screen (which may be CSR with no additional selective pressures, CSR preceded by a 100C 10min heat-kill step, CSR with 100mM GuSCN in the aqueous phase).

5.3.8 Variant Polymerase Characterization

5.3.8.1 Plasmid Construction

For single-mutant variants, TFO-WT in 2B-T plasmid was mutated using a Q5 site-directed mutagenesis kit (New England Biolabs E0554) following the manufacturer-recommended protocol. For multi-mutant variants, TFO coding sequences containing the desired mutations and 35-base flanks homologous to the linearized plasmid backbone were ordered as gBlock dsDNA fragments (Integrated DNA Technologies) and cloned into 2B-T plasmid (Addgene plasmid #29666) using NEBuilder HiFi DNA Assembly Master Mix (New England Biolabs E2621S) following the manufacturer-recommended recipe for assembling two dsDNA fragments (2:1 molar ratio of TFO insert to 2B-T vector, 0.015pmol total fragments, 1x NEBuilder master mix in 10µL reactions incubated at 50°C for 60 minutes followed by a 4°C hold). All TFO variants

(including TFO-WT plasmid as a positive control) were then transformed into T7 Express lysY/Iq *E. coli* cells (New England Biolabs C3013I), plated onto LB+agar+carbenicillin plates and grown overnight at 37°C.

5.3.8.2 Protein Production

For TFO-WT and TFO variant polymerase enzymes, the following medium-throughput protein production method was developed. Colonies were inoculated into 2.1mL LB broth with 100ug/mL carbenicillin (LB+carb) and grown overnight at 30°C, 250rpm. The following morning, 0.5mL culture was reserved for glycerol stocks, 1.5mL culture was reserved for plasmid purification and Sanger sequencing validation, and the remaining 100µL culture was subcultured into 10mL fresh LB+carb and grown at 37°C, 250rpm until OD600 reached 0.4-0.6, then induced with 0.4mM IPTG. Cells were further incubated for 2 hours at 37°C 250rpm. Cells were then pelleted at 5000g for 10 minutes, supernatant was discarded, and cell pellets were stored at -80°C.

TFO enzyme was purified from cell pellets via heat clarification followed by immobilized metal affinity chromatography using NEBExpress® Ni Spin Columns (New England Biolabs S1427S). Up to 0.1mL of cell pellet was transferred to a new tube and resuspended in 0.5mL lysis/binding buffer (20mM sodium phosphate, 300mM NaCl, pH 7.4) supplemented with 1mg lysozyme from chicken egg white (Millipore Sigma). Cell suspensions were then heated to 80°C for 10 minutes, then cell debris was pelleted at 12,000g for 15 minutes. Supernatant was then transferred to a new 2mL tube on ice. The manufacturer's instructions were then followed to prepare Ni Spin Columns, bind, wash, and elute protein. Elutions were pooled, dialyzed for 2 hours into 15mL 2x polymerase buffer base (20mM Tris-HCl, 200mM KCl, pH 7.5) in a Slide-A-Lyzer dialysis device with 20 kDa molecular weight cutoff (Thermo Scientific™ 88402), then dialyzed again into 15mL fresh 2x polymerase buffer base for 2 hours to overnight. After dialysis, polymerase sample was diluted with an equal volume of glycerol and

supplemented with DTT and Triton X-100 to achieve a final 1x polymerase storage buffer consisting of 10mM Tris-HCl, 100mM KCl, 50% v/v glycerol, 2mM DTT, 0.1% v/v Triton X-100, pH 7.5.

Following purification, polymerase variant stocks were analyzed via SDS-PAGE to confirm purity and normalize concentrations to each other based on relative intensities of the target protein band (63.062kDa including polyhistidine tag and linker). Bst DNA Polymerase Large Fragment from New England Biolabs (product number M0275S, lot number 10044729, 0.077mg/mL, 67kDa, 1.16µM) was included as a quantitative standard.

TFO-WT and TFO-P460V stocks were concentrated enough to normalize to each other and use directly in the LAMP-based thermostability assay detailed below. However, all other TFO variants expressed more poorly than TFO-WT (especially the variants that combined 3 or more high-scoring mutations from the CSR+GuSCN screen) and were too dilute to use directly in LAMP. The altered charge properties of these variants may have caused a loss of solubility and expression yield. To correct for this, all TFO stocks were concentrated using Amicon centrifugal filters with 30kDa molecular weight cutoff (Millipore Sigma UFC203024) and normalized by mass once more via SDS-PAGE before being used in the LAMP-based GuSCN resistance assay.

5.3.8.3 Thermostability Activity Assay

25µL reactions were prepared each containing 1x Thermopol buffer (New England Biolabs B9004SVIAL), 2mM supplemental MgSO4 (New England Biolabs B1003SVIAL), 0.4mM each dNTPs, 1x GAPDH LAMP primer mix (prepared as described[57]), 1M betaine (Sigma Aldrich B0300), 1x EvaGreen intercalating dye (Biotium 31000), 20pg GAPDH dsDNA template (Integrated DNA Technologies gBlock with sequence as described[57]), and 0.087µg TFO polymerase variant. To prevent polymerase activity during reaction setup, master mix containing all reagents except polymerase was first prepared at room temperature and added to individual reaction tubes. 2.5µL of TFO polymerase (0.035mg/mL) was added to the lid of

each tube, then tubes were closed and simultaneously spun on a minicentrifuge and vortexed before quickly being transferred to a pre-heated Bio-Rad CFX96 real-time PCR thermal cycler. Reactions were incubated at 68°C for 1 hour with plate reads taken every 30 seconds.

5.3.8.4 Guanidinium Thiocyanate Resistance Activity Assay

10µL reactions were prepared each containing 1x Thermopol buffer (New England Biolabs B9004SVIAL), 2mM supplemental MgSO4 (New England Biolabs B1003SVIAL), 0.4mM each dNTPs, 1x GAPDH LAMP primer mix (prepared as described[57]), 1M betaine (Sigma Aldrich B0300), 1x EvaGreen intercalating dye (Biotium 31000), varying concentrations of GuSCN (Sigma-Aldrich 50983), 8pg GAPDH dsDNA template (Integrated DNA Technologies gBlock with sequence as described[57]), and 0.048µg TFO polymerase variant. To prevent polymerase activity and denaturation during reaction setup, master mix containing all reagents except polymerase was first prepared at room temperature and added to individual reaction tubes. 2µL of TFO polymerase (0.024mg/mL) was added to the lid of each tube, then tubes were closed and simultaneously spun on a minicentrifuge and vortexed before quickly being transferred to a pre-heated Bio-Rad CFX96 real-time PCR thermal cycler. Reactions were incubated at 68°C for 250 minutes with plate reads taken every 30 seconds.

5.4 Results and Discussion

5.4.1 Wild-Type Thin Fingers Polymerase Exhibits Sufficient Resistance to Heat and Guanidinium to Enable Screening

A polymerase for the proposed CSR-DMS screen should be able to withstand thermal cycling, retain at least some baseline activity in harsh chemistries used as selective pressures, and ideally exhibit some pre-existing traits useful for downstream applications. The most important trait is thermostability (TS), which is essential to any PCR-based workflow, including CSR. TS ensures that a polymerase will not denature during the melting steps of PCR and is also handy in direct amplification workflows in which

heat is used to lyse cells and virions. Also important is strand-displacement (SD) activity, as virtually all isothermal amplification mechanisms used in nucleic acid diagnostics, including LAMP[4], require a polymerase that extends through double-stranded DNA and displaces competing strands. Reverse transcription (RT) is also essential for the detection of RNA targets. While some DNA polymerases possess RT activity, most are not sufficiently sensitive against RNA targets, and must be combined with a separate reverse transcriptase to kick off amplification. As we will focus our work on a single enzyme, we will use a polymerase with sufficient RT activity to act alone on RNA targets. Finally, because we wish to use guanidinium-induced denaturation as an example selective pressure, some baseline guanidinium resistance (GR) is important to resolve the effect of stabilizing and destabilizing mutations.

No known polymerases possess all four properties (TS, SD, RT, and GR) required for our approach, to our knowledge. *Bst* 3.0[6] and OmniAmp[96] polymerases have RT and SD but lack sufficient TS for thermal cycling. A Klentaq-Bst chimera (v5.9[57]) exhibits strong SD and TS, but its RT activity is unknown and its parent enzymes do not perform RT. GR is not typically determined for polymerases because most workflows are not designed to intentionally include guanidinium during amplification.

We conducted activity assays on wild-type Thin Fingers polymerase ("TF-WT") to determine its baseline TS, SD, RT, and GR (**Figure 12**). These assays revealed that TF-WT possesses sufficient activity in each category to enable CSR-DMS and future applications in POC NAATs. Notably, it retains activity after at least 35 PCR cycles and in the presence of 10mM GuSCN (100mM GuSCN without thermal cycling). Because 100mM GuSCN allowed (delayed) polymerase activity at 68°C, but not under repeated thermal cycling, we reasoned that 100mM GuSCN would be a viable level for an inhibitory but not overly harsh selective pressure via CSR-DMS.

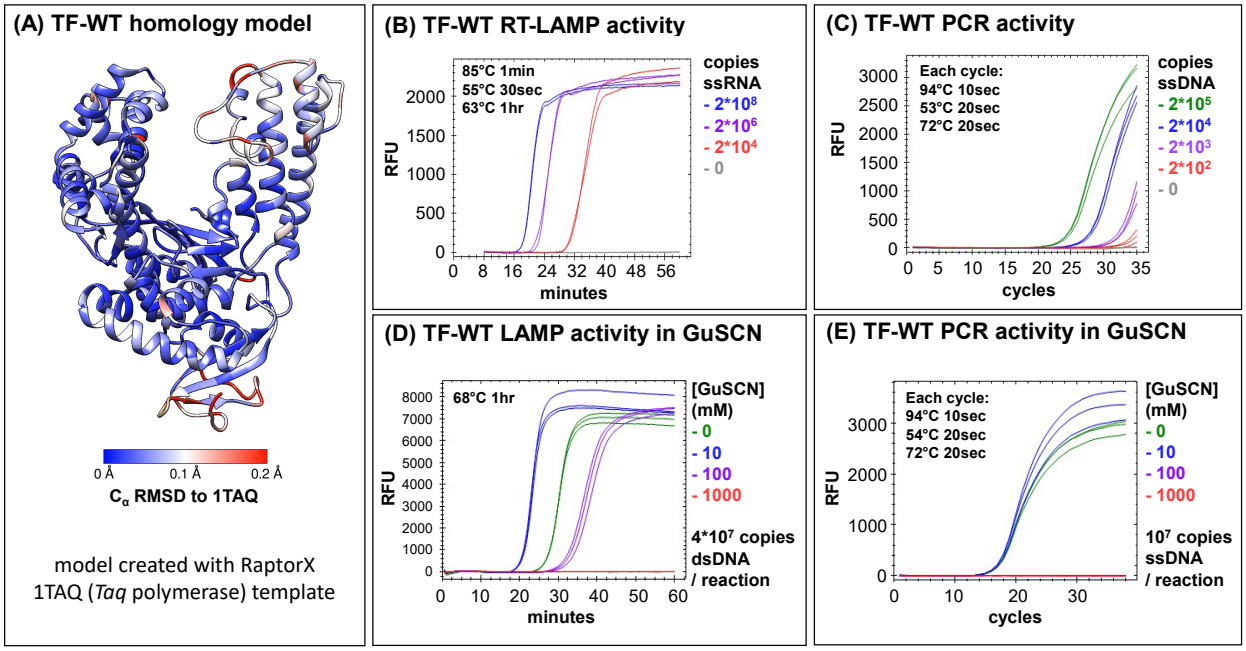

Figure 12. TF polymerase, a novel polymerase useful for RNA diagnostics. *(A) Homology model of TF-WT, generated with RaptorX[97] using 1TAQ[98] (Taq polymerase) as a template. TF-WT has 83.5% sequence identity to 1TAQ. Structural alignment with 1TAQ performed in UCSF Chimera[99]. (B) RT-LAMP with TF-WT demonstrates RT and SD capability. (C) PCR with TF-WT demonstrates TS capability. (D) TF-WT LAMP activity peaks near 10mM GuSCN, then decreases until undetectable at 1M. No-template controls (NTCs) (not shown) did not amplify for >90 minutes. (E) TF-WT PCR activity is inhibited by 100mM and 1M GuSCN. NTCs (not shown) did not amplify. The combination of thermal cycling and GuSCN has a strong denaturing effect, which presents barriers for PCR diagnostics, but we may exploit this as a selective pressure.*

5.4.2 CSR-DMS Design Uses Barcodes to Identify Polymerase Variants

CSR has previously been used to propagate polymerase genes through iterative rounds of selection. This approach is necessary for the original purpose of CSR: to enrich a library for high-fitness variants so strongly that they can be identified through low-throughput random sampling and characterization of individual clones. However, targeting the coding sequence for amplification has drawbacks. Regions of interest for mutagenesis and CSR selection can be large (often spanning the entire polymerase coding sequence, which in our case is 1620 base pairs). PCR efficiency tends to drop with amplicon length, and this decline may be even steeper in CSR because polymerase enzyme and plasmid concentrations are poorly controlled. Low amplification efficiency during CSR could stifle enrichment of the most active variants and introduce noise if some amplicons stochastically fail to fully extend to opposing primer sites, while non-specific amplification could produce sequence-able “junk” amplicons that consume valuable sequencing reads. Furthermore, CSR amplicons longer than a few hundred bases cannot be

sequenced directly via Illumina sequencing[100] and must be either tiled or fragmented to fit within the maximum read length (an approach that can also mask variants with multiple mutations). Despite these incentives for a small CSR amplicon, we still desired a saturated variant library that explores the single-mutant sequence space for the full-length polymerase gene, because such a library could be multipurpose (useful for any selective pressure) and agnostic to the location of mutational hotspots (important for selective pressures based on denaturing conditions, under which stabilizing mutations may appear far from active sites).

In order to shorten CSR amplicon length without sacrificing our ability to search the full polymerase gene, we used a subassembly approach, in which random DNA barcodes are cloned into the plasmid library and associated with specific variants using long-read, high-fidelity PacBio sequencing. After generating this barcode-variant map, the barcode alone can be targeted for CSR amplification and sequencing (**Figure 13**). This approach allows for flexibility in CSR primer design (primers can be designed to target any desired site for barcoding and screened for favorable characteristics) and simplicity in amplicon sequencing (short reads are sufficient and sequencing errors are easy to identify).

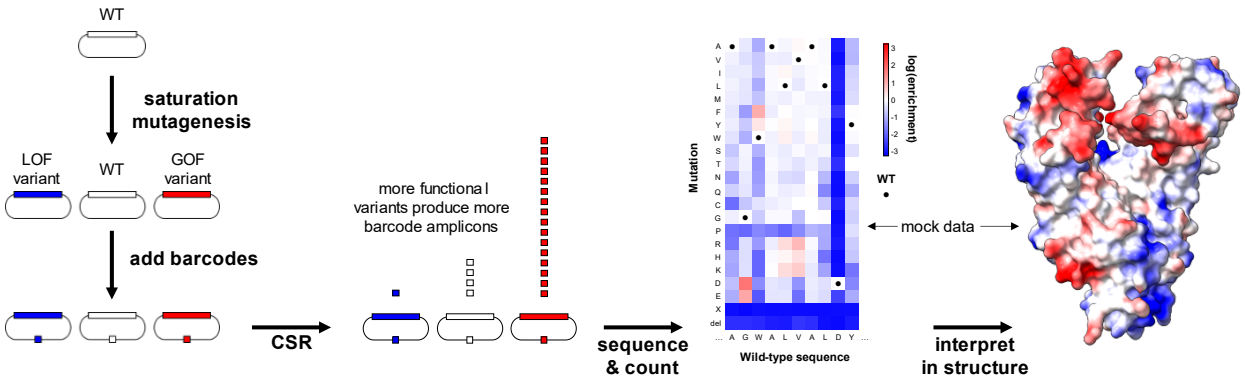

Figure 13. CSR-DMS workflow. *Wild-type polymerase sequence is mutated so every single-residue mutant is represented in library. This can be achieved with various saturation mutagenesis methods; we ordered a library from Twist Bioscience. Polymerase libraries are sampled, then subjected to CSR (**Figure #**), then sampled again. Polymerase variants (or barcodes) are sequenced, counted, and assigned a functional score based on enrichment across experimental replicates (normalized to WT score). Functional scores can be interpreted in the context of the polymerase structure and the scores of related variants to attempt to understand the biophysical mechanism by which mutations affect polymerase activity or stability.*

We screened several CSR primer designs *in vitro* in PCR conditions resembling CSR to identify a primer pair with short time to liftoff, robustness to annealing temperature gradients, generation of a single specific product with a consistent melt peak, high sensitivity and amplification efficiency against the plasmid template, and no or infrequent product in no-template controls. The primer pair that performed best overall across these screens was chosen as the site for plasmid barcoding (and CSR amplification in later experiments).

Careful preparation and sequencing of the barcoded library was necessary to ensure that the library represented nearly all single-mutant variants (roughly 10^4) with sufficient barcode-to-variant ratio (roughly 10x, for a barcoded variant library size of 10^5), and that a variant-to-barcode map could be generated using a PacBio Sequel II sequencing run with sufficient read count (a typical Sequel II run produces roughly 10^6 reads, allowing 10x coverage of each barcoded variant). PacBio sequencing confirmed that our library was successfully cloned and barcoded with the vast majority of single-amino-acid mutants represented, along with a subset of higher-order mutants (**Figure 14**).

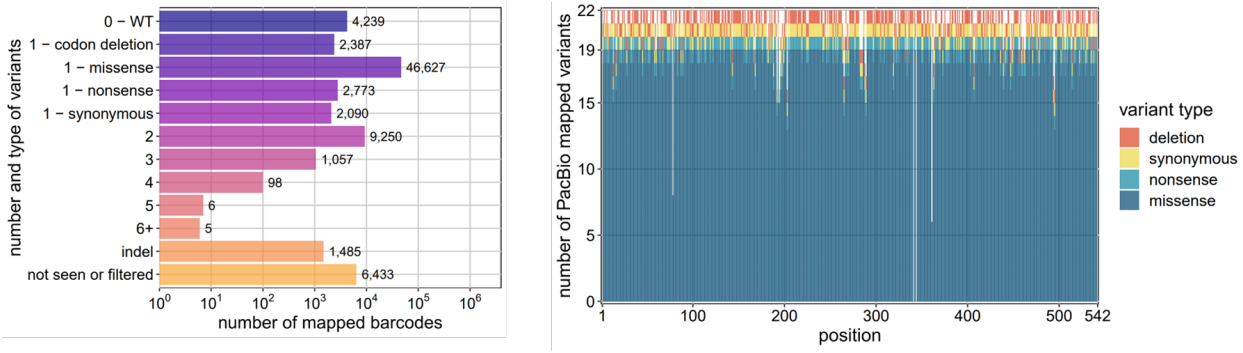

Figure 14. PacBio sequencing of barcoded library. *(LEFT) Number of mapped barcodes for different types of variants. (RIGHT) Variant coverage for all positions in the library. Nearly all single-mutant variants were represented in the barcode-variant map after quality filtering. Sites with poor variant representation generally corresponded to those with low yields in the original library synthesis (according to the QC report from Twist Bioscience – for example, sites 340 and 343 failed synthesis according to the QC report, and were likewise entirely missing from the barcode-variant map).*

5.4.3 Mock CSR-DMS Exhibits Strong Enrichment of Wild-Type Polymerase Over Inactive Variant

To validate that our CSR-DMS workflow could strongly enrich a library for active polymerase variants after a single round of selection, we ran several mock selections and made numerous changes to our protocols, primer, and library designs. Key changes include using a tissue homogenizer to finely control emulsification parameters, codon-optimizing the polymerase gene for *E. coli* B expression and lower overall GC content, and switching to the barcode-only amplification approach described above. A more detailed discussion of this process is available in the Supporting Information. We eventually arrived at a workflow that could enrich the wild-type polymerase (TFO-WT) to overcome a >100-fold excess of inactive variant (TFO-XX) and dominate the library after a single round of selection (**Figure 15**).

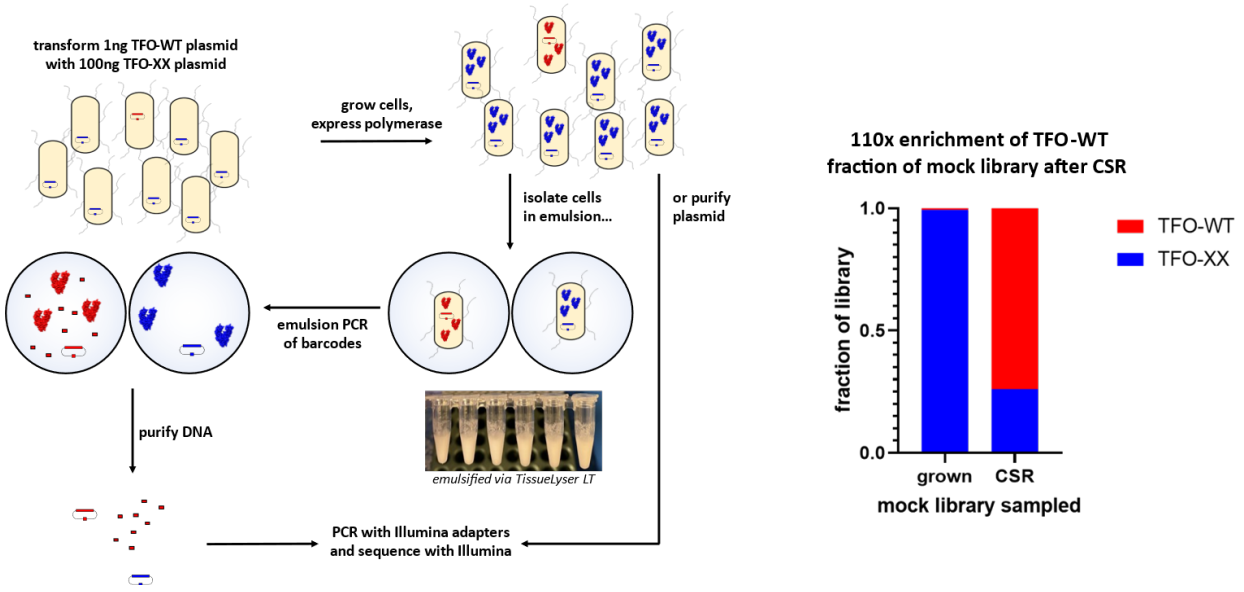

Figure 15. Mock CSR-DMS selection. *(LEFT) Workflow for mock selection. TFO-WT is co-cultured with a large excess of inactivated TFO-XX, then subjected to CSR amplification of barcodes (tagged AAA-24N for WT and TTT-24N for XX). The library is sampled before and after CSR and sequenced with the appropriate adapters. (RIGHT) Results of mock selection. TFO-WT is present in the grown (pre-CSR) library at roughly 0.67% (of total AAA and TTT tags). After CSR and recovery PCR, TFO-WT is represented at roughly 74% - an enrichment of 110-fold.*

We designed the TFO-XX variant to closely mimic wild-type (to control for metabolic burden on expressing cells), but with complete loss of catalytic activity. We targeted an aspartic acid residue

corresponding to Asp-610 in *Taq* polymerase; this residue has been shown to be essential for catalytic activity in a mutational scan of the *Taq* active site and is highly conserved across bacterial Family A polymerases[90]. The D318A mutation induced in TFO-XX was predicted (and later confirmed; see activity assay results below) to completely lose catalytic activity.

After a single round of CSR-DMS selection, TFO-WT enriched itself from 0.67% of a library otherwise dominated by TFO-XX (before selection) to roughly 74% (after selection) (enrichment roughly 110-fold). The enrichment demonstrated in this mock selection is comparable to other examples in literature where the wild-type polymerase overcomes a >100-fold excess of inactive variant after a single round of selection[55,57] and was deemed sufficient to proceed with CSR-DMS selections of a fully saturated library. Furthermore, the TFO WT vs. XX enrichment shown here can be used as a benchmark to judge whether future selections achieved comparable enrichment for active variants.

5.4.4 Differences in Variant Growth Prior to CSR-DMS Reveal Toxic Polymerase Domains

After validating our CSR-DMS approach in the mock selection, we proceeded with construction and screening of the barcoded TFO variant library. We ran three replicate CSR-DMS selections of the library. To identify and account for changes in variant frequency during cell growth and protein expression, we sequenced the original plasmid library (sampled before transformation into expressor cells) and each replicate's grown library (sampled after transformation, cell growth, and protein expression, immediately before CSR). We expected minor differences in variant frequency in the grown libraries relative to original, possibly due to sampling error during transformation or differential effects of each variant on host cell metabolism. In contrast, we observed a substantial increase in the frequency of some nonsense variants in the grown libraries relative to the original library. Interestingly, there was a sharp transition in growth enrichment for nonsense variants; nonsense mutations at sites from the N-terminus to codon 250 grew extremely well relative to all other variants, whereas nonsense mutations

at sites from codon 251 to the C-terminus generally grew slightly worse than or equivalent to the average variant. The bimodal distribution of nonsense mutants' enrichment during growth and expression suggests that polymerase expression is toxic to cells not just due to metabolic burden, but potentially due to a deleterious effect of the protein itself on host physiology. We hypothesize that Lys250 completes the formation of a nucleic acid binding domain, which could interfere with a number of processes including replication, transcription, or translation. Truncating proteins after Lys250 does not generally rescue cell growth and may even form catalytically dead polymerase fragments that are more toxic than full-length variants (which would also bind nucleic acids but at least retain functionality). This hypothesis is supported by the fact that Lys250 and nearby residues form part of the polymerase "thumb" domain, which is thought to bind dsDNA and play a role in processivity[101], and that certain missense variants in the thumb domain display similar enrichment during cell growth, suggesting that a loss of affinity for nucleic acids can partially reverse the toxicity of the thumb domain.

The stark difference in growth between certain nonsense variants and most other variants complicates CSR-DMS analysis, but also provides an opportunity for quality filtering. Nonsense variants increase from ~5% of the original library to ~60-70% of the grown libraries. This reduces read count of all other variants in the grown libraries, which can lead to increased noise, but also highlights the importance of using grown libraries rather than the original library as a baseline for variant frequencies prior to CSR. Furthermore, when examining distributions of individual barcodes, we noticed some outlier barcodes that increased in frequency during cell growth as if they were nonsense variants, even if they mapped to full-length polymerase variants and other barcodes for the same variants decreased in frequency during cell growth. We hypothesized that these barcodes mapped to clones with some defect that gave them nonsense-like growth and activity; they may have had plasmid backbone or host cell mutations that prevented polymerase expression, or may have actually been nonsense variants that were misassigned during subassembly. To avoid the skewed variant frequencies and enrichments caused by nonsense and

nonsense-like clones, we filtered out all barcodes with average enrichment greater than 2 during cell growth. Implementing this quality filter greatly reduced the noise of variant scores and enabled more accurate normalization of scores to WT-like activity.

5.4.5 CSR-DMS Produces Sequence-to-Function Map of Polymerase Activity

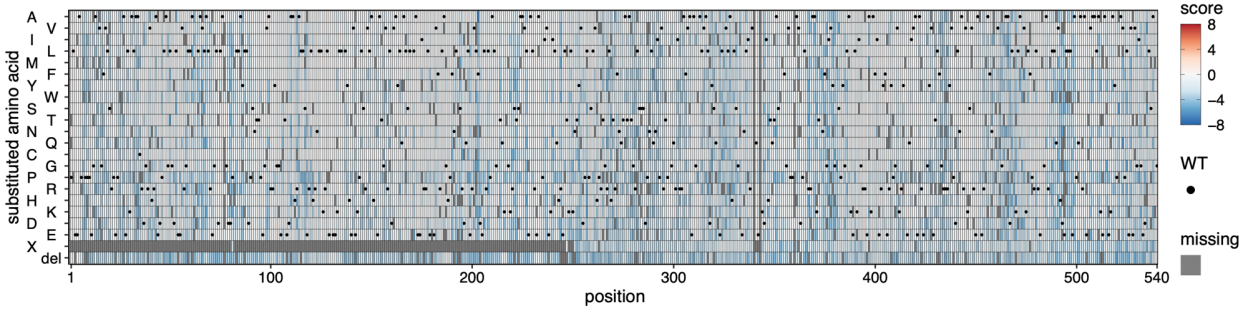

Figure 16. Sequence-to-function map of polymerase variant scores under CSR relative to grown library.

The sequence-to-function map of variant scores under CSR relative to the grown library (**Figure 16**) quantifies the relative abilities of polymerase variants to copy their own coding sequences in CSR with no additional selective pressure. Because CSR is essentially a form of PCR, the scores shown here are expected to correlate with PCR activity. Under our normalization method, a score near 0 connotes WT-like activity. Because wild-type TF polymerase already exhibits high PCR activity, we expected most variants to perform similar to or worse than WT, with few or none exhibiting a higher score. That expectation was upheld – essentially no variants outperformed WT, but loss-of-function mutations cluster distinctively in regions that contact dsDNA or perform other catalytic activities (such as the magnesium-coordination activity of D318).

The underlying mechanism by which PCR activity is affected may differ across variants. For a polymerase to be active in PCR, it must survive thermal cycling, bind to double-stranded DNA with high affinity, catalyze nucleotide addition at the 3' end of the extending strand, and move along the extending strand with high processivity. The role that each variant plays in affecting these processes may be inferred by examining the polymerase structure and its predicted interactions with a DNA template.

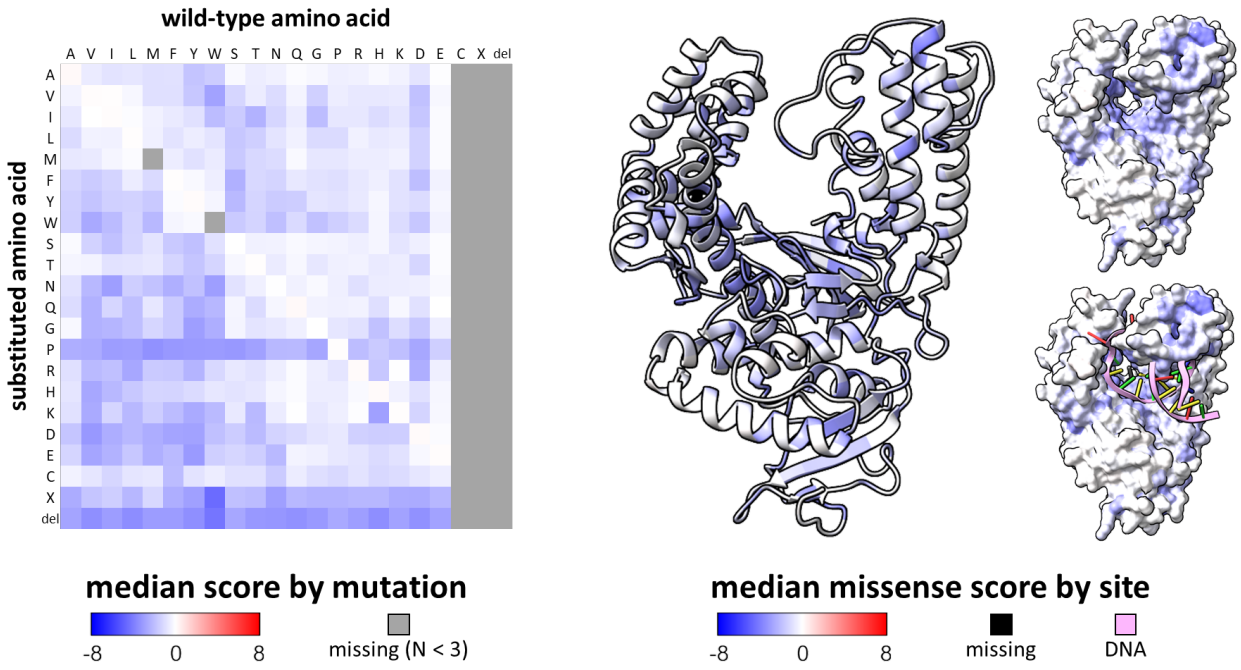

Figure 17. Median CSR scores highlight functional roles of residues. *(LEFT) Substitution matrix contains all possible residue-level mutations; scores represent the median CSR score of each mutation across all relevant sites. Diagonal represents median synonymous variant scores. Mutations with sample size N < 3 are omitted, including mutations from cysteine (only one cysteine is present in the WT sequence), synonymous mutations to methionine and tryptophan (these amino acids are encoded by one codon each, thus synonymous variants do not exist), and mutations from stop codons or deletions (not present in the WT sequence). (RIGHT) Median missense scores at each site mapped to polymerase homology model. Cartoon and surface models of the polymerase are shown. Model with DNA has been structurally aligned to a crystal structure[102] of Taq polymerase bound to DNA (PDB reference 3RTV); only the DNA backbone (pink) and base cartoons are shown.*

Figure 17 shows a substitution matrix of median CSR scores by type of mutation and models of TFpol polymerase colored by median CSR scores of missense variants at each site. The substitution matrix confirms that amino acid substitutions with similar chemistries are generally more tolerable than substitutions that change chemistries (for example, the aromatic side chains phenylalanine (F), tyrosine (Y), and tryptophan (W) generally tolerate mutations to each other better than mutations to non-aromatic side chains). Missense mutation scores mapped to the structure reveal that missense mutations are less favorable in the hydrophobic core, the enzyme active site, and where contacts are made with DNA, compared to the protein exterior, where missense mutations are generally well-tolerated. These results validate the ability of CSR-DMS to probe variants for activity, as the median scores generally align with expectations that residues involved in DNA binding and extension are less

mutable than residues on the surface (which are expected to contribute mainly to solubility and proper folding).

5.4.6 CSR-DMS Tolerates Additional Selective Pressures to Identify Stabilized Variants

In addition to the CSR-only selective pressure discussed above, our selections incorporated two more CSR conditions with additional selective pressures: a screen for thermostability by heating emulsions to 100°C for 10min immediately prior to thermal cycling, and a screen for guanidinium resistance by including 100mM GuSCN in the emulsion aqueous phase.

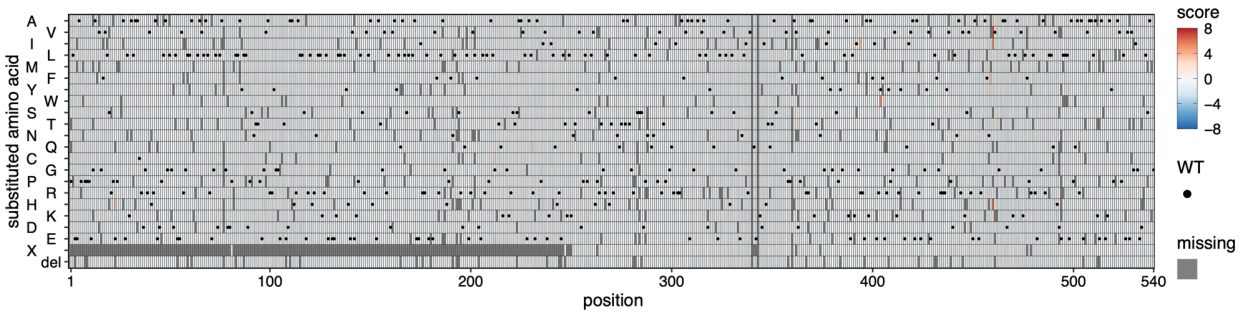

Figure 18. Sequence-to-function map of polymerase variant scores under CSR, preceded by a 10min 100°C heat-kill, relative to grown library.

Figure 18 shows a heatmap of variant scores under the thermostability screen. This screen appeared to kill polymerase activity for nearly the entire library, as evidenced by the lack of enrichment for most variants. However, some missense variants scored highly with obvious trends or putative stabilizing interactions. **Figure 19** shows the four sites in the wild-type structure with the highest-scoring variants.

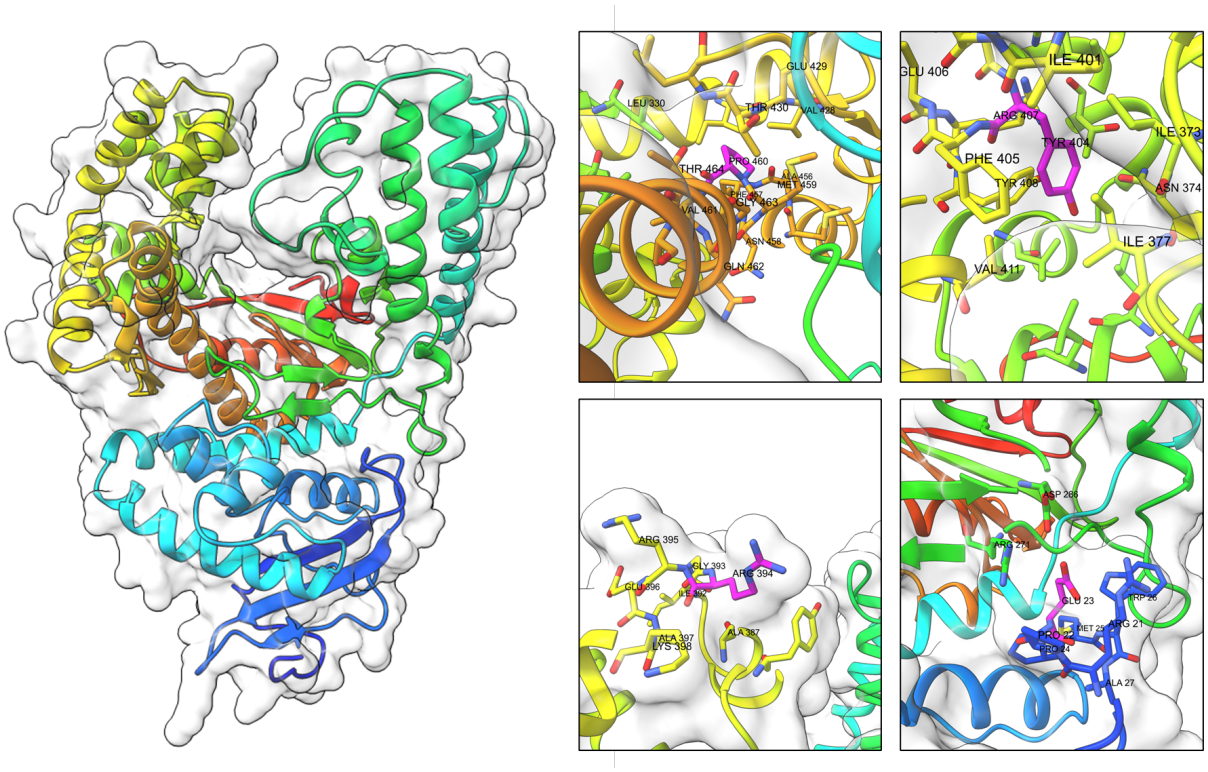

Figure 19. Residues favored for mutation under thermostability screen. *Clockwise from top left: P460 (favored for mutation to various residues, mostly hydrophobic), Y404 (favored for mutation to other aromatic residues, tryptophan and phenylalanine, which lack the polar phenol group of tyrosine), E23 (favored for mutation to histidine, which may form a hydrogen bond with the backbone carboxyl group of H269 and thereby prevent unfolding at the interface between the palm and thumb domains), R394 (favored for mutation to hydrophobic residues, which may prevent an undesired interaction in a partially unfolded state, potentially with Y404).*

P460 appears to disrupt an alpha helix in the fingers domain of the WT polymerase. Several missense variants at this site score well, especially small hydrophobic residues like valine, isoleucine, and alanine, but also histidine. Proline is known to disrupt alpha helices[103] and it is likely that missense variants are favored here to prevent disruption of the helix (and ideally pack well into the hydrophobic core or form bonds with nearby residues). Y404W and Y404F also score highly. Tyrosine, tryptophan, and phenylalanine are similar in that they all have large aromatic side chains and contribute to stability of the fingers domain by packing into the hydrophobic core and possibly aromatic stacking with F405. However, the phenol group of tyrosine enables polar interactions with water that may stabilize a partially unfolded state. Mutations to other aromatic side chains at this site likely avoid undesirable interactions with water while maintaining interactions with nearby residues in the hydrophobic core.

R394I, R394L, and R394V score highly, but are perplexing because R394 appears on the surface of the fingers domain. It is possible that R394 forms an undesired salt bridge in a partially unfolded state. The proximity of R394 and Y404 suggests that the region of the fingers domain in which they reside is prone to denaturation, perhaps even due to an undesired interaction between R394 and Y404. E23H scores highly and may form a hydrogen bond that secures this loop in the palm domain to the base of the thumb domain at the backbone carboxyl group of H269. We have run molecular dynamics simulations of the wild-type polymerase at 335K and 373K (**Figure B4**) and are currently analyzing the behavior of P460, Y404, R394, and E23 in these simulations to further develop explanations of stabilizing mutations at these sites.

Overall, thermostability-conferring mutations appear to work through a variety of stabilizing mechanisms familiar to biophysicists. This is not entirely surprising – as heat affects all residues regardless of charge, hydrophobicity, or location, it can disrupt salt bridges, hydrophobic packing, and hydrogen bonding alike, and the diversity of disrupted interactions is matched by a diversity of stabilizing mutations. In this sense, heat is a useful selective pressure because it probes a large swath of sequence space and its effects are relatively easy to model when we try to rationalize the mechanism behind stabilizing mutations. In the case of CSR, heat is also an easy selective pressure to implement, as the system must already tolerate thermal cycling (though the severity of the pressure in future experiments should ideally be tuned to maximize the range of variant scores).

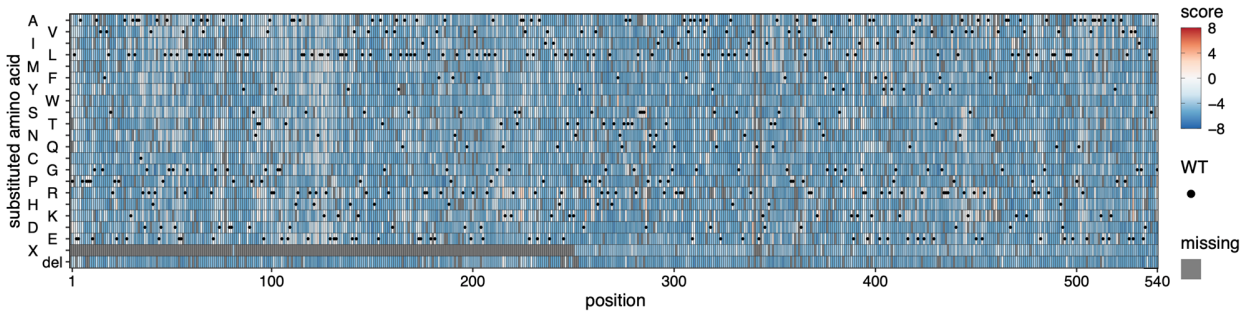

Figure 20. Sequence-to-function map of polymerase variant scores under CSR with 100mM GuSCN relative to grown library.

The guanidinium resistance screen differed from the thermostability screen in several ways. It displayed a wide range of enrichment values across the library (**Figure 20**), implying that 100mM GuSCN was a sufficiently gentle selective pressure to enable relative scoring for most variants (unlike the comparatively harsh thermostability screen), while still lowering activity significantly overall. Of note in the guanidinium resistance sequence-function map is an apparent benefit of mutations to positively charged residues, most notably arginine or lysine. Unlike the thermostability map, in which stabilizing mutations tend to cluster at individual sites, the guanidinium resistance map displays regions spanning several nearby sites where mutations to arginine and lysine are preferred. These sites are generally in the main DNA-binding cleft. We hypothesize that these are regions where guanidinium cations disrupt DNA binding and catalysis either by shielding the negatively charged phosphodiester backbone of DNA or by altering the electrostatic environment of catalytic sites such as the region of the palm domain surrounding D318 and E528. Mutations to positively charged side chains in these regions could compete with guanidinium cations for DNA binding and prevent guanidinium from interacting with catalytic sites.

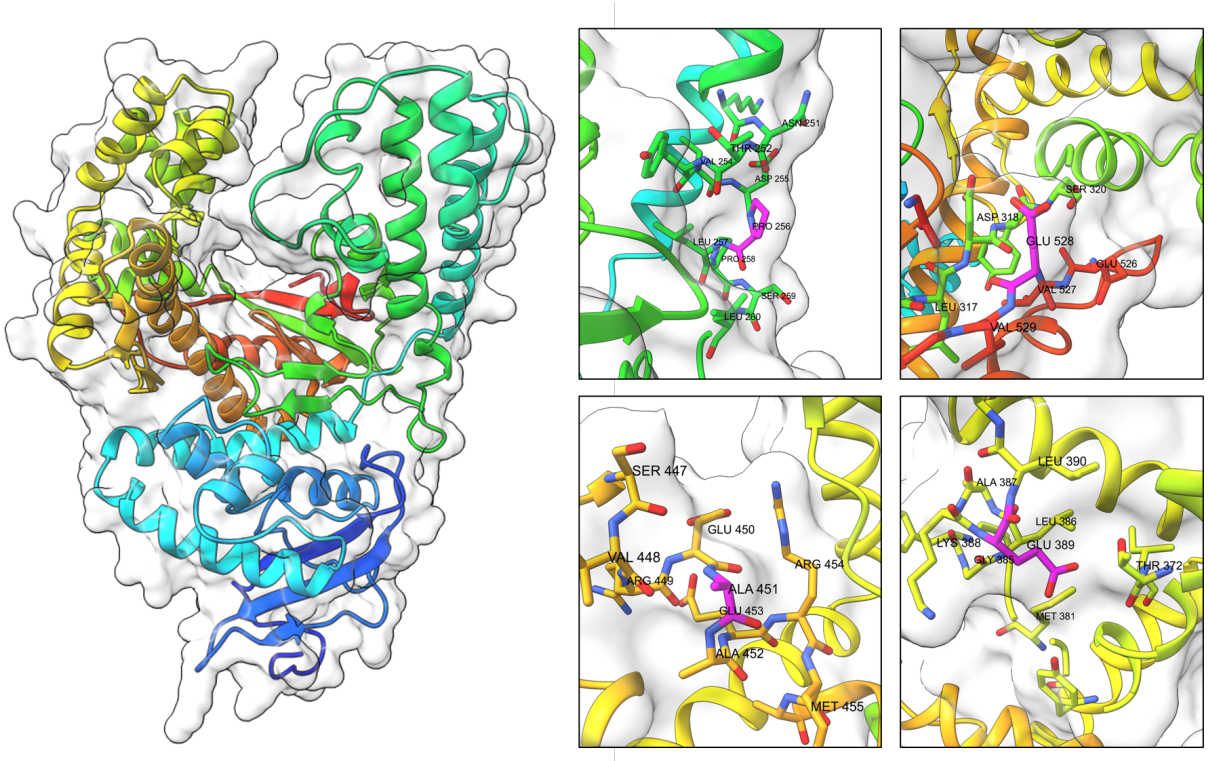

Figure 21. Residues favored for mutation under guanidinium resistance screen. *Clockwise from top left: P256 (favored for mutation to lysine or arginine), E528 (favored for mutation to histidine, lysine, or arginine), E389 (favored for mutation to arginine or various hydrophobic residues), A451 (favored for mutation to arginine). All sites are surface residues.*

The structural context of the highest-scoring variants in the guanidinium resistance screen support the notion that surface electrostatic interactions favor mutations to positively charged side chains. **Figure 21** shows the four sites in the wild-type structure with the highest-scoring variants. All four sites are surface-exposed residues in the DNA-binding cleft that score highly when mutated to arginine, histidine, or lysine. P256K is the highest-scoring variant in the selection and may also benefit from loss of a helix-breaking proline. E528H and E528K are the second- and third-highest-scoring variants, respectively, and are notable for their proximity to D318 and E526. The combined effect of these acidic side chains is a highly negative surface electrostatic potential near these sites in the wild-type polymerase. As previously noted, D318 coordinates two magnesium cations essential for catalysis[90]; the negative potential at this site may attract guanidinium cations and disrupt catalysis. It should be noted, however, that E528R and E528K score highly in the thermostability screen as well, which suggests a more general susceptibility of the site to denaturation (perhaps due to electrostatic repulsion between D318 and E528). A simple explanation for the favorability of positive side chains at site 528 could be formation of a stabilizing salt bridge with D318 (assuming catalytic activity is maintained), but this is not mutually exclusive with the possibility of additional resistance to guanidinium binding. A451R and E389R scored fourth- and fifth-highest respectively and similarly add positive charges to DNA-binding surfaces.

The overarching message of the guanidinium screen is that mutations to positively charged residues (or in some cases, mutations from negatively charged residues) at the protein surface confer some protection against guanidinium. This is useful knowledge especially because the mechanism by which guanidinium denatures proteins is contentious. Molecular dynamics simulations have invoked stacking with aromatic side chains[104], electrostatic interactions with charged side chains[105], and attenuation of the hydrophobic effect[106]. Guanidinium may act through several mechanisms, the relative strengths of

each depending on the protein in question. In the case of this DNA polymerase, it appears that electrostatic interactions are by far the most impactful, and surface charge engineering is a potentially effective way to counteract chaotropes if it can be done without disrupting interactions with the desired ligands. An interesting reinforcement of this idea was demonstrated by Paik et al.[107], who designed variants of *Bacillus stearothermophilus* DNA polymerase with fusion domains that had engineered positively charged mutations and found that (unlike the parent polymerase) these variants were active in 2M urea, a polar chaotrope that may also disrupt DNA binding.

Overall, the observation that charged surface residues play a strong role in mediating the effects of chemical denaturants serves as a confirmation of the validity of our scan results and of the utility of CSR-DMS overall. Unlike heat denaturation, which affects all atoms of the protein, chemical denaturation disproportionately affects surface residues because only they are in direct contact with solvent. It is therefore reasonable to expect that surface residues will be most sensitive to mutation in DMS with a chaotropic selective pressure, as we observed. The benefits of using a synthetic library saturated with single mutants at all sites is also apparent, as many of the highest-scoring mutations require multiple base changes per codon (which would be extremely rare under simpler mutagenesis methods such as error-prone PCR or doped oligonucleotide synthesis) and sensitive sites are widely distributed in both primary sequence and three-dimensional space. Unlike previous deep mutational scans that targeted the polymerase active site to identify residues that drive polymerase catalysis and substrate specificity[61,62], we needed a library spanning the entire coding sequence because the denaturing effects of heat and chaotropes are not necessarily limited to catalytic sites. A library that covers the entire coding sequence is also multi-purpose; it can easily be used to screen polymerases under various selective pressures with no need to target mutations to a specific region or category that is assumed to be most relevant to the selective pressure.

5.4.7 Activity Assays of High-Scoring Variants Validate CSR-DMS Predictions

To validate that CSR-DMS accurately identifies variants with improved activity under a selective pressure, and to quantify this improvement, we cloned some of the highest-scoring variants to test for activity and stability *in vitro*. We ordered site-directed mutagenesis primers to generate the top three highest-scoring single-mutant variants from the CSR+heat and CSR+GuSCN screens (excluding mutations that target the same site as a higher-scoring mutation, e.g. E528K which scores highly but not as highly as E528H). We also ordered synthetic dsDNA gene fragments that combined several of the highest-scoring single mutations from the CSR+heat and CSR+GuSCN screens into multi-mutant variants. These multi-mutants may resist denaturation better than any single mutant, as the effects of mutations may be additive or even synergistic, but there is also risk in combining several mutations in one variant because they may interact deleteriously with each other (e.g. P460V and M459F in the CSR+heat screen each scored highly in isolation but may rely on wild-type structural context that is altered when the two mutations are combined). Some of the high-scoring variants from the CSR+heat and CSR+GuSCN screens also appear to have partial loss of function relative to WT in the CSR-only screen; this may be minor for a single mutant, but combining such mutations may result in a dead enzyme. To maximize our chances of identifying highly stabilized multi-mutant variants and gain some inkling of the point of diminishing or deleterious returns when combining mutations, we aimed to test variants that combine the top three, five, or ten highest-scoring variants from the CSR+heat and CSR+GuSCN screens.

rationale	mutation(s)	CSR score	CSR error	CSR+heat score	CSR+heat error	CSR+GuSCN score	CSR+GuSCN error
TFO-WT control		0.00	N/A	0.00	N/A	0.00	N/A
TFO-XX control	D318A	-2.79	0.08	-0.80	0.08	-5.75	0.17
1st CSR+heat	P460V	-0.88	0.12	6.43	0.13	2.80	0.35
2nd CSR+heat	Y404W	-0.08	0.15	5.46	0.39	1.89	0.24
3rd CSR+heat	R394I	-0.09	0.13	3.85	0.91	2.30	0.43
Top 3 CSR+heat	P460V, Y404W, R394I	N/A	N/A	N/A	N/A	N/A	N/A
Top 5 CSR+heat	P460V, Y404W, R394I, E23H, M459F	N/A	N/A	N/A	N/A	N/A	N/A
Top 10 CSR+heat	P460V, Y404W, R394I, E23H, M459F, E528R, R231Q, K470F, G212C, F272W	N/A	N/A	N/A	N/A	N/A	N/A
1st CSR+GuSCN	P256K	-1.01	0.21	0.65	0.18	3.49	0.14
2nd CSR+GuSCN	E528H	-0.59	0.12	0.80	0.05	3.43	0.07
3rd CSR+GuSCN	A451R	-0.63	0.18	0.67	0.07	3.28	0.13
Top 3 CSR+GuSCN	P256K, E528H, A451R	N/A	N/A	N/A	N/A	N/A	N/A
Top 5 CSR+GuSCN	P256K, E528H, A451R, E389R, A224K	N/A	N/A	N/A	N/A	N/A	N/A
Top 10 CSR+GuSCN	P256K, E528H, A451R, E389R, A224K, V339D, R394L, D286H, T93R, F272W	N/A	N/A	N/A	N/A	N/A	N/A

Table 2. Variants designed for cloning and activity assays. *TFO-WT and TFO-XX (previously cloned for protein production and mock selection) included as positive and negative controls, respectively, for LAMP activity (without added heat or GuSCN). Single mutants were cloned via site-directed mutagenesis using mutagenic primers on a TFO-WT plasmid. Multi-mutants were cloned via Gibson assembly of synthetic dsDNA coding sequences into the linearized plasmid backbone.*

Table 2 summarizes the variants we cloned for activity assays and their respective CSR-DMS scores and standard errors (N=3 experimental replicates for all single-mutant variants). Unfortunately, after we cloned, expressed, and pelleted cultures with these variants, Sanger sequencing revealed that some variants had cloning errors that we did not have time to resolve. These variants were Y404W, Top3Heat, and Top5Heat (which had large deletions and therefore were not purified); R394I (which was multiclonal between R413 and R413Q and therefore not purified); and Top3GuSCN (which had an additional undesired L330F mutation – we chose to continue with purification and testing of this variant but named it "Top3*GuSCN" to denote the additional mutation). After purifying and normalizing enzyme stocks from the remaining variants, we evaluated their activity relative to WT and relative to their CSR-DMS scores in LAMP assays that impose gradient heat spikes prior to amplification or gradient concentrations of GuSCN included in the amplification mix.

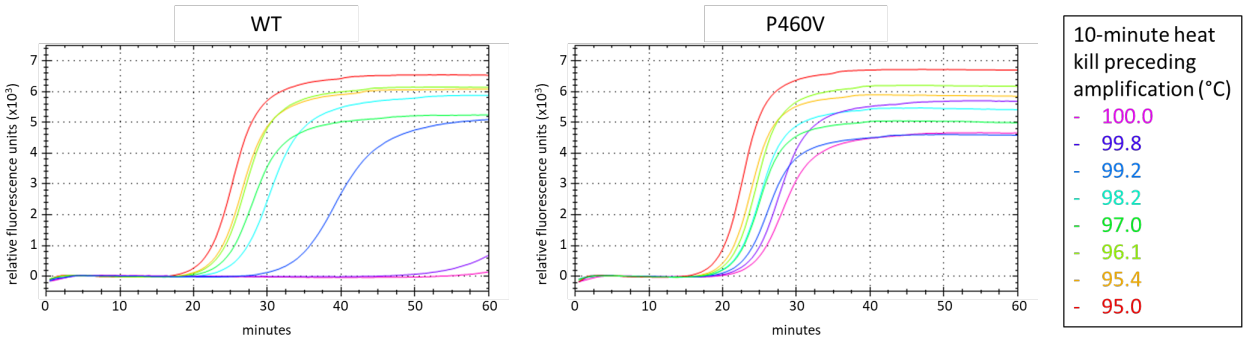

Figure 22. P460V variant is more thermostable than WT. *LAMP reactions were heat-killed for 10 minutes on a gradient from 95-100°C, then incubated at 68°C.*

Figure 22 demonstrates the relative thermostability of TFO-WT and TFO-P460V in LAMP reactions preceded by a 10-minute heat spike on a gradient from 95°C to 100°C. WT retains some activity after heating to these high temperatures (as expected due to its PCR activity), but is substantially denatured by heat-kill temperatures near 100°C, which delay liftoff from roughly 20 minutes to nearly 60 minutes.

P460V (the highest-scoring variant from the CSR+heat screen) is more resistant to heat-kill temperatures near 100°C, with liftoff delayed by less than 10 minutes. These results validate the prediction of the CSR+heat screen that P460V is substantially more thermostable than WT. Crucially, P460V does not appear to have lost any baseline activity, as demonstrated by its strong performance relative to WT even in the absence of a heat-kill step, as shown in the guanidinium resistance screen.

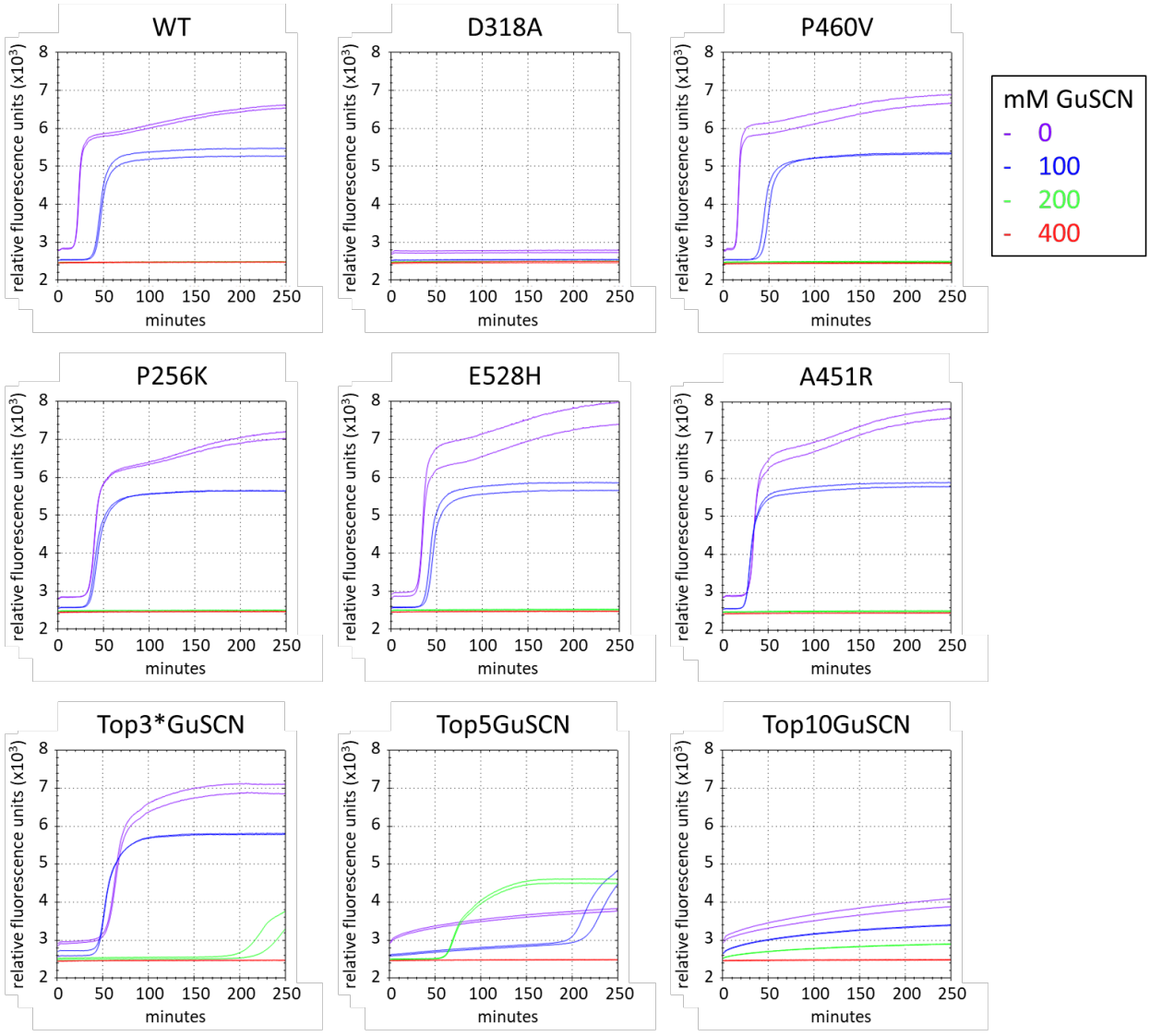

Figure 23. Top-scoring mutations from CSR+GuSCN screen increase GuSCN tolerance in TFO variants. *LAMP reactions containing final concentrations of 0, 100, 200, or 400mM GuSCN were incubated at 68°C. Total incubation time of 250 minutes is shown to demonstrate reactions with delayed liftoff. Fluorescence curves are not baseline subtracted to demonstrate non-specific activity of certain variants. TOP ROW: Control variants, including TFO-WT, TFO-D318A ("TFO-XX" from mock selection), and TFO-P460V (previously shown to have enhanced thermostability). MIDDLE ROW: Single-mutant TFO variants with the 3*

*highest-scoring mutations from the CSR+GuSCN screen. BOTTOM ROW: Multi-mutant TFO variants that combine the top 3, 5, or 10 highest-scoring mutations from the CSR+GuSCN screen (note: Top3*GuSCN additionally contains an undesired L330F mutation that was introduced during cloning, but could not be re-cloned due to time constraints. CSR scores predict this mutation to be slightly deleterious (average CSR score -1.42)).*

Figure 23 shows the resistance of all cloned TFO variants to various concentrations of GuSCN in LAMP. TFO-WT activity is delayed by 100mM GuSCN and killed by 200mM GuSCN (as expected from preliminary characterization of TF-WT). TFO-D318A ("TFO-XX" variant used in mock selection) shows no activity under any conditions, confirming loss of catalytic activity. P460V behaves similarly to WT, with slightly earlier liftoff than WT in the no-GuSCN condition (potentially related to thermostability in reaction or during storage), but no GuSCN tolerance to note. This was unexpected, as P460V scored quite highly in the CSR+GuSCN screen; it seems likely that P460V may have enriched well in this screen due to enhanced thermostability alone (which would still be important under the combined denaturing effect of GuSCN and thermal cycling).

The highest-scoring mutations from the CSR+GuSCN screen exhibit enhanced resistance to GuSCN (although sometimes at the cost of delayed or disrupted baseline activity). Each single-mutant variant is slower than WT in the no-GuSCN condition, but faster than WT in 100mM GuSN. Notably, A451R is faster in 100mM GuSCN than in no GuSCN. Multi-mutant variants exhibited a similar trend: as more top-scoring mutations from the CSR+GuSCN screen are built into the polymerase, optimal activity is shifted to conditions with increasing GuSCN, to the point that Top3*GuSCN performs best in a 100mM GuSCN environment and Top5GuSCN performs best in a 200mM GuSCN environment. These two variants are the only Thin Fingers variants we have yet tested that exhibit any activity in 200mM GuSCN. Also of note is significant non-specific activity exhibited by Top5GuSCN and Top10GuSCN. The amplification profile of this non-specific activity is atypical for conventional primer artifacts or non-specific priming (which typically exhibit an exponential curve similar to the target amplification). We suspect these polymerases may be prone to ab initio synthesis (in which DNA strands are spontaneously synthesized from free dNTPs) due to the drastically altered charge properties of these multi-mutant variants, which may bind

dNTPs with increased affinity. GuSCN may partially counteract this phenomenon by shielding free dNTPs, just as we suspect it shields the phosphodiester backbone of DNA strands.

The surprising result that some positively-charged variants perform better in the presence of certain GuSCN concentrations than with no GuSCN points to a rather fascinating scenario. Just as many polymerases that tolerate high temperatures ("thermostable") also exhibit optimal activity at high temperatures ("thermophilic"), these GuSCN-resistant variants are also GuSCN-"loving" or "guaniphilic" polymerases. The adaptations that polymerases make in the course of natural (or in this case, artificial) selection and evolution are rarely without tradeoffs. Building positive charges onto a polymerase's DNA binding surface to increase affinity to the negatively-charged DNA backbone does not necessarily translate to improved DNA replication activity because it could harm other important characteristics, such as affinity for the transition state during catalysis and processivity and translocation down the growing DNA strand. The presence of GuSCN may simply shift the optimal equilibrium of these traits to one that favors additional positive surface charges.

Overall, the enhanced activity of certain TFO variants in elevated GuSCN concentrations presents an exciting opportunity for point-of-care diagnostics with minimal sample preparation. As previously discussed, GuSCN (and guanidinium hydrochloride, GuHCl) at molar concentrations is a useful denaturant in sample lysis and denaturation buffers, as it can simultaneously free nucleic acids from cell membranes and virion capsids with also protecting them from nucleases in the sample, but it also inhibits polymerase activity at much lower concentrations and must therefore be removed through stringent sample purification or significantly diluted. Bender et al.[108] found that 4M GuHCl is necessary to completely inactivate ribonuclease activity from blood serum and note that a PCR that tolerates up to 50mM GuHCl would require 80-fold dilution of a denatured sample to reach tolerable levels, which could bring analyte concentrations unacceptably low. Our results suggest that the Top5GuSCN variant could enable a workflow in which a chemically denatured sample is diluted 20-fold (or less, depending

on the requisite GuSCN concentration) directly into a LAMP reaction mix without loss of polymerase activity. Other work currently undertaken by members of our group suggest that large-volume LAMP reactions up to 200µL can maintain the sensitivity and specificity of smaller, more conventional volumes. A 20-fold dilution factor for a denatured sample strikes us as within the realm of possibility for a point-of-care nucleic acid test.

5.5 Conclusions

CSR-DMS is a powerful method for polymerase screening that combines the high throughput and efficiency of compartmentalized self-replication with the comprehensive and quantitative resolution of deep mutational scanning. By fully exploring the single-mutant sequence space of a polymerase subjected to a selective pressure, CSR-DMS can identify functional variants after a single round of selection, with no need for iterated selections and random sampling of clones as is often done in conventional directed evolution. Furthermore, by returning information about negatively enriched variants, CSR-DMS can illuminate structures and sequence features that are most sensitive to a selective pressure, which is useful for identifying residues essential for activity or stability and understanding the mechanisms of selective pressures. While CSR-DMS suffers from some noise, as all high-throughput screens do, it also returns information that can be used to quantify noise (such as the distribution of synonymous or nonsense variant scores), which has not previously been examined for CSR. Trends from the sequence-function maps can also be used to increase confidence in variant scores (e.g. multiple high-scoring mutations with similar side-chain chemistries at the same site are more likely to represent real biophysical phenomena than isolated mutations with no contextual trend) and suggest general strategies for engineering proteins with increased fitness under a selective pressure.

In the context of our search for a guanidinium-resistant polymerase, this ability to identify trends is useful for many reasons. First, without knowledge of the general fitness landscape of the protein in

response to guanidinium thiocyanate, we might misinterpret some highly enriched variants to act through some local effect, such as stabilizing electrostatic interactions with nearby charged residues or DNA, rather than the general observation that positively charged surface residues at many sites appear to increase GuSCN resistance (which suggests an interaction with the denaturant itself). Second, we can now propose promising strategies for rational design of GuSCN-resistant proteins that are not limited to polymerases. This is particularly useful for diagnostics, where accessory enzymes may be used to support nucleic acid amplification (such as recombinases, helicases, or dedicated reverse transcriptases), but could also be used more generally in the design of orthogonal protein systems that are active in conditions that are too harsh for most proteins (analogous to many thermostable enzymes used today, but without the need for instrumentation).

CSR-DMS is not without drawbacks. Constructing the barcoded library and generating the barcode-variant map is both laborious and expensive, so it is most economical when the library can be used to study multiple selective pressures. The return for this initial investment is the wealth of DMS data returned and the relative ease of running single-round screens rather than multi-round directed evolution campaigns. However, to mitigate noise and increase the accuracy of variant scores, some experimental replication is likely necessary unless one is interested only in the highest-scoring variants. It may be possible to use the width of the synonymous variant distribution to roughly quantify noise in single-replicate screens and identify missense variants that fall above or below that noise as real effects, but ultimately experimental replicates are essential to quantify variant-level noise. Another drawback of CSR-DMS as described in this work is that it is limited to a single round of selection because barcodes alone are amplified, and polymerase coding sequences cannot be propagated through multiple rounds of selection. While it is tempting to consider re-designing the CSR-DMS primers to copy barcodes and coding sequences in a single amplicon, we caution that amplification efficiency (and therefore enrichment) would likely suffer due to the increased length of the amplicon and difficult secondary

structures of regulatory elements like promoters and terminators. A good way to simulate iterative rounds of selection with increasing selective pressures may be to run a range of selective pressures in a single experiment and calculate composite scores for variants based on a regression of the scores yielded by each value of the selective pressure. This method does not allow for increased diversification of the enriched library by gene shuffling or further mutagenesis, as is sometimes practiced between rounds of directed evolution[63], but if changes to the library are desired in light of knowledge uncovered by initial screens, it may be possible to perform site-directed mutagenesis on the barcoded library to effectively change the "wild-type" sequence to contain a desired single mutation without breaking the barcode-variant linkage previously established for other mutations.

Overall, the utility of CSR-DMS is evident in the staggering density of the information produced by our screens. CSR-DMS data is highly multi-dimensional; it can be compressed, transformed, and manipulated to tell many stories about the protein fitness landscape. With the proper care taken to avoid the pitfalls of noise and multiple hypothesis testing, CSR-DMS can be used to examine what a selective pressure does to a protein, where its effects localize, what kinds of residues or features are sensitive to it, and how its effects can be overcome. The power of this knowledge extends beyond the identification of solutions to a protein engineering problem and into true understanding of the question – a loftier but more worthwhile goal.

5.6 Acknowledgments

We thank Nuttada Panpradist for creating the lyophilized Covid-19 LAMP reaction mix. We thank Snehal Nariya, Raining Wang, Gabriel Boyle, and Sriram Pendyala for advice on DMS barcoding and sequencing.

5.6.1 Author Contributions

I.T.H. conceived and developed the overall plan for CSR-DMS and conducted experiments, analysis, and writing except where noted. N.A.P. contributed to CSR-DMS design and conducted PacBio subassembly,

Illumina sequencing, DMS quality control, and variant scoring. E.C.K. conducted TF-WT cloning and contributed to CSR-DMS design. R.L.P. and M.K.W. conducted library preparation for Illumina sequencing. M.C.C. assisted with homology modeling and molecular dynamics simulations. Q.W. assisted with the development of the protein purification workflow and activity assay analysis. V.D., D.M.F., and B.R.L. advised the project and reviewed the manuscript.

5.6.2 Funding

This work was supported by the National Institute of Allergy and Infectious Diseases of the National Institutes of Health (R21AI156017, R61AI140460, and R33AI140460) and by the National Human Genome Research Institute of the National Institutes of Health (RM1HG010461). The research was supported by the PRISM (Protein Interactions and Stability in Medicine and Genomics) center funded by the Novo Nordisk Foundation (NNF18OC0033950). I.T.H. was supported, in part, by the National Institute of General Medical Sciences of the National Institutes of Health under award number T32GM008268. N.A.P. was supported, in part, by the National Heart, Lung, and Blood Institute of the National Institutes of Health (F30HL151075).

5.6.3 Competing Interests

A patent application has been filed on Thin Fingers polymerase and a provisional patent application has been filed on CSR-DMS and polymerase variants resulting from this work. E.C.K. is an inventor on the US patent application for Thin Fingers polymerase. I.T.H., N.A.P., E.C.K., D.M.F., and B.R.L. are inventors on US provisional patent application 63/459,883, filed on April 17, 2023 by the University of Washington. I.T.H., E.C.K., Q.W., and B.R.L. hold equity in a startup company that has licensed Thin Fingers polymerase and supports ongoing work in the B.R.L. laboratory at the University of Washington; B.R.L. and E.C.K. serve as scientific advisors. The company played no role in the funding, study design, data analyses, or reporting of results for this study.

6 Conclusions and Future Directions

6.1 Efficacy of CSR-DMS

CSR-DMS improves upon the throughput of conventional CSR by ensuring that every variant is scored, not just a random sample of the most highly enriched variants. This enables a broader understanding of the effects of a selective pressure on the protein fitness landscape. Because there is some unavoidable noise in our screens, it is important to understand that individual variant scores are not necessarily trustworthy (depending on the measured error across experimental replicates and the observed spread of variants score with a known or expected value, such as synonymous or nonsense variants), but trends in the variant scores increase both confidence in and understanding of the mechanism by which a mutation affects fitness. For example, because several mutations at P460 score highly in the CSR+heat screen (a screen where most variants barely enrich relative to WT and signal-to-noise ratios are low), we can conclude that the variant scores at this site likely indicate a true gain of function, because random noise is extremely unlikely to favor so many variants at the same site. Furthermore, because several mutations at this site are positively enriched (not all of which have similar chemistries), we can conclude that the primary benefit of these mutations is a loss of a destabilizing proline rather than any stabilizing interactions formed by the new side chains. Contrast this with the abundance of mutations to positively charged side chains in the CSR+GuSCN screen with little apparent pattern in the wild-type residue, which suggests a beneficial effect of the new residues rather than a deleterious effect of the wild-type residues. If these mutations were identified through random, low-throughput sampling of a CSR-enriched library by cloning and Sanger sequencing, they would be much more difficult to interpret or trust without further experimental investigation.

One drawback of CSR-DMS as described here is that we only examined single-mutant variants. In our library construction and subassembly, we actually did generate multi-mutant variants (likely through

random mutagenesis during library synthesis, PCR, or cell growth) and assign barcodes to them. However, these variants are harder to score accurately due to their low abundance in the library, and harder to interpret because multiple mutations represent multiple variables with unresolved relative contributions and because similar variants that would be useful for identifying trends are rare due to the size of multi-mutant sequence space. For these reasons, we have not discussed them in our initial analysis, though we are looking into ways to score and investigate them.

If one wanted to screen multi-mutant variants intentionally, it should be relatively straightforward to generate the proper library using error-prone PCR (which uses a low-fidelity polymerase to randomly introduce DNA base changes) (this was used in the original CSR study)[55] or gene shuffling (which randomly recombines molecules from a library of single-mutant variants to generate multi-mutant variants)[109]. Either method could even use our saturated single-mutant variant library as a template to generate multi-mutant variants with good uniformity. While this uniformity helps to reduce noise and increase variant scoring accuracy (due to consistent barcode-variant ratios and sequencing depth), it does not change the reality that the library sequence space increases exponentially with each mutation (e.g. a 540-residue polymerase has roughly 10^4 single missense variants, 10^8 double missense variants, 10^{12} triple missense variants, and so on), such that each variant becomes far apart from any others in sequence space and trends remain hard to identify. Though it is tempting to think that one could scale CSR selections up to accommodate such throughput (1mL of *E. coli* culture at OD600=1 is nearly 10^9 cells), there are several other bottlenecks that limit the achievable library size, including transformation yields, sequencing depth, and even PCR sampling. In this project, the most significant limit on library size was PacBio sequencing capacity; a single PacBio Sequel II run typically produces ~10^6 HiFi reads, and ideally the library size is several times smaller than this so multiple reads per molecule can be used to generate a barcode-variant map (we used a minimum of 3 reads per barcode as a cutoff).

The sequencing constraints described above effectively limit the size of a CSR-DMS library to about 10^5 variants; this project screened a library of roughly 10^4 single-mutant variants and was still constrained by noise. For this reason, I would not recommend trying to push CSR-DMS library size too high; on the contrary, if one is interested in screening multi-mutant variants with a specific application in mind, sampling the entire sequence space may be futile, but a higher priority should be increasing the number of mutations per variant (even if coverage of that sequence space is low)[63] and limiting overall library size so there is more coverage per variant in selections and variant scores become more trustworthy.

6.2 Important Parameters for Validation, Maintenance, and Improvement of CSR-DMS Accuracy

Quantifying the noise of a CSR-DMS selection is essential for interpretation of variant scores. One way to do so is to calculate the standard error of variant scores across experimental replicates[95]. Another important sanity check, however, is to examine the distribution of variant scores by category of mutation. **Figure 24** shows such distributions for various library comparisons from our CSR-DMS screens. An important initial sanity check is that synonymous variants (which should have identical amino acid sequences and therefore identical polymerase activity) have scores very similar to WT. In our case, this was only true for most selections after we filtered out barcodes with grown/original enrichment > 2 (see Results and Discussion section of main polymerase chapter for justification). It also remains an issue with the CSR+heat libraries (probably because polymerase activity was so low in those selections that the distributions are dominated by cell growth effects), though trends in high-scoring missense variants are still apparent in heatmaps.

Second, the width of the synonymous variant score distribution is an important way to quantify inter-variant noise. While standard error calculations are a decent way to estimate the error in an individual variant's score across replicates (which should approach zero with an increasing number of replicates),

there are still factors that may affect the scores of different variants with identical polymerase activity, such as hidden genomic or backbone mutations that affect cell growth and polymerase expression, slight differences in transcription and translation for different codons, varying amplification efficiency for different barcodes, and sampling errors due to inadequate sequencing coverage. The synonymous variant distribution is a good way to resolve all these possible factors into a single range of "WT-like" activity. A missense variant may score above or below WT with seemingly low standard error, for example, but if it does not lie far from the center of the synonymous variant distribution, then it may in fact possess WT-like activity. This can even be quantified by expressing variant scores as a percentile of synonymous scores or by binning variants into "loss of function", "WT-like", or "gain of function" bins according to cutoffs defined by the synonymous variant distribution (e.g. a certain number of standard deviations above or below the mean synonymous variant). We see in the CSR+GuSCN libraries, for example, that the synonymous variant distributions are particularly wide, suggesting a high level of noise for those assays. While we are confident that the highest-scoring missense variants from those assays likely represent true biophysical phenomena (due to non-random trends in the fitness landscape), this noise makes it hard to trust the score for any single variant from these screens, and we are investigating ways to filter or bin these scores for various levels of confidence before publishing these results in a journal article.

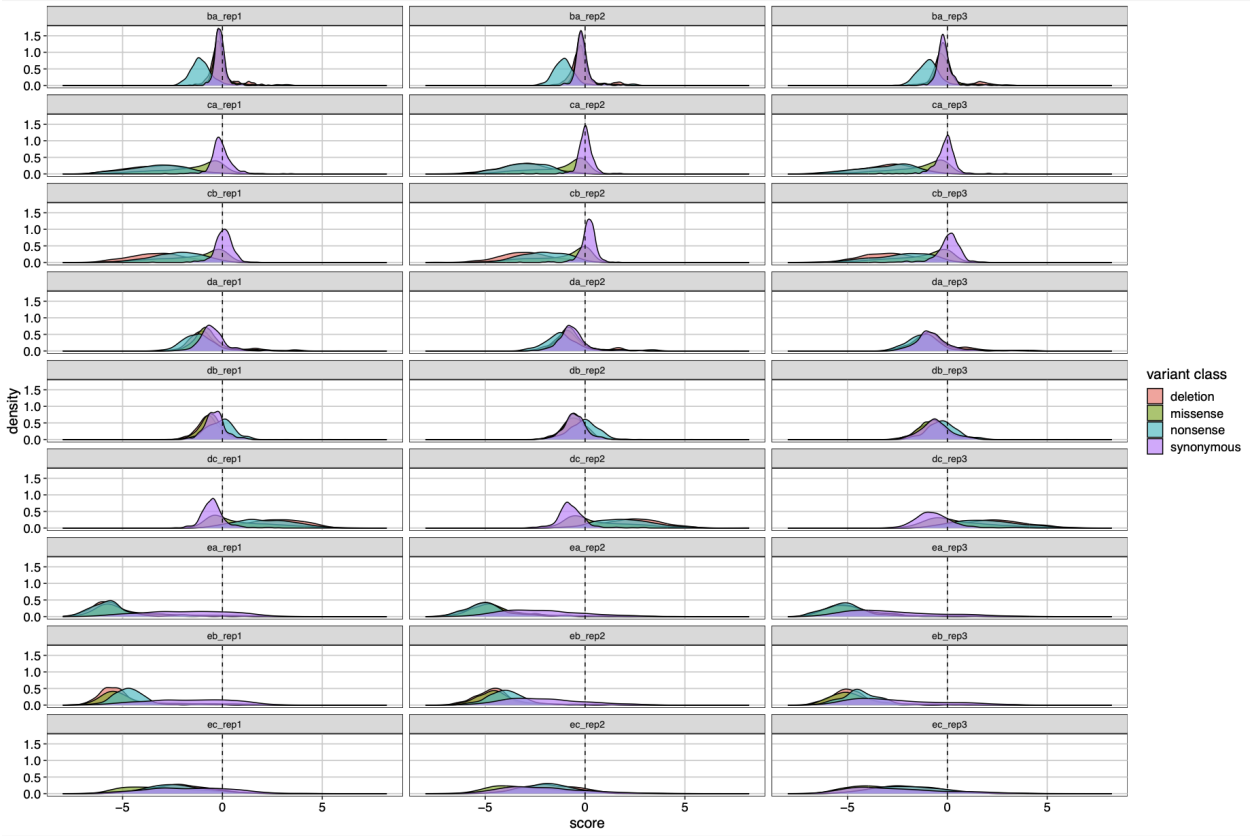

Figure 24. Distributions of variant scores at the level of mutational class. *(Barcodes with grown/original enrichment > 2 have been filtered out). A = original library, B = grown library, C = CSR library, D = CSR+heat library, E = CSR+GuSCN library. Plot titles represent comparisons of libraries for each experimental replicate (e.g. "cb_rep1" = variants scored by enrichment in CSR library relative to grown library in experimental replicate 1). Dotted line represents WT score (0 in all cases due to normalization).*

For future CSR-DMS experiments, an effective way to reduce noise would likely be to increase the barcode-variant ratio, so variants have higher coverage for a given number of transformants and noise can be evaluated at the barcode level (potentially even within a single experimental replicate). Our library was somewhat under-barcoded at roughly 4.5 barcodes per missense variant, which may have contributed to noise. An ideal library would have as many barcodes per variant as sequencing depth permits (in practice, 10-20 barcodes per variant is a good target). A higher barcode-variant ratio is useful for accurate scoring, but it also requires more sequencing depth, both in PacBio subassembly (a good target is 10 reads per barcode on average) and Illumina measurement of CSR libraries (a good target is 100 reads per barcode on average).

It is also important to choose selective pressure harshness wisely, otherwise one might fall into a regime where the pressure is so harsh that only a few missense variants enrich at all (as we experienced in our CSR+heat screen) – or, at the other end of the scale, the pressure is so gentle that enrichment barely changes relative to a CSR-only baseline and the selective pressure's effect is hard to differentiate from noise. For this project, selective pressures were chosen based on preliminary activity assays (in which we observed that TFO-WT tolerated 100mM GuSCN in LAMP, but not PCR, and that TFO-WT could tolerate a 10min heat spike with virtually no loss of activity for a gradient of temperatures 90-98°C but not at 100°C). Ideally, the selective pressure should be as harsh as possible (to maximize single-to-noise ratio of gain-of-function variants over WT-like variants) while still preserving a quantitative range of variant scores for all variants with at least some activity. In practice, this is nearly impossible to get right the first time, especially because selective pressures may act differently in CSR than in preliminary activity assays (for example, a 10 minute 100°C heat spike seemed harsher in CSR than in activity assays).

One of the best ways to both improve the accuracy of variant scoring and ensure that variant scores fall within a useful quantitative range is to run a titration of selective pressure harshness in the same experiment. For example, in the CSR+heat screen, it may have been best to run a temperature gradient for 10 minutes rather than just 100°C for 10 minutes. The best condition for in-depth analysis could be chosen retroactively after preliminary sequencing and scoring. Alternatively, the variant scores from each individual condition could be combined into a composite score by plotting scores against harshness of selective pressure and performing regression analysis (note that the best curve to fit to data might depend on the selective pressure, and there is no reason to expect it to be linear).

A final note is to ensure not to bottleneck the library at any point during library construction (beyond what is desired when barcoding to achieve the desired barcode-variant ratio) or selection. Assuming the subassembled library is a certain size, transformation yields should exceed that size by as much as possible (at least 10x), emulsions should contain several orders of magnitude more cells than barcodes

(relatively easy to achieve, as an *E. coli* culture at OD600 = 1 should be roughly 10^9 cells/mL), and all cloning and PCR steps should have large input masses to avoid sampling error. Sequencing and comparing PCR technical replicates is a good way to make sure that libraries were not bottlenecked or otherwise biased during post-selection sequencing preparation.

6.3 Adaptability of CSR-DMS

CSR-DMS should easily incorporate any selective pressure that has been previously demonstrated in a CSR study in the literature (as long as it still produces barcodes that can be sequenced). It should similarly be straightforward to incorporate any selective pressure that is compatible with emulsion PCR; most small molecules are probably allowable unless they react with emulsion oil phase or prematurely lyse cells. Some examples of selective pressures that are promising for incorporation into CSR-DMS are discussed in the next section.

Sequencing of CSR-DMS libraries does not necessarily need to have high coverage. For a sequence-function map that accurately quantifies variant scores over several orders of magnitude, sequencing depth is paramount, especially when interested in loss-of-function variants. For this reason we used an Illumina sequencing kit that would yield roughly 100-200 reads per barcode on average. However, if the priority is to identify the most functional variants, much lower read counts may be sufficient, as long as the most abundant variants are not subject to substantial sampling error. If variant frequencies in the original library are already established (as we have done for the TFO saturated variant library), these frequencies could potentially be used as inputs for calculation of variant enrichment in low-read-count CSR product libraries. This approach relies on an assumption that variant frequencies are relatively unchanged in the grown library (which would require high read counts to properly evaluate), an assumption that we know is false for some nonsense and missense variants, but these variants could be filtered out or ignored during downstream data analysis. The advantage of a low-read-count sequencing

approach is rapid turnaround time and low cost; some commercial services, such as the AmpliconEZ service offered by Genewiz, can return 200,000 reads per sample for $55 with a two-week turnaround at the time of writing.

6.4 Incorporating Novel Selective Pressures into CSR-DMS

6.4.1 Inhibitors (Beyond Guanidinium)

The simplest selective pressures to incorporate into CSR-DMS are likely small-molecule protein denaturants, such as urea or SDS, that can be added to the CSR aqueous phase just as we demonstrated with guanidinium thiocyanate. While GuSCN is a common denaturant in lysis buffers, especially for RNA diagnostics where RNase denaturation is needed, urea and surfactants like SDS are also frequently used in lysis buffers because they possess similar protein denaturant activity[110]. Urea and SDS are also similar to guanidinium in that they are model protein denaturants used in laboratory experiments such as unfolding experiments and denaturing gel electrophoresis[86].

Incorporating small-molecule denaturants into CSR is straightforward – simply add it to the aqueous phase – but requires validation to ensure that the denaturant does not prematurely lyse *E. coli* cells or break the emulsion at the specific concentration used for selection, as we demonstrated with 100mM GuSCN. The most direct way to validate cell and emulsion compartment integrity in the presence of a denaturant would be to examine an emulsion of GFP-expressing cells under a fluorescence microscope; fluorescent cells should be visible before thermal cycling, and compartment size should be 1-10µm before and after thermal cycling. A mock selection may also serve to validate enrichment of a known active variant against an inactive variant with denaturant present, but if this enrichment is worse than a no-denaturant control, it may be difficult to discern whether the denaturant is acting solely on polymerase activity (as desired) or introducing noise by breaking cell or emulsion integrity.

6.4.2 Reverse Transcription

Enzymes capable of reverse transcription (RT) are essential for RNA diagnostics and sequencing, but are typically distinct from DNA polymerases used to amplify the resulting complementary DNA (cDNA). This is because most dedicated reverse transcriptases lack the thermostability of and processivity of dedicated DNA polymerases[111], while many DNA polymerases have poor or absent RT activity[112]. Some polymerases used in diagnostics, such as Bst 3.0 or TF polymerase, have some inherent or inducible RT activity, but we have found that this activity is often slower or less sensitive than dedicated reverse transcriptases (this is why we combined WarmStart RTx with TF polymerase in Covid-19 diagnostics)[44,64].

However, there are major drawbacks to using dedicated reverse transcriptases. High prices for purchase and licensing of third-party enzymes contribute significantly to the costs of RNA diagnostics. Additionally, reverse transcriptases are often active and stable at temperatures lower than DNA polymerases used in diagnostics, which can complicate assay workflows and devices and introduce opportunities for non-specific products to form. Finally, an assay is only as robust as its weakest component, and our work to develop DNA polymerases with enhanced stability and chaotrope resistance via CSR-DMS is rendered moot if the assay also requires the inclusion of a dedicated reverse transcriptase that has not been engineered to share these properties.

For these reasons, it may be of interest to screen DNA polymerases for RT activity. Fortunately, this has already been demonstrated for CSR, and is easy to adapt into CSR-DMS. RT-CSR is an approach developed by the Ellington Lab that selects for DNA polymerases with RT activity by incorporating RNA bases into CSR primers[56]. A DNA polymerase must be able to generate cDNA from these RNA bases, or the resulting amplicons will lack the tags necessary for recovery PCR. The Ellington Lab demonstrated that RT-CSR could generate variants of KOD polymerase capable of RT even though the wild-type enzyme possessed no detectable RT activity.

RT activity can be evaluated in CSR-DMS in much the same way that it was evaluated in the RT-CSR study. Because TF polymerase already possesses some baseline RT activity, the initial selective pressure need not be gentle. CSR-DMS primers could use chimeric RNA recovery tags or be made completely of RNA. If this proves insufficient to discern gain-of-RT-function variants from WT, it may be possible to build long RNA spacers into CSR-DMS primers to lengthen the RNA sequence that must be copied before the recovery tag is reached. However, secondary structure of extremely long CSR-DMS primers may prove problematic for this approach. An alternative may be to shorten extension time during thermal cycling, so polymerase variants are forced to quickly reverse-transcribe CSR-DMS primers.

6.4.3 Strand Displacement

Strand displacement (SD) activity is essential for most isothermal nucleic acid amplification mechanisms, including loop-mediated isothermal amplification (LAMP)[4], recombinase polymerase amplification (RPA)[5], and (unsurprisingly) strand displacement amplification (SDA)[113]. Although TF polymerase itself possesses strand displacement activity, it may be of interest to improve this activity (perhaps for long amplification), to study loss-of-SD-function in a sequence-function map, or to engineer it anew in a polymerase that lacks strand displacement activity (which is true of the Klenow fragment of *Taq* polymerase and many of its derivatives). Strand displacement selection has previously been demonstrated by Milligan *et al.* in a method they call high-temperature isothermal compartmentalized self-replication (HTI-CSR)[57]. They used hyperbranched rolling circle amplification (RCA), which relies on SD activity, to amplify concatemers of entire plasmid sequences. In doing so, they were able to enrich a library of Bst-KlenTaq polymerase chimeras for variants that were both strand-displacing (which KlenTaq lacks) and thermostable (which Bst lacks).

HTI-CSR might be a valid way to introduce an SD selective pressure – it is simple and previously validated – but it suffers from some drawbacks. Because it copies entire plasmids, its efficiency is likely inherently

lower than a barcode amplification approach, which will decrease signal-to-noise of enrichment. Also, unless recovery PCR tags can be engineered into the amplicons (not possible for RCA but potentially possible for hyperbranched RCA), removal of template plasmid DNA by DpnI will be necessary and ideally quite stringent. A potential alternative is to run a selection similar to CSR-DMS using thermal cycling and barcode-targeting primers, but add a blocking oligonucleotide that binds to the primers between the recovery tag and the plasmid-binding sequence and prevents full extension and generation of the recovery PCR primer binding site unless the polymerase possesses sufficient SD activity to displace the blocking oligonucleotide. It is important to add a chain terminator to the blocking oligonucleotide so it is not extensible itself. A blocking oligonucleotide would likely be a very gentle selective pressure, which could be useful for engineering SD anew into a polymerase that doesn't already possess it, but might be too gentle for TF polymerase, where we expect nearly all variants to retain strong SD activity. Thus, a blocking oligonucleotide could potentially be engineered to have an especially high melting temperature. One way to do this is increasing length or GC content, but that can lead to deleterious secondary structures during CSR itself or difficult downstream amplification during sequencing preparation. A potential alternative is to use a blocking oligo made of high-melting-temperature modified bases such as locked nucleic acids[114].

6.4.4 Lesion Bypass

Lesion bypass is an important capability for polymerases used to copy damaged DNA. This could be ancient DNA (such as from archaeological or paleontological samples) or environmental DNA that has been degraded (e.g. from ultraviolet light). One of the most common DNA lesions is an abasic site, where the nucleobase has been cleaved from the deoxyribose[115]. This is often the result of spontaneous depurination. Many DNA polymerases cannot easily extend through abasic sites and other DNA lesions, but those that can are known as "lesion bypass" polymerases and are often Y-family DNA polymerases[116,117]. However, natural lesion bypass polymerases may lack other capabilities essential for

biotechnological applications, such as thermostability or strand displacement. It is therefore potentially useful to try to engineer lesion bypass into a polymerase with several preexisting useful capabilities rather than engineer those capabilities into a natural lesion bypass polymerase.

CSR has previously been used to evolve polymerases with enhanced lesion bypass activity by using primers with mismatched bases near the 3' end, which simulate the effects of many kinds of DNA damage[115]. A similar approach would be easy to implement in CSR-DMS. Alternatively, it could be possible to use CSR-DMS primers with abasic or otherwise damaged sites separating recovery PCR tags from the plasmid-binding sequence. By tuning the number of damaged sites that the polymerase must extend through to generate the recovery PCR binding site, the selective pressure harshness can be titrated. Interestingly, this approach could be used to determine not just which polymerases can extend through damaged sites, but also the profile of base incorporations that the polymerase makes when doing so. This would be accomplished by including this region in the sequencing run, either by sequencing the entire amplicon, or by redesigning the barcode read primers to bind upstream of this region.

6.5 Expanding CSR-DMS to Study Other Enzymes

6.5.1 Multi-Enzyme Amplification Systems

Many isothermal amplification methods use multiple enzymes to copy DNA, such as helicase-dependent amplification (HDA)[118], strand displacement amplification (SDA)[113], and recombinase polymerase amplification (RPA)[5]. It may be of interest to engineer these "helper" enzymes to have similar stability to a polymerase, such as thermostability or chaotrope resistance, for a specific application. CSR-DMS is best-suited to study libraries of DNA polymerases because it uses PCR activity of the polymerase to copy barcodes representing the variants. However, alternative "helper" enzymes and proteins may be screened via a system resembling CSR-DMS if the system can be designed to make replication of helper

enzyme variant coding sequences dependent on the activity of the encoded proteins. This is achieved by redesigning the library to express helper enzyme variants, including a polymerase with the aqueous CSR phase, and making the polymerase activity dependent on the helper enzyme. A mock selection of such a "cooperative CSR" system was explored in the original CSR paper[55] to select for a wild-type nucleoside diphosphate kinase (which converted the supplied dNDPs into dNTPs needed for polymerase activity) over an inactive variant.

To perform an analogous "cooperative CSR-DMS", a variant library of the helper enzyme must be cloned, barcoded, and subassembled in a similar manner to what was done with TF polymerase for our study. Then, a DNA polymerase (and any other helper enzymes besides the one being screened) must be added to the CSR aqueous phase and other buffer components and thermal parameters should be tuned to amplify barcodes in a manner similar to the desired amplification system (for example, divalent cation concentrations should ideally match those of the target isothermal amplification mechanism). The barcodes can then be sequenced and counted to generate a sequence-function map of the helper enzyme activity in the desired amplification system. There are some difficulties with this approach, however. Because protein expression in CSR is poorly controlled, the concentration of helper enzyme is also poorly controlled, which complicates the study of amplification systems that are sensitive to the helper enzyme concentration (or its molar ratio to other enzymes). This problem may be difficult to surmount for such sensitive systems, but it also serves as a harsh selective pressure by itself that would likely favor helper enzyme variants whose activity is less dependent on concentration. Another constraint is the fact that CSR-DMS requires thermal cycling to lyse cells and drive primer binding, which limits screening to thermostable proteins. This may be acceptable or even favorable if thermostability is a characteristic desired of helper enzyme variants (a likely scenario), but systems like RPA (which operates at a relatively low range of 37-42°C[5]) may be incompatible with thermal cycling. In this case, the HTI-CSR study[57] by Milligan *et al.* (previously discussed) is a useful reference, as their initial screens

avoided thermal cycling by including lysozyme to lyse cells and a nicking enzyme to nick plasmids at a site conducive to amplification of variant coding sequences.

6.5.2 Self-Replicating Biomolecules

CSR-DMS may be useful in the study of self-replicating biomolecules (a theoretical stepping stone in the evolution of life from prebiotic organic molecules to fully replicative cells). Hypotheses for the origin of life on Earth must explain the chicken-and-egg problem posed by ribosomes, which are large molecular machines composed of RNA and proteins that all living organisms use for protein translation (which is itself necessary for reproduction)[119]. If ribosomes are made of RNA and proteins, but are also responsible for protein synthesis (including proteins that copy nucleic acids), then how were the first ribosomes made? The "RNA World" hypothesis posits that the first self-replicating biomolecules were RNA polymers, as RNA can catalyze reactions like proteins (and has indeed been found to be the catalytic component of ribosomes) but also serve as replicable genetic material (like DNA). While several forms of catalytic RNA enzymes ("ribozymes") have been identified and many act on RNA substrates[119], few are capable of self-replication in any form, all of which have constraints (such as poor efficiency, substrate specificity, or fidelity) that make them unlikely to truly represent the first self-replicating RNA molecules.

CSR-DMS could potentially be used to study the features of RNA oligomers that enable or enhance self-replication. In theory, such a system would be simple to set up. A library of randomly synthesized RNA oligomers, or oligomer variants based on known imperfect self-replicators, could be mixed with free monomers such as nucleoside triphosphates and compartmentalized in an emulsion as with conventional CSR. Any self-replicating RNA molecules would face an inherent selective pressure – yield of copies of itself – which could be studied by purifying, sequencing, and scoring RNA sequences or sequence features. This system would require a serious investment in design and development, as it

differs in many ways from all previous systems discussed, but it would be a compellingly unique application of CSR-DMS and an exciting foray into research on the origin of life.

7 List of Publications and Presentations

7.1 Journal Articles Included in This Dissertation

Hull, I. T.; Kline, E. C.; Gulati, G. K.; Kotnik, J. H.; Panpradist, N.; Shah, K. G.; Wang, Q.; Frenkel, L.; Lai, J.; Stekler, J.; Lutz, B. R. Isothermal Amplification with a Target-Mimicking Internal Control and Quantitative Lateral Flow Readout for Rapid HIV Viral Load Testing in Low-Resource Settings. *Anal. Chem.* **2022**, *94* (2), 1011–1021. https://doi.org/10.1021/ACS.ANALCHEM.1C03960.

Hull, I. T.; Kline, E. C.; Gulati, G. K.; Kotnik, J. H.; Panpradist, N.; Shah, K. G.; Wang, Q.; Frenkel, L.; Lai, J.; Stekler, J.; Lutz, B. R. Addition to "Isothermal Amplification with a Target-Mimicking Internal Control and Quantitative Lateral Flow Readout for Rapid HIV Viral Load Testing in Low-Resource Settings." *Anal. Chem.* **2022**, *94* (15), 6071–6071. https://doi.org/10.1021/ACS.ANALCHEM.2C01256.

Hull, I. T.; Popp, N. A.; Kline, E. C.; Powell, R. L.; Wheelock, M. K.; Childers, M. C.; Wang, Q.; Daggett, V.; Fowler, D. M.; Lutz, B. R. High-Resolution Polymerase Screening via Compartmentalized Self-Replication, Deep Mutational Scanning, and Molecular Dynamics Simulations. (Manuscript in preparation).

7.2 Other Journal Articles

Panpradist, N.; Kline, E.; Atkinson, R. G.; Roller, M.; Wang, Q.; **Hull, I. T.**; Kotnik, J. H.; Oreskovic, A. K.; Bennett, C.; Leon, D.; Lyon, V.; Gilligan-Steinberg, S. D.; Han, P. D.; Drain, P. K.; Starita, L. M.; Thompson, M. J.; Lutz, B. R. Harmony COVID-19: A Ready-to-Use Kit, Low-Cost Detector, and Smartphone App for Point-of-Care SARS-CoV-2 RNA Detection. *Sci. Adv.* **2021**, *7* (51), eabj1281. https://doi.org/10.1126/sciadv.abj1281.

Kline, E. C.; Panpradist, N.; **Hull, I. T.**; Wang, Q.; Oreskovic, A. K.; Han, P. D.; Starita, L. M.; Lutz, B. R. Multiplex Target-Redundant RT-LAMP for Robust Detection of SARS-CoV-2 Using Fluorescent Universal Displacement Probes. *Microbiol. Spectr.* **2022**, *10* (4). https://doi.org/10.1128/spectrum.01583-21.

Creighton, R. L.; Doan, M. A.; Tobos, C. I.; Guo, T.; Faber, K. A.; Han, Y.; Chiew, C.; **Hull, I. T.**; Malakooti, M. H.; Woodrow, K. A. High Resolution 3D Deposition of Electrospun Fibers on Patterned Dielectric Elastomers. (Manuscript under review at *Advanced Materials Technologies*).

7.3 Patent Applications

Roller, M.; Kline, E.; Atkinson, R.; Panpradist, N.; Leon, D.; **Hull, I.**; Wang, Q.; Lutz, B. R. Amplification Device. 63/049,758, 2020.

Roller, M.; Kline, E.; Atkinson, R.; Panpradist, N.; Leon, D.; **Hull, I.**; Wang, Q.; Lutz, B. R. Kit for Sample Collection and Preparation for Amplification. 63/049,941, 2020.

Panpradist, N.; Lutz, B. R.; Roller, M.; Kline, E.; **Hull, I.**; Wang, Q.; Leon, D.; Atkinson, R. G. SYSTEMS AND METHODS FOR DETECTING SARS-COV-2 RNA. 63/165,029, 2021.

Kline, E.; Roller, M.; Atkinson, R. G.; Panpradist, N.; Leon, D.; **Hull, I.**; Wang, Q.; Lutz, B. R. KITS, METHODS, POLYPEPTIDES, SYSTEMS AND NON-TRANSITORY, MACHINE-READABLE STORAGE MEDIA FOR DETECTING A NUCLEIC ACID. PCT/US2021/041035, 2021.

Kline, E.; Roller, M.; Atkinson, R.; Panpradist, N.; Leon, D.; **Hull, I.**; Wang, Q.; Lutz, B. KITS, METHODS, POLYPEPTIDES, SYSTEMS AND NON-TRANSITORY, MACHINE-READABLE STORAGE MEDIA FOR DETECTING A NUCLEIC ACID. 18/004,489, 2023.

Hull, I.; Lutz, B.; Kline, E., Fowler, D., Popp, N. SYSTEMS AND METHODS FOR HIGH-RESOLUTION POLYMERASE SCREENING. (U.S. provisional patent application in preparation). 63/459,883, 2023.

7.4 Conference Presentations

A Simple Test for HIV Treatment Failure Using Competitive Recombinase Polymerase Amplification. Biomedical Engineering Society Annual Meeting. Philadelphia, PA. October 19, 2019. Oral presentation.

8 Appendix A: Supporting Information for Isothermal Amplification with a Target-Mimicking Internal Control and Quantitative Lateral Flow Readout for Rapid HIV Viral Load Testing in Low-Resource Settings

Additional experimental methods, results, and discussion, including oligo and template sequences, regression analysis parameters, lateral flow strip images, survey design, oligo-template sequence alignment, and MATLAB script.

8.1 RPA Primer, Probe, and Template Sequences

The synthetic HIV template used in this work contains a majority consensus sequence generated from a 2017 web alignment of 3666 HIV-1 genomes from the Los Alamos National Laboratory (LANL) HIV Sequence Database[25]. All base numbering described below corresponds to the HXB2 reference genome (GenBank: K03455.1). The RPA assay detects bases 4756-4896; we designed a template containing bases 4733-4931 of the majority consensus sequence. Base 4830 was changed from A to G to prevent a mismatch with the HIV probe (this base is an A or G in roughly 77% or 22% of HIV-1 genomes in the 2017 web alignment, respectively, but is a G in roughly 58% of subtype B sequences; we believe that Boyle *et al.*[22] may have designed their assay against an alignment enriched for subtype B). The IAC template was identical to the HIV template, but with the IAC probe sequence substituted for the HIV probe sequence. We also designed three variant HIV templates to determine the effect of HIV genetic polymorphism on the assay. These templates were based on a 2002 alignment of HIV-1 group M subtype consensus sequences from the LANL HIV Sequence Database. One variant template contained a subtype B sequence, another contained a subtype C sequence, and the third contained a “Franken”-subtype

challenge sequence combining all mutations from the majority consensus that are present in at least one subtype consensus (see **Figure A6** for alignment with highlighted mutations).

All sequences are listed in **Table A1** as ordered from IDT using the manufacturer's modification codes. Primers and probes were ordered as custom DNA oligonucleotides, while templates were ordered as gBlocks (double-stranded DNA molecules).

Description	Sequence (5'-3')
RPA forward primer	/5BiosG/TGGCAGTATTCATTCACAATTTTAAAAGAAAAGG
RPA reverse primer	CCCGAAAATTTTGAATTTTTGTAATTTGTTTTTG
HIV RPA nfo probe	/5DiGN/TGCTATTATGTCTACTATTCTTTCCCCTGC/idSp/CTGTACCCCCCAATCCCC/3SpC3/
IAC RPA nfo probe	/56-FAM/TGTCTTCTATATCCCTACGTACTCCCATGC/idSp/CTCTCTTCTCCCCCAGTA/3SpC3/
HIV gBlock template	GTAAAACGACGGCCAGTTAATACGACTCACTATAGAGCTGAACACCTTAAGACAGCAGTACAAATGGCAGTAT TCATTCACAATTTTAAAAGAAAAGGGGGGATTGGGGGGTACAGTGCAGGGGAAAGAATAGTAGACATAATAGC AACAGACATACAAACTAAAGAATTACAAAAACAAATTACAAAAATTCAAAATTTTCGGGTTTATTACAGGGAC AGCAGAGACCCAATTGTCATAGCTGTTTCCTG
IAC gBlock template	GTAAAACGACGGCCAGTTAATACGACTCACTATAGAGCTGAACACCTTAAGACAGCAGTACAAATGGCAGTAT TCATTCACAATTTTAAAAGAAAAGGTACTGGGGGGAGAAGAGAGTGCATGGGAGTACGTAGGGATATAGAAGAC AACAGACATACAAACTAAAGAATTACAAAAACAAATTACAAAAATTCAAAATTTTCGGGTTTATTACAGGGAC AGCAGAGACCCAATTGTCATAGCTGTTTCCTG
HIV subtype B consensus sequence gBlock template	GTAAAACGACGGCCAGTTAATACGACTCACTATAGGGCTGAACATCTTAAGACAGCAGTACAAATGGCAGTAT TCATCCACAATTTTAAAAGAAAAGGGGGGATTGGGGGGTACAGTGCAGGGGAAAGAATAGTAGACATAATAGC AACAGACATACAAACTAAAGAATTACAAAAACAAATTACAAAAATTCAAAATTTTCGGGTTTATTACAGGGAC AGCAGAGATCCACTTGTCATAGCTGTTTCCTG
HIV subtype C consensus sequence gBlock template	GTAAAACGACGGCCAGTTAATACGACTCACTATAGAGCTGAGCACCTTAAGACAGCAGTACAAATGGCAGTAT TCATTCACAATTTTAAAAGAAAAGGGGGGATTGGGGGGTACAGTGCAGGGGAAAGAATAATAGACATAATAGC AACAGACATACAAACTAAAGAATTACAAAAACAAATTATAAAAATTCAAAATTTTCGGGTTTATTACAGAGAC AGCAGAGACCCTATTGTCATAGCTGTTTCCTG
HIV "Franken"-subtype gBlock template	GTAAAACGACGGCCAGTTAATACGACTCACTATAGGGCTGAGCATCTTAGAACAGCAGTACAGATGGCAGTAT TCATCCACAATTTTAAAAGAAAAGGGGGGATTGGGGGATACAGTGCAGGGGAAAGAATAATAGACATAATAGC ATCAGATATACAAACTAGAGAACTACAAAAACAGATCTTAAAAATTCAAAAATTCCGGGTTTATTACAGAGAC AGCAGAGATCCTCTTGTCATAGCTGTTTCCTG

Table A1. Sequences for RPA primers, probes, and templates. *IDT modification codes are included for primers and probes. Templates contained flanking M13 PCR primer sites and T7 promoter sites to enable in-house DNA and RNA production, respectively. Underlined bases are M13 forward PCR primer sites. Thick-underlined bases are T7 RNA polymerase promoter sites. Double-underlined bases are M13 reverse PCR primer sites.*

8.2 Non-Linear Regression Analysis Results

Results from non-linear regression analysis of data from scanned images or cell phone photos are shown in **Table A2**. HIV input copy number and HIV signal fraction were fit via least squares regression to four-parameter logistic curves defined by the following model:

$$Y = Bottom + (X\text{^}Hillslope) * (Top - Bottom)/(X\text{^}HillSlope + EC50\text{^}HillSlope)$$

where X represents input HIV copy number and Y represents HIV signal fraction.

	Scanner analysis, 200-copy DNA increments (Fig. 2)	Scanner analysis, 10-fold DNA increments (Fig. 2)	Cell phone analysis, 200-copy DNA increments (Fig. 2)	Cell phone analysis, 10-fold DNA increments (Fig. 2)	Scanner analysis, 10-fold RNA increments (Fig. 5)
Best-fit values					
Bottom	-0.01431	-0.0214	0.08073	0.1335	-0.004993
Top	0.8021	1.051	0.5842	1.024	0.9579
EC50	359.7	670.5	75.9	850.6	2894
HillSlope	0.517	0.5767	0.7038	0.4156	0.8901
95% confidence intervals					
Bottom	-0.03005 to 0.001428	-0.07062 to 0.02631	0.06642 to 0.09504	0.08415 to 0.1819	-0.09095 to 0.07384
Top	0.6626 to 1.617	1.002 to 1.107	0.5464 to 0.7635	0.9600 to 1.113	0.8527 to 1.101
EC50	194.0 to 13850	455.0 to 998.8	55.26 to 98.39	445.8 to 1802	1460 to 6365
HillSlope	0.2993 to 0.7350	0.4824 to 0.6936	0.3201 to 1.110	0.3303 to 0.5192	0.5369 to 1.521
Goodness of fit					
Degrees of Freedom	29	17	29	17	17
R squared	0.9939	0.9907	0.992	0.9851	0.9514
Adjusted R squared	0.9932	0.989	0.9912	0.9824	0.9428
Sy.x	0.01333	0.04439	0.01212	0.04188	0.1016
Normality of residuals					
D'Agostino-Pearson omnibus (K2)	5.597	2.177	0.9421	0.03899	2.555
P value	0.0609	0.3367	0.6243	0.9807	0.2787
Passed normality test (alpha=0.05)?	Yes	Yes	Yes	Yes	Yes

Table A2. Non-Linear Regression Analysis Results. *Best-fit sigmoidal curves and related parameters were generated individually from each experiment using GraphPad Prism 9.2.0.*

This analysis is a useful way to predict future performance of a competitive assay or to interpolate unknown values. However, we caution that it requires validation to avoid misleading results. The fact that our best-fit curves differed across experiments, when they theoretically should be nearly identical, is evidence that large datasets and stringent cross-validation are needed to define a curve that accounts for all sources of assay variability, and training data should ideally be produced under various conditions to avoid over-fitting these models to data produced under a highly controlled laboratory environment.

8.3 IAC Exhibits Similar Sensitivity and Signal to HIV

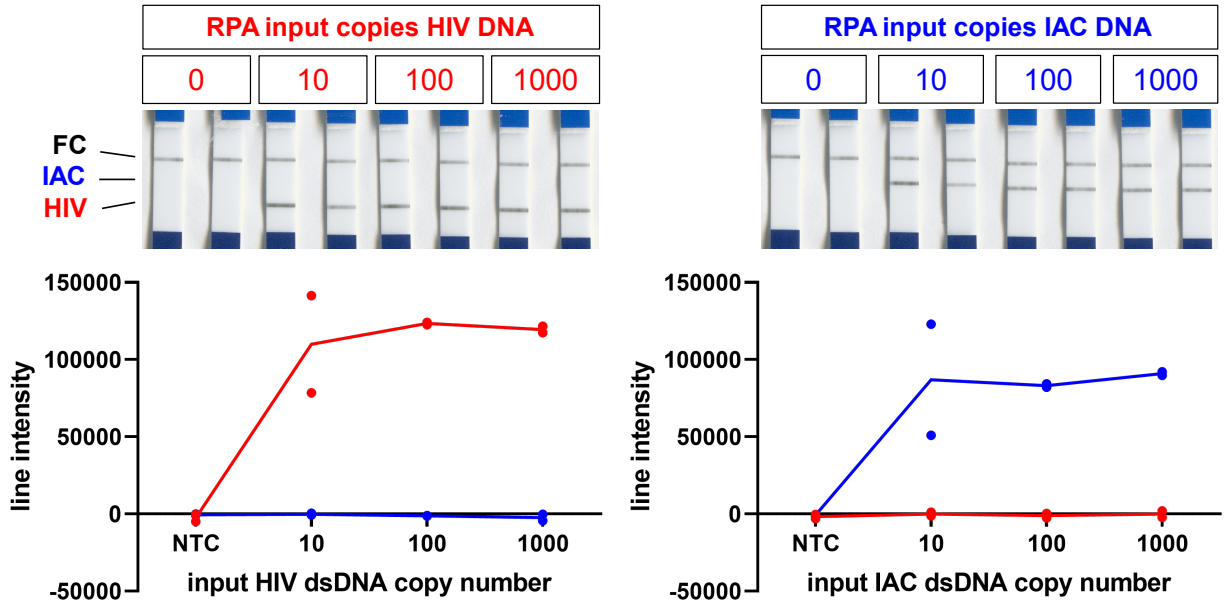

Figure A1. Competitive RPA assay sensitively detects HIV and IAC, with signal saturation regardless of copy number. *Note that the lateral flow assays in this experiment were performed using 10µL RPA reaction input and 140µL PCRD extraction buffer. Dots represent replicate assays while connecting lines represent sample means (N=2).*

In RPA nfo reactions with the HIV and IAC probe mixed at 50% of the recommended total probe concentration each, we amplified varying copy numbers of HIV or IAC DNA, then ran the products on PCRD FLEX lateral flow strips (**Figure A1**). Both targets were detectable at 10 input copies of DNA (the lowest tested), with similar capture line intensities for all positive reactions regardless of input template or copy number. In fluorescence-based assays using RPA exo chemistry (not shown), we have seen similar behavior, implying that the signal saturation is not due to exhaustion of the lateral flow detection beads, but due to an inherent tendency of RPA assays to saturate when a certain amplicon concentration has been reached. This has two major implications for our RPA-based viral load assay. First, we cannot rely on endpoint signal of HIV amplicons alone to determine input copy number, as inputs of varying copy number tend to saturate with the same endpoint signal. Second, if the IAC and HIV targets amplify with similar sensitivity and efficiency as seen above, then we can expect their combined signal to saturate around the same intensity as an equivalent amount of HIV or IAC targets

alone. Furthermore, our probes appear not to be cross-reactive, as the IAC capture line showed no signal in the presence of exclusively HIV targets (and vice versa). Therefore, while the sum of HIV and IAC signals is expected to saturate, the ratio of HIV signal to IAC signal is expected to resemble the ratio of HIV input copy number to IAC input copy number.

8.4 Justification for Use of 1µL RPA Reaction in Lateral Flow

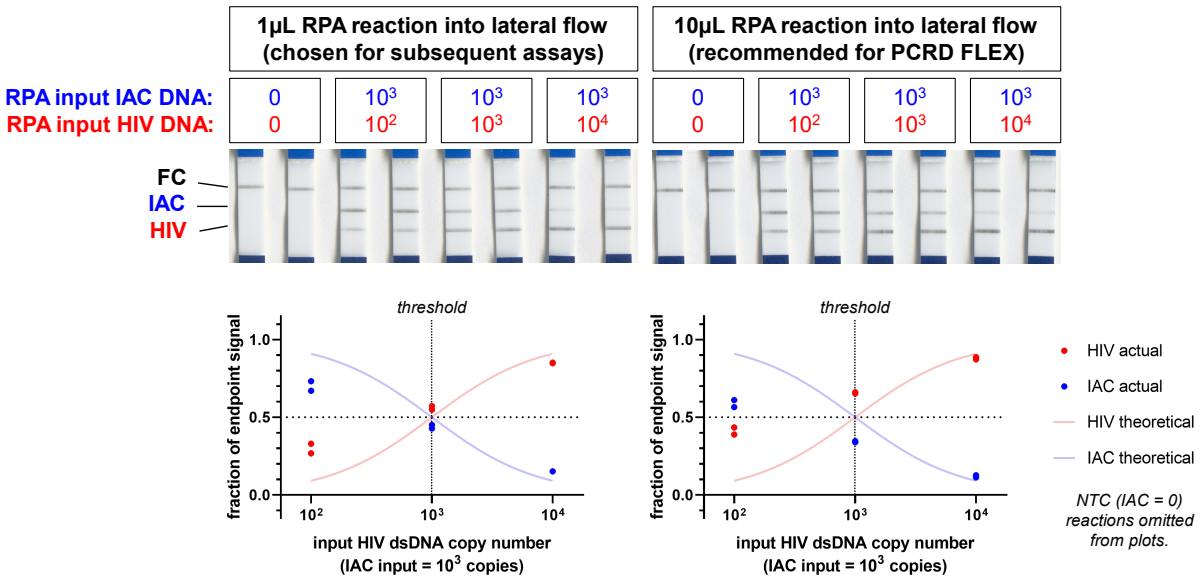

Figure A2. Competitive RPA assay run with varying RPA reaction volume input to lateral flow assay. *(LEFT) PCRD FLEX lateral flow assays run with 1µL RPA reaction input and 149µL PCRD extraction buffer. (RIGHT) PCRD FLEX lateral flow assays run with 10µL RPA reaction input and 140µL PCRD extraction buffer. Dots represent replicate assays while connecting lines represent sample means (N=2).*

Although the PCRD FLEX brochure recommends mixing 10µL nucleic acid amplification products with 140µL PCRD extraction buffer before wicking through strips, we suspected that these volumes were chosen to maximize qualitative detection of targets by using an excess of nucleic acid product. This poses a problem for quantitative use - if there is an excess of nucleic acid product, then some of the streptavidin-coated beads could be labeled with both HIV and IAC amplicons and preferentially bind to the HIV (anti-DIG) line because it is encountered first during fluid flow, which in turn could artificially inflate HIV signal relative to IAC signal. Indeed, we found that when we co-amplified 10^3 copies each of HIV and IAC and used 10µL of the RPA product in the lateral flow assay, the HIV signal fraction was much

higher than the HIV input fraction of 0.5, contrary to the desired behavior of our assay (**Figure A2**, right). Using the same RPA reaction products, we then tried a smaller 1µL input into lateral flow and found that the signal fractions aligned much better with the input fractions, as desired (**Figure A2**, left). For this reason, we used 1µL RPA product in all subsequent lateral flow assays. We suspect that an even smaller volume could improve quantification further, but risks a loss of sensitivity, so we decided that 1µL was sufficient.

8.5 Survey Design

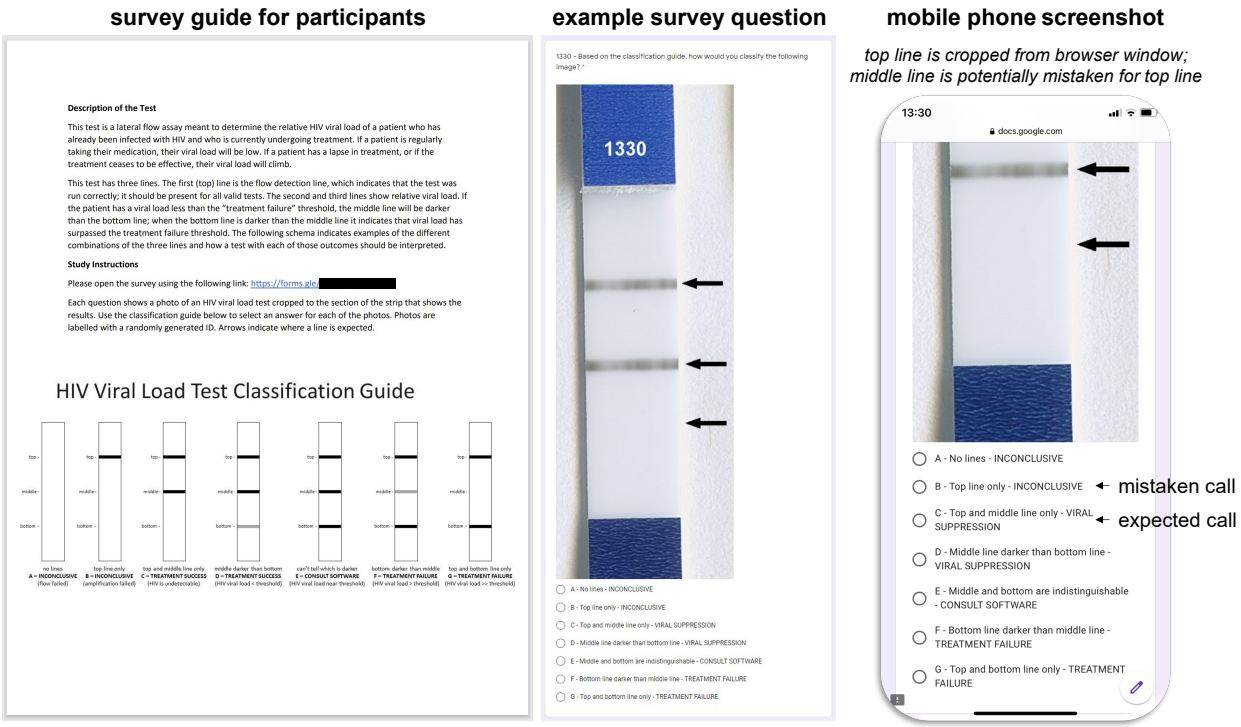

Figure A3. Survey for naked-eye analysis of lateral flow strips. *(LEFT) Survey guide provided to participants via PDF. Options C and D suggest successful HIV treatment under current WHO guidance and are thus combined in calculations, as are options F and G, which both represent treatment failure. However, we included this distinction in the survey options to better understand respondents' analysis of low-intensity capture lines and because alternative clinical guidelines may distinguish between e.g. "HIV undetectable" and "HIV detectable but virologically suppressed" results. (CENTER) Example survey question. All images of strips were labeled with a random numeric ID and arrows to indicate the expected location of capture lines (as is commonplace on plastic cassettes for lateral flow strips). (RIGHT) Screenshot of a survey question from a mobile phone web browser. Note the unintended cropping of the top capture line (present in the survey image with positive signal, but not shown here), which may have confused survey volunteers into mistakenly choosing option B instead of option C. Similar cropping was observed on a personal computer web browser (not shown).*

The survey for naked-eye interpretation of lateral flow strip images was conducted online, with an email containing a survey guide and a link to the survey on Google Forms sent to all participants. Screenshots

of the survey guide and examples of survey questions are in **Figure A3**. Participants were not instructed to take the survey on any specific browser or platform, and we assume multiple of these were used by the 21 participants.

There were three unexpected erroneous calls in **Figure 5** by Participants 3 and 17, in which the participants claimed not to see certain lines (both HIV and IAC for Participant 3, leading to a "B" call, and HIV for Participant 17, leading to a "C" call) that were seen by all other participants. We believe these errors are an artifact of the survey method, wherein participants viewed the images through a web browser window that may have cropped out certain capture lines (**Figure A3**, right). We therefore believe these errors would be unlikely to occur in a real-world setting where naked eye analysis is carried out on tangible strips in cassettes that clearly mark capture line regions.

8.6 IAC Input is Tunable to Represent Various Clinical Thresholds, Sample Volumes, or Sample Preparation Yields

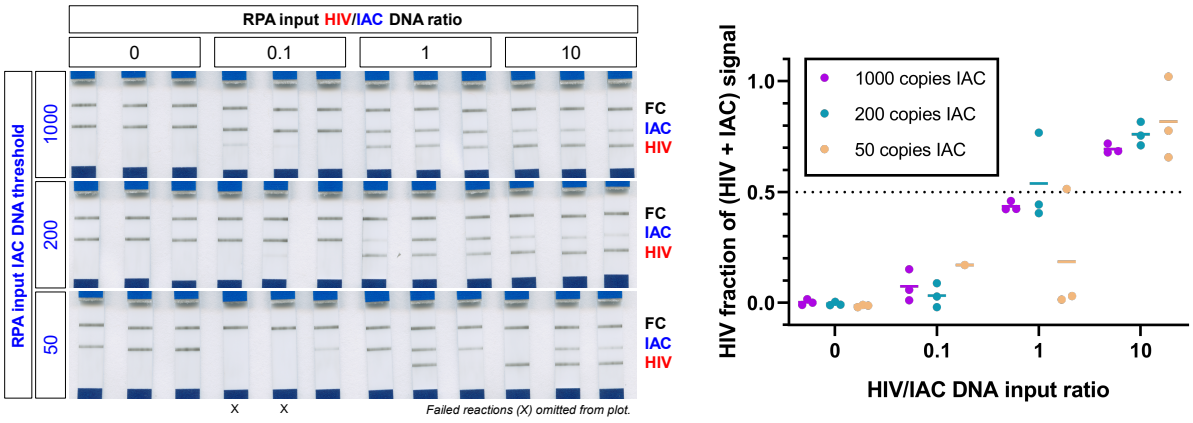

Figure A4. Competitive RPA assay with various IAC inputs to simulate different thresholds for treatment failure. *RPA reactions were run with varying copy numbers of IAC DNA and varying ratios of HIV DNA relative to IAC, then wicked through lateral flow strips for endpoint signal analysis via scanner and ImageStudio Lite. (LEFT) Images of strips. (RIGHT) Software analysis of strips. Dots represent replicate assays while horizontal lines represent sample means (N=3).*

For competitive RPA to be broadly useful for quantification, it must be effective at various IAC thresholds. An IAC threshold of 1000 copies simulates the expected copy number of HIV RNA purified from a 1mL sample of HIV-positive plasma at the WHO-designated threshold for treatment failure (1000

copies RNA/mL)[14]. The CDC, however, uses a stricter 200 copies/mL threshold to prevent HIV transmission[15]. Also, while a venous blood draw is required for collection of 1mL plasma, fingerstick samples are much lower volumes (typically around 50µL, though they can approach 200µL[20]). Finally, the HIV RNA input to competitive RPA might be less than the copy number collected in a sample, whether due to sample preparation with < 100% yield or constraints on the volume of purified RNA that can be added to an RPA reaction. For these reasons, a lower IAC threshold may be necessary. We therefore demonstrated the feasibility of competitive RPA using IAC thresholds of 50, 200, and 1000 copies (**Figure A4**).

For all reactions with HIV inputs an order of magnitude or more different from IAC, the higher endpoint signal matched the predominant input template, as desired. For 2 out of 3 reactions with 50 copies of IAC and an HIV/IAC input ratio of 0.1 (i.e. 5 copies of HIV DNA), amplification appeared to have failed, with neither the IAC nor HIV capture lines exceeding background intensity. We believe these reactions likely failed because they were near the limit of detection for both targets. As these strips would be classified as inconclusive, they were omitted from analysis.

These results imply that a competitive IAC enables this HIV VL assay to accommodate various treatment failure thresholds, sample volumes, or sample preparation yields. For example, if the IAC is added early in the workflow as a sample processing control (e.g. an encapsulated RNA bacteriophage with the IAC sequence incorporated into its genome[120]), then it can control for premature lysis and ribonuclease-mediated degradation of RNA during sample preparation. This flexibility of IAC input further implies that competitive RPA may be used in other non-HIV semi-quantitative applications with various IAC thresholds, assuming the sensitivity of the assay is sufficient. Indeed, the competitive IAC is a useful control that may indicate when the assay approaches its limit of detection, as demonstrated by the two failed reactions with a 50-copy threshold.

However, the sensitivity loss at such low copy numbers does pose barriers to clinical implementation of this assay. The justifications described above for choosing 1000-, 200-, or 50-copy thresholds assume that the entire volume of purified RNA can be added to an RPA reaction, but achieving this in reality would require special attention to choose a sample preparation workflow that concentrates RNA to a small volume and to design an RPA reaction formulation that can accommodate said volume, neither of which were addressed in this work. Viral RNA extraction kits that use conventional silica column adaptations of the Boom method[73] have limited ability to concentrate HIV RNA without modifications. The QIAamp Viral RNA Kit (Qiagen), for example, processes 140µL of plasma and elutes in 60µL by default. Meanwhile, the TwistAmp nfo Kit (TwistDx) accommodates a sample volume up to 13.2µL by default. Thus, pairing these kits with no modifications would result in a maximum of ~31 copies of HIV RNA purified from a plasma sample at the WHO VL threshold being added to the reaction – a troubling consideration, given the assay's inconsistent results with a 50-DNA-copy threshold above. However, it is possible to concentrate HIV RNA further, for example by passing larger volumes of sample through a column over multiple steps (as described in the QIAamp Viral RNA Kit), choosing higher-volume columns (e.g. 1mL maximum in the QIAamp UltraSens Virus Kit, Qiagen), pre-concentrating the plasma with a centrifugal filter, or eluting in smaller volumes. These methods are all somewhat conventional, but increase assay complexity. Alternatively, developing an RPA formulation that accommodates a larger sample volume could simplify the assay. Incorporating all oligos into the lyophilized pellet and combining the rehydration buffer and magnesium acetate solution would leave room for a 20.5µL sample input and reduce pipetting steps. Finally, there are design considerations we would recommend for this application or for any POC diagnostic: choosing a more sensitive assay[47] and the minimum sample volume necessary (ideally fingerstick) to achieve quantitative results.

8.7 Competitive IAC Controls for Amplification Inhibition

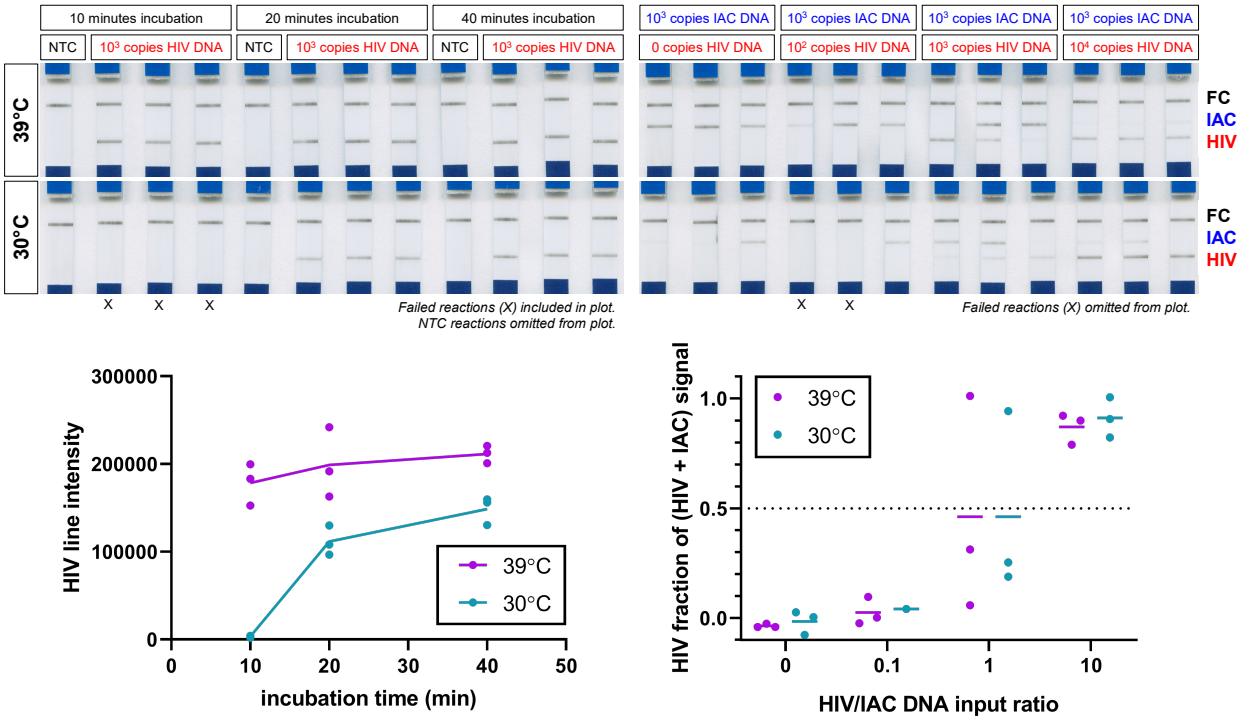

Figure A5. RPA at varying temperature to demonstrate robustness of competitive RPA regardless of sensitivity or reaction rate. *(LEFT) Lateral flow strip results for RPA run on 10^3 copies HIV DNA (no IAC included) at 30°C or 39°C. Dots represent replicate assays while connecting lines represent sample means (N=3). (RIGHT) Lateral flow strip results for competitive RPA run with 10^3 copies IAC DNA and varying HIV inputs at 30°C or 39°C. Dots represent replicate assays while horizontal lines represent sample means (N=3).*

One of the strongest advantages of competitive RPA is that the IAC controls for assay inhibition in a quantitative manner. One example of inhibition is the effect of temperature on amplification. RPA performs best at 37-42°C[5], though this HIV assay has been shown to tolerate temperatures as low as 30°C[12]. This wide temperature tolerance range is ideal for point-of-care nucleic acid tests because it enables the use of imprecise yet inexpensive heating mechanisms such as chemical heaters[12] or even body heat[121]. However, temperatures outside the ideal incubation range can adversely affect assay speed and sensitivity. To demonstrate this, we amplified 1000 copies of HIV DNA at the default 39°C or at 30°C for various lengths of time (**Figure A5**, left). Although the assay reliably detected the HIV input after the default 20 minutes of incubation regardless of temperature, the signal at 20 minutes was weaker for the 30°C reactions. At 10 minutes, the 39°C reactions had already produced a signal but the

30°C reactions had not. Taken together, this shows that the assay is delayed at a sub-optimal temperature and may suffer sensitivity loss.

However, the competitive IAC serves as a control against which HIV amplification may be normalized to negate the effects of inhibition. To demonstrate this, we co-amplified 1000 copies of IAC DNA with varying DNA copy numbers, using (HIV/IAC) input ratios of 0, 0.1, 1, or 10, at 30°C or 39°C (**Figure A6**, right). At both temperatures, the assay maintained its ability to correctly identify the dominant input template based on dominant endpoint signal.

The cause of the variation in the HIV=IAC condition is perplexing to us, as other experiments have shown much less variation, but it is possible that the manual mixing step in this experiment was delayed relative to other experiments because of the more complex setup requiring two thermal cyclers, which resulted in inconsistent initiation of HIV or IAC amplification. The mixing step 5 minutes into RPA incubation has been shown to significantly enhance assay sensitivity and reproducibility, particularly in reactions with high volume or low target inputs[13]. This is presumably caused by localized depletion of reagents around amplicons, which may be heterogeneously distributed early in the reaction (the low temperature and high viscosity of RPA limit diffusive or convective mixing). Such heterogeneities may randomly favor HIV or IAC amplification in certain reactions, and delayed mixing may have propagated such variation in this experiment. Furthermore, the HIV or IAC signal fractions should be more sensitive to changes in HIV input when the HIV and IAC inputs are similar rather than when one target is in great excess (see theoretical curves in **Figure 2**). Future development of competitive RPA assays would therefore benefit from an evaluation of the mixing step's impact on quantification, particularly because a mixing step increases POC assay complexity. We note that the RPA manufacturer sells instruments that perform automatic mixing during incubation, which could be used in low- to mid-throughput clinical settings. For ideal POC use, however, we recommend automating the RPA mixing step, which may be

accomplished through acoustic[122,123] and/or paper-based[124,125] microfluidic mixing, or choosing an alternative NAT chemistry that does not require mixing.

Here, a non-ideal temperature was chosen as an example of inhibition because it is likely to occur in a low-resource test format using inexpensive equipment. However, various sources of inhibition could presumably be accounted for by the IAC. For example, some denaturants commonly used in sample preparation can inhibit amplification if they are not properly removed during the final steps of sample preparation[126]. If RPA amplification is inhibited by these substances, the competitive IAC would likely either lose amplification efficiency accordingly and still report a proper test result, or fail entirely and yield an inconclusive test (which is preferable to a false negative).

8.8 High-Probability Mutations in HIV Sequence Do Not Affect Thresholding

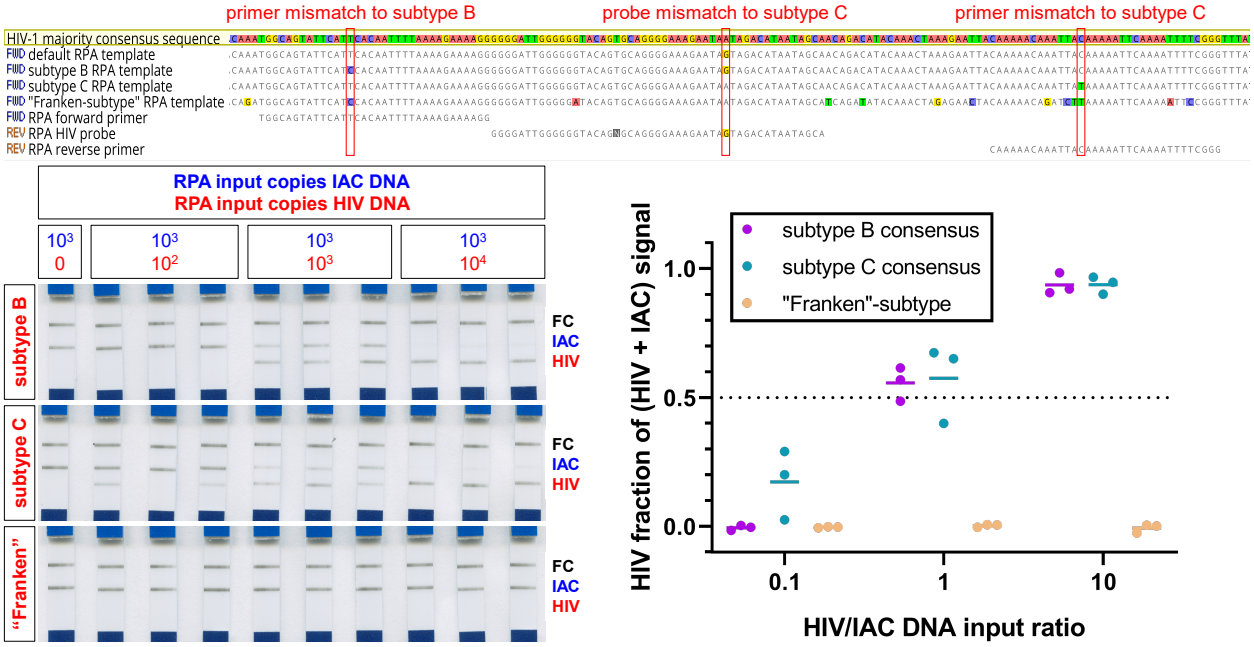

Figure A6. Reactivity and accuracy of competitive RPA assay on HIV sequences with mutations relative to the IAC. *(TOP) Sequence alignment of HIV templates and RPA primers/probe to a majority consensus sequence for HIV-1. The RPA primers and probe were originally designed to maximize HIV genomic coverage[22], and they match an HIV-1 majority consensus sequence nearly exactly, aside from a single G/A polymorphism in the probe site. This base occurs as a G or A in essentially equal proportions for all HIV sequences according to our internal assessment; for our default RPA template we use a majority consensus sequence with the G variant to match the probe. Subtype B has a mismatch to the forward primer, while subtype C has mismatches to the probe and the reverse primer. Because these mismatches are far from the primer 3' sites or the probe cleavage site, they are unlikely to affect detection. The "Franken-subtype" template incorporates any mutation that an HIV-1 subtype consensus sequence exhibits relative to the overall HIV-1 majority consensus sequence, and has 9 total mismatches to the primers and probe. (BOTTOM) Lateral flow strip results for competitive RPA run with 10^3 copies IAC DNA and varying copy*

numbers of HIV DNA of varying subtype. Reactivity and quantitative response are maintained for subtype B and subtype C, but not for the "Franken-subtype" template. Dots represent replicate assays while horizontal lines represent sample means (N=3).

We have so far shown the competitive RPA assay to be robust to various IAC thresholds and assay inhibition. However, in our view, the biggest risk to its accuracy is HIV genomic polymorphism. HIV-1 is an extremely diverse virus with a high mutation rate. While most assay interferences should equally affect HIV and IAC amplification efficiency and thereby have little effect on assay function, a mutation in the HIV target could prevent primer/probe binding and decrease HIV amplification efficiency relative to the IAC. In severe cases, the VL could be underestimated or even undetected. While the original qualitative version of this HIV *pol* RPA assay has previously been shown to detect many HIV genomic variants (up to 9 total mismatches to the primers and probe)[22] with high *sensitivity*, it is unclear how polymorphism might affect HIV amplification *efficiency* and thus the accuracy of our competitive RPA assay. We therefore designed polymorphic HIV templates to test the effect of common mutations.

We designed templates based on majority consensus sequences of HIV-1 Group M subtypes. Group M causes over 90% of HIV/AIDS infections worldwide and is further divided into various subtypes, of which subtype C is predominant (comprising 46.6% of all HIV-1 infections worldwide[127]), followed by subtype B (comprising 12.1% of all HIV-1 infections worldwide[127] and roughly 95% of all HIV-1 infections in the United States[38]). The remaining Group M subtypes are numerous but comprise roughly 10% or less each of global HIV-1 prevalence[127]. We therefore designed HIV templates with a subtype C consensus sequence, subtype B consensus sequence, and a "Franken"-subtype (with all mutations that differ from the HIV-1 majority consensus sequence included in one sequence). The full template sequences are displayed in **Table A1**.

We then co-amplified 1000 copies of IAC DNA with varying DNA copy numbers of above templates, using (HIV/IAC) input ratios of 0.1, 1, or 10 (**Figure A6**). The assay maintained the ability to match dominant endpoint signal with dominant input template for subtypes B and C, but showed no HIV

amplification for the “Franken”-subtype. This implies that the assay is robust to common/expected HIV mutations, but it may deliver false negative results when the HIV sequence has too many mutations compared to the intended assay design. While we expect such highly mutant sequences to be rare (the “Franken”-subtype mostly has mutations from subtypes of low global prevalence), this is the only risk for the assay that is expected to inhibit HIV amplification *relative* to IAC amplification, causing potential false negatives for treatment failure. Therefore, when PWH cohorts are expected to have high HIV sequence diversity[38,127] relative to the HIV-1 majority, subtype B, or subtype C consensus sequences, we advise caution and pre-validation of the assay against endemic HIV strains before clinical use.

8.9 Competitive RPA is Compatible with Genomic HIV RNA from Clinical Samples

25µl of plasma from an HIV$^+$ donor was diluted to 140µL total in Tris-buffered saline (pH 7.4) with 0.1%w/v Bovine Serum Albumin, then processed using a QIAamp Viral RNA Mini Kit (Qiagen 52906), with a final elution volume of 60µL. 5µL of the resulting elution was sampled in triplicate for determination of copy number using RT-qPCR. The remaining HIV-1 genomic RNA was added directly (without further dilution) in various volumes to achieve the HIV RNA copy numbers specified in RT-RPA reactions.

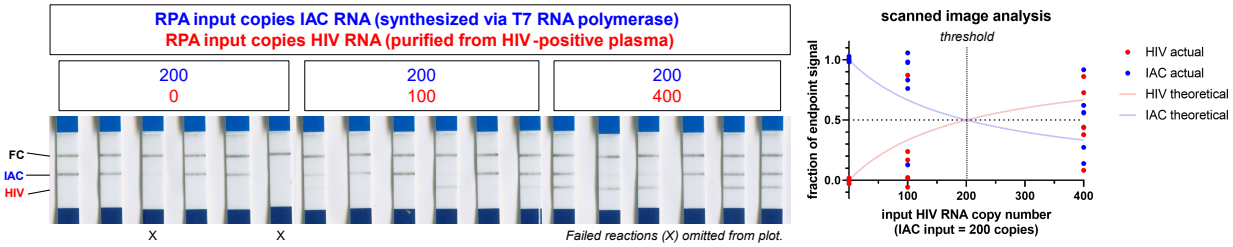

Figure A7. Accuracy of the RPA assay against HIV RNA purified from HIV-positive plasma. *The RPA assay was performed with 200 copies of IAC RNA and varying copy numbers of HIV RNA purified from a clinical plasma sample. The IAC copy number was selected to represent a treatment failure threshold of 1000 copies/mL for a 200µL fingerstick blood sample (alternatively, a threshold of 5000 copies/mL for a 40µL fingerstick blood sample).*

To determine the sensitivity and accuracy of the competitive RPA assay for semi-quantitative determination of HIV viral load using genomic HIV RNA, we ran various copy numbers of HIV RNA in the RPA assay with 200 copies of added IAC RNA (simulating the WHO viral load threshold of 1000

copies/mL for a 200 µL blood sample) (**Figure A7**). A 2-fold (~0.3 $\log_{10}$) range of HIV copy number was chosen to determine whether the resolution of the assay is comparable or superior to the 2-fold error typical of qPCR. The assay was marginally effective at matching the dominant endpoint signal with dominant input template. 4/6 NTC reactions and 5/6 100-copy reactions correctly produced a dominant IAC signal (2/6 NTC reactions failed). The assay may have slightly underestimated HIV copy number, as 4/6 400-copy reactions produced a dominant IAC signal (replicates limited due to small amount of clinical RNA available). This may be due to inaccuracies in our quantification of the HIV RNA prior to experiments. Unlike the synthetic IAC (which was quantified via Qubit High-Sensitivity RNA Assay), this clinical HIV RNA was quantified via RT-qPCR due to insufficient mass for fluorometry, and it is possible that the HIV copy number was overestimated at this stage. Another source of error could be mutations in the HIV sequence relative to the IAC, as discussed in the previous section (the HIV in this plasma sample is known to be subtype B, but its sequence has not been determined), though our results from the previous section indicate that common subtype B sequences should be tolerated by the assay. One other complication could be potential RNase contamination and degradation of the extracted HIV RNA stock from its original plasma sample matrix, which is unlikely to affect the IAC stock due to its synthetic origin. A POC workflow, with IAC integrated into sample preparation and no RNA storage step, could mitigate this potential issue. Nevertheless, the dominant signal switches roughly within a 2-fold range around the IAC threshold, and we have found the assay to be quite accurate for wider ranges of HIV copy number using synthetic templates. In a clinical VL test, the IAC would be most effective if it is added to plasma to account for sample loss during RNA extraction - while such development is outside the scope of this work, we suggest incorporating the IAC into clinical workflows as an “Armored RNA” target enclosed in a non-pathogenic viral capsid (e.g. MS2 bacteriophage[120] or phage-like particle[128]).

8.10 MATLAB Script for Analysis of Cell Phone Photos of Lateral Flow Strips

```
%% Process lateral flow strips and analyze them for RPA (3 test lines)
```

```
% Copyright (C) 2020 Kamal Shah
% Run in MATLAB R2019a for best results
% last edited on 2020/02/15
%
function processImagesForIanv2()
clc
clear
close all
%% start by getting images
% change myPath to the folder in which you have the images
myPath='C:\Users\Qin\Desktop\HIV VL LFA_quantification\190918 new\';
myPhones={'iPhone 11'};
myImages=struct('Folder',[],'File',[],'Phone',[],'Experiment',[],'ImageIndex',[],'Image',[]);
myIndex=1;
for i=1:length(myPhones) %number of phones
    for e=1:2 %two experiments
        myPathLong=[myPath,myPhones{i},'\Set ',num2str(e),'\'];
        myFileNames=dir(myPathLong);
        myImageIndex=1;
        for f=1:length(myFileNames) %iterate over all files
            myFile=myFileNames(f).name;
            if strlength(myFile)<=4 %only consider image files, not the junk contributed by
hidden files
                continue;
            end
            myFolder=myFileNames(f).folder;
            myImage=imread([myFolder,'\',myFile]);
            myImages(myIndex).Folder=myFolder;
            myImages(myIndex).File=myFile;
            myImages(myIndex).Phone=myPhones{i};
            myImages(myIndex).Experiment=e;
            myImages(myIndex).ImageIndex=myImageIndex;
            if size(myImage,1)<=size(myImage,2)
                myImage=imrotate(myImage,-90);
            end
            myImages(myIndex).Image=myImage;

            myIndex=myIndex+1;
            myImageIndex=myImageIndex+1;
        end
    end
end
%% Get positions of individual lateral flow strips
myStructLFAs=struct('Phone',[],'Experiment',[],'ImageIndex',[],'LFA',[],'NC',[],'Profile',[],'AUC
',[],'AUCcontrol',[],'AUCiac',[],'AUCsample',[],'AUCbg1',[],'AUCbg2',[],'AUCgray',[]);
myIndex=1;
for i=1:length(myImages)
    myImage=myImages(i).Image;
    myPhone=myImages(i).Phone;
    myExperiment=myImages(i).Experiment;
    myImageIndex=myImages(i).ImageIndex;
    %resize images to uniform size
    myImage=imresize(myImage,[2000 NaN]);

    % we know that the solid blue rectangle always is the largest,
    % and nitrocellulose comes after it, followed by the dark region

    myBlueMask=myImage(:,:,3)>2*mean(myImage(:,:,1:2),3);
    myImage=single(myImage);

    %find biggest blue rectangles
    connComps=bwconncomp(myBlueMask);
    numPixels=cellfun(@numel,connComps.PixelIdxList);
    [myBiggest,myIndices]=maxk(numPixels,3);

    % remove everything else
    connComps.PixelIdxList(setxor(1:length(numPixels),myIndices))=[];
    connComps.NumObjects=length(myIndices);

    myLabels=labelmatrix(connComps);
```

```
    % crop to each lateral flow strip
    for j=1:3
        myIndices=any(myLabels==j,1);
        myIndices=find(myIndices);
        myStart=max([min(myIndices)-10,1]);
        myEnd=min([max(myIndices)+10,size(myImage,2)]);
        myLFA=uint8(myImage(:,myStart:myEnd,:));
        myStructLFAs(myIndex).LFA=myLFA;
        myStructLFAs(myIndex).Phone=myPhone;
        myStructLFAs(myIndex).Experiment=myExperiment;
        myStructLFAs(myIndex).ImageIndex=myImageIndex;
        myIndex=myIndex+1;
    end
end

%iterate over each LFA and find nitrocellulose
for i=1:length(myStructLFAs)
    myLFA=myStructLFAs(i).LFA;
    myLFAgamma=rgb2lin((single(myLFA)./255.0));
    %find the 2 blue rectangles that border the nitrocellulose
    myBlueMask=myLFAgamma(:,:,3)>2*mean(myLFAgamma(:,:,1:2),3);

    %find biggest blue rectangles
    connComps=bwconncomp(myBlueMask);
    numPixels=cellfun(@numel,connComps.PixelIdxList);
    [myBiggest,myIndices]=maxk(numPixels,2);

    % remove everything else
    connComps.PixelIdxList(setxor(1:length(numPixels),myIndices))=[];
    connComps.NumObjects=length(myIndices);
    myLabels=labelmatrix(connComps);

    %nitrocellulose is in between the 2 areas
    myProfile1=any(myLabels==1,2);
    myProfile2=any(myLabels==2,2);

    myIndicesCombined=[find(myProfile1,1,'first'),
find(myProfile1,1,'last'),find(myProfile2,1,'first'), find(myProfile2,1,'last')];
    myIndicesCombined=sort(myIndicesCombined);
    myStart=myIndicesCombined(2);
    myEnd=myIndicesCombined(3);

    myNC=myLFAgamma(myStart:myEnd,:,:);
    myStructLFAs(i).NC=myNC;

    %now get signal profiles of middle of nitrocellulose
    myFraction=[0.90 0.5]; %get 90% of length and 50% across width
    myVerStart=floor(size(myNC,1)*(1-myFraction(1))/2);
    myVerEnd=size(myNC,1)-myVerStart;
    myHorStart=floor(size(myNC,2)*(1-myFraction(2))/2);
    myHorEnd=size(myNC,2)-myHorStart;
    myProfile=squeeze(mean(myNC(myVerStart:myVerEnd,myHorStart:myHorEnd,:),2)); %profile across
width of strip
    myProfile=-myProfile; %invert profiles
    myStructLFAs(i).Profile=myProfile;
    %now get AUCs
    [myPeaks,myLocs,myWidths,myProms]=findpeaks(myProfile(:,2),'SortStr','descend');
    myPeakStruct=struct('Peaks',myPeaks,'Locs',myLocs,'Widths',myWidths,'Prominances',myProms);
    myStructLFAs(i).AUC=myPeakStruct;
end

%% use LFAs that have 3 lines to determine where to look for lines in the others
myPositives=table([1;2],{5;3:12},'VariableNames',{'Experiment','ImageIndex'});
for p=1:size(myPositives,1) %first find rows of myStructLFAs to consider
    myPositivesRow=myPositives(p,:);
    if p==1
        myIndices=ismember([myStructLFAs.Experiment]',myPositivesRow{1,'Experiment'});
        myIndices=myIndices &
ismember([myStructLFAs.ImageIndex]',myPositivesRow{1,'ImageIndex'}{1,1});
    else
```

```
        myIndices=myIndices |
(ismember([myStructLFAs.Experiment]',myPositivesRow{1,'Experiment'}) &
ismember([myStructLFAs.ImageIndex]',myPositivesRow{1,'ImageIndex'}{1,1}));
    end
end

%then find the location of the 3 lines
myStructLFAsPos=myStructLFAs(myIndices); %RAM inefficient but good enough for now
myPeakStructMax=struct('Control',[],'IAC',[],'Sample',[],'Metadata',[],'Widths',[]);
for i=1:length(myStructLFAsPos)
    myAUCs=myStructLFAsPos(i).AUC;
    myLocs=myAUCs(1).Locs(1:3);
    myPeaks=myAUCs(1).Peaks(1:3);
    myWidths=myAUCs(1).Widths(1:3);

    [myLocs,myIndices]=sort(myLocs,'ascend'); %sort by position
    myPeaks=myPeaks(myIndices);
    myWidths=myWidths(myIndices);

    myPeakStructMax(i).Control=myLocs(1);
    myPeakStructMax(i).IAC=myLocs(2);
    myPeakStructMax(i).Sample=myLocs(3);
    myPeakStructMax(i).Metadata={myLocs,myPeaks, myWidths};
    myPeakStructMax(i).Widths=myWidths;
end

%then figure out where the lines should be:
myLocsMean=mean([[myPeakStructMax.Control]',[myPeakStructMax.IAC]',[myPeakStructMax.Sample]'],1);
myLocsStd=std([[myPeakStructMax.Control]',[myPeakStructMax.IAC]',[myPeakStructMax.Sample]'],[],1)
;
myWidthsMean=mean([myPeakStructMax.Widths]',1);
myWidthsStd=std([myPeakStructMax.Widths]',[],1);

%then establish start and end indices (order is control, IAC, then sample)
myAlpha=0.5; %this is a threshold for what fraction to get
myIndicesStart=myLocsMean-myWidthsMean-tinv(1-
myAlpha,length(myPeakStructMax))*sqrt(myLocsStd.^2+myWidthsStd.^2);
myIndicesEnd=myLocsMean+myWidthsMean+tinv(1-
myAlpha,length(myPeakStructMax))*sqrt(myLocsStd.^2+myWidthsStd.^2);

%background regions between the sample and IAC lines (5) and IAC and
%control lines (4):
myIndicesStart(4:5)=myIndicesEnd(1:2);
myIndicesEnd(4:5)=myIndicesStart(2:3);
myLineWidths=myIndicesEnd-myIndicesStart;

% get AUC for each profile at the locations of the lines for all LFAs
for i=1:length(myStructLFAs)
    myProfile=-double(myStructLFAs(i).Profile); %invert profile
    myAUCgray=nan(size(myIndicesStart));
    for c=1:5 %1-3 are control, IAC, and sample lines; 4 and 5 are the 2 background regions

myAUC=trapz(myProfile(ceil(myIndicesStart(c)):floor(myIndicesEnd(c)),:))./myLineWidths(c); %area
under the curve, normalized to width of line

myAUCgray(c)=trapz(mean(rgb2gray(myProfile(ceil(myIndicesStart(c)):floor(myIndicesEnd(c)),:)),2))
./myLineWidths(c); %area under the curve, normalized, converted to grayscale

        switch c %this area is verbose for readability's sake
            case 1
                myControl=myAUC;
                myStructLFAs(i).AUCcontrol=myControl;
            case 2
                myIAC=myAUC;
                myStructLFAs(i).AUCiac=myIAC;
            case 3
                mySample=myAUC;
                myStructLFAs(i).AUCsample=mySample;
            case 4
                myBG1=myAUC;
                myStructLFAs(i).AUCbg1=myBG1;
```

```
            case 5
                myBG2=myAUC;
                myStructLFAs(i).AUCbg2=myBG2;
                myStructLFAs(i).AUCcombined=[myControl, myIAC, mySample, myBG1, myBG2];
                myStructLFAs(i).AUCgray=1-myAUCgray; %to get into range [0,1]
        end
    end
end

%these are output variables that you can view (double-click them in the
%workspace to see them as a spreadsheet, which you can copy into Excel)
%I (Kamal) used myOutputStructSmall when exporting to excel
myOutputStruct=rmfield(myStructLFAs,{'LFA','NC','Profile','AUC','AUCcontrol','AUCiac','AUCsample'
,'AUCgray'});
myOutputStructSmall=rmfield(myStructLFAs,{'LFA','NC','Profile','AUC','AUCcontrol','AUCiac','AUCsa
mple','AUCcombined','AUCbg1','AUCbg2'});
keyboard
%writetable(struct2table(myOutputStructSmall), 'output data.xlsx');
Return
```

9 Appendix B: Supporting Information for High-Resolution Polymerase Screening via Compartmentalized Self-Replication, Deep Mutational Scanning, and Molecular Dynamics Simulations

9.1 Sequences

9.1.1 Primer Sequences

Name	Sequence (5'-3')
forward CSR-DMS primer	TCTAGAGCTAACGGACGTATACGTAGCCAGCAGCATCCTGCGATG
reverse CSR-DMS primer	CGTTCTCGGTATATGCTGCATACTGCTGCTGCAAAACGTCTGCG
forward AmpliconEZ-recovery primer	ACACTCTTTCCCTACACGACGCTCTTCCGATCTTCTAGAGCTAACGGACGTATACG
reverse AmpliconEZ-recovery primer	GACTGGAGTTCAGACGTGTGCTCTTCCGATCTCGTTCTCGGTATATGCTGCATAC
forward adapter-recovery primer	CCGCGTGATTACGAGTCGTCTAGAGCTAACGGACGTATACG
reverse adapter-recovery primer	GGGTTAGCAAGTGGCAGCCTCGTTCTCGGTATATGCTGCATAC
forward adapter-recovery-CSR primer	CCGCGTGATTACGAGTCGTCTAGAGCTAACGGACGTATACGTAGCCAGCAGCATCCTGCGATG
reverse adapter-recovery-CSR primer	GGGTTAGCAAGTGGCAGCCTCGTTCTCGGTATATGCTGCATACTGCTGCTGCAAAACGTCTGCG
forward index-adapter primer	AATGATACGGCGACCACCGAGATCTACACNNNNNNNNCCGCGTGATTACGAGTCG
reverse index-adapter primer	CAAGCAGAAGACGGCATACGAGATNNNNNNNNGGGTTAGCAAGTGGCAGCCT
forward barcode read primer	CAGGGCGCTGACTTCCGCGTTTCCAGA
reverse barcode read primer	CCTGAGCAACAACATGAATGGTCTTCGGTTTCCGTGTTTCGTAAAG
forward index read primer	ACCGAGAACGAGGCTGCCACTTGCTAACCC
reverse index read primer	CGTCCGTTAGCTCTAGACGACTCGTAATCACGCGG

Table B1. Primer sequences. *Note that read primers were ordered HPLC-purified to minimize crosstalk in Illumina sequencing.*

9.1.2 Thin Fingers Codon-Optimized (TFO) DNA Sequence

CCACTGGAGGAGGCGCCTTGGCCGCCGCCGGAAGGGGCTTTCGTCGGCTTTGTACTCTCGCGCCCGGAACCAATGTGGGCGGAGCTGAAAGCTCTGG

CAGCCTGCCGGGATGGCCGTGTGCATCGGGCAGAAGATCCATTGGCGGGACTGGGTGACCTCGAGGAGGTGCGTGGCCTGCTGGCCAAAGATCTTGC

GGTCCTTGCATTGCGGGAGGGTCTGGATCTGGCTCCTGGGGATGACCCGATGCTGCTGGCTTATCTGCTGGATCCGTCGAATACCACTCCGGAAGGG

GTGGCACGTCGCTACGGGGGTGAATGGACTGAAGATGCCGCCCATCGTGCACTGCTGTCGGAACGTCTGCATCGTAACCTCTTGAAGCGCCTCGAGG

GTGAAGAGAAACTGCTTTGGTTATATCACGAAGTTGAAAAACCGCTCTCTCGTGTTCTGGCGCATATGGAAGCGACCGGGGTACGTTTAGATGTTGC

GTATTTGCAGGCCCTTTCTCTGGAACTTGCGGAAGAAATCCGCCGCCTCGAGGAAGAAGTCTTTCGCTTGGCGGGCCACCCGTTCAACCTGAATTCC

CGTGATCAGCTGGAACGGGTGCTGTTTGATGAGCTTCGTCTTCCGGCCTTGGGAAAAACGCAAAAAACTGGCAAGCGCTCTACCAGTGCTGCGGTGT

TAGAAGCCTTACGTGAGGCGCATCCGATCGTTGAAAAAATTCTCCAGCACCGGGAGCTGACAAAACTGAAAAATACCTATGTGGATCCGTTACCGAG

CTTAGTTCACCCGCGGACGGGCCGCTTGCATACCCGCTTCAATCAAACGGCCACGGCCACGGGTCGTCTGAGTAGCTCGGACCCGAATCTGCAAAAT

ATCCCAGTACGCACACCGTTGGGCCAGCGCATCCGCCGTGCTTTTGTTGCAGAGGCTGGTTGGGCGTTGGTGGCGTTGGATTATAGCCAGATCGAAT

TACGCGTCCTGGCACATTTGTCAGGAGATGAAAACCTGATTCGGGTCTTTCAGGAGGGTAAGGACATTCACACCCAAACCGCAAGCTGGATGTTCGG

CGTCCCGCCGGAAGCGGTTGATCCACTGATGCGGCGGGCAGCGAAAACGATTAACTTTGGCATTGTTTATGGCATGAGTCCGTACGGTCTGGCGAAA

GAACTGAAAATTGGCCGCCGTGAGGCAAAAGCGTTTATCGAACGCTATTTTGAACGCTACCCGGGTGTGAAACGGTATATGGAACAGATTGTGGCTG

AAGCCCGTGAAAAAGGTTATGTGGAGACCCTTTTCGGCCGCCGGCGCTACGTCCCGGACCTGAATGCCCGTGTGAAATCAGTACGTGAAGCAGCGGA

ACGCATGGCCTTTAACATGCCTGTGCAGGGCACCGCCGCAGACCTCATGAAACTCGCAATGGTGAAATTATTCCCTCGCCTCCGTGAGATGGGAGCC

CGCATGTTACTGCAGGTACACGATGAGCTGTTACTGGAGGCGCCACAAGCGCGTGCGGAAGAAGTGGCGGCTTTGGCCAAGGAAGCGATGGAAAAGG

CCTATCCGTTAGCCGTGCCTCTGGAGGTTGAAGTGGGTATCGGGGAGGACTGGCTTTCCGCCAAGGGC

9.1.3 Thin Fingers Polymerase Sequence

PLEEAPWPPPEGAFVGFVLSRPEPMWAELKALAACRDGRVHRAEDPLAGLGDLEEVRGLLAKDLAVLALREGLDLAPGDDPMLLAYLLDPSNTTPEG

VARRYGGEWTEDAAHRALLSERLHRNLLKRLEGEEKLLWLYHEVEKPLSRVLAHMEATGVRLDVAYLQALSLELAEEIRRLEEEVFRLAGHPFNLNS

RDQLERVLFDELRLPALGKTQKTGKRSTSAAVLEALREAHPIVEKILQHRELTKLKNTYVDPLPSLVHPRTGRLHTRFNQTATATGRLSSSDPNLQN

IPVRTPLGQRIRRAFVAEAGWALVALDYSQIELRVLAHLSGDENLIRVFQEGKDIHTQTASWMFGVPPEAVDPLMRRAAKTINFGIVYGMSPYGLAK

ELKIGRREAKAFIERYFERYPGVKRYMEQIVAEAREKGYVETLFGRRRYVPDLNARVKSVREAAERMAFNMPVQGTAADLMKLAMVKLFPRLREMGA

RMLLQVHDELLLEAPQARAEEVAALAKEAMEKAYPLAVPLEVEVGIGEDWLSAKG

9.2 Preliminary Mock Selection (T7 Primers)

9.2.1 Plasmid Construction

TF-WT was cloned into 2B-T plasmid (Addgene plasmid #29666) via ligation-independent cloning and transformed into T7 Express LysY/Iq cells (New England Biolabs C3013I) as previously described[44].

9.2.2 Inactive Mutant Design

TF-WT in 2B-T plasmid was mutated using a Q5 site-directed mutagenesis kit (New England Biolabs E0554) following the manufacturer-recommended protocol. The mutations induced are depicted in **Figure B1**. The D-A mutation was chosen to knock out polymerase activity, as the aspartic acid residue coordinates two magnesium ions essential for catalysis[90]. The two synonymous mutations upstream were included to improve discernment of the two variants by next-generation sequencing and qPCR. TF-XX sequence was verified by Sanger sequencing.

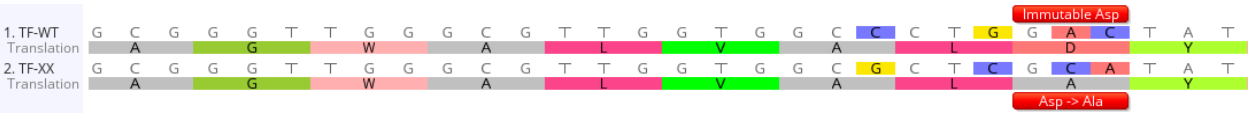

Figure B1. Mutations induced in TF-XX. *Immutable[90] aspartic acid corresponding to D610 in Taq polymerase was mutated to alanine.*

9.2.3 Culture and Expression

Colonies of TF-WT and TF-XX were inoculated into 10mL 2x YT broth with 100µg/mL carbenicillin in 50mL sterile conical tubes covered with AirPore sheets (Qiagen). Cultures were incubated overnight at 30°C, 250rpm. The following morning, 100µL of each culture was subcultured into 10mL fresh media and grown at 37°C until exponential phase was reached (OD600 = 0.4-0.6). Cultures were induced with 0.4mM IPTG and allowed to express for 2 hours. Culture OD600 measurements were taken and equivalents of 0.25mL of each culture at OD600=1.0 were combined (for a final ratio of 1:1 WT:XX cells) and transferred to new microcentrifuge tubes for further processing.

9.2.4 Emulsion PCR

1.2mL of oil phase was prepared fresh for each condition: 54µL Span 80, 4.8µL Tween 80, 0.6µL Triton X-100, and 1140.6µL light mineral oil (all from Sigma Aldrich). Oil phase was aliquoted into 2mL tubes, to each of which a rubber stopper from a 1mL syringe was added, vortexed, and chilled on ice.

0.3mL of aqueous phase was prepared fresh for each condition and chilled on ice: 30µL 10x ThermoPol buffer, 7.8µL of (10mM each) dNTPs, 15µL 10µM T7 forward primer, 15µL 10µM T7 reverse primer, 50µL 6x GuSCN, and 182.2µL water.

The previously aliquoted TF-WT and TF-XX cells were pelleted at 1500g for 15 min. Supernatant was removed and cells were resuspended in 1mL tris-buffered saline (TBS). Cells were pelleted and resuspended in fresh TBS as above once more, then pelleted and resuspended in 0.3mL of ice-cold aqueous phase. The cell-aqueous phase mixtures were then added to the 1.2mL oil phase aliquots and emulsified on a Qiagen TissueLyser LT at 42 Hz for 4 min at 4°C (this step was skipped for solution controls). Following emulsification, 100µL aliquots of emulsions were distributed into PCR tubes (six 100µL tubes per condition) (for solution controls, 80µL oil phase and 20µL cells+aqueous phase were individually added to PCR tubes). Emulsions were placed onto a Bio-Rad T100 thermal cycler and

incubated as follows: 95°C for 1 minute, 20 cycles of (95°C for 10 seconds, 50°C for 15 seconds, 68°C for 3 minutes), 68°C for 8 minutes. Emulsions may be kept at 4°C overnight.

9.2.5 Emulsion Breaking and DNA Purification

Emulsions were combined into a single 1.5mL tube per condition and centrifuged for 10 min at 12,000g. The top oil layer was removed. To the bottom emulsion layer, 150µL (approximately 1:1 v/v) of chloroform was added and vortexed for 10 to 20 seconds, until the bottom layer appeared dissolved. The entire mixture was added to a PhaseLock tube (VWR 10847-802) and centrifuged for 2 min at 16,000g. The top aqueous layer was transferred to a new 1.5mL tube, further purified using an Invitrogen PureLink PCR Purification Kit following the manufacturer recommended instructions, and eluted with the maximum volume of water preheated to 60°C. The eluted DNA was digested with DpnI (New England Biolabs R0176S) following the manufacturer recommended instructions and purified once more with the PureLink kit.

9.2.6 Amplicon Sequencing

233bp amplicons containing the Asp-Ala mutation site and tagged with Illumina sequencing adapters were generated via PCR. 10µL reactions were prepared each containing 1x PrimeTime master mix (Integrated DNA Technologies), 500nM forward primer tagged with Illumina adapter, 500nM reverse primer tagged with Illumina adapter, and 1µL purified mock CSR amplicon. Reactions were placed on a Bio-Rad T100 thermal cycler and incubated at 95°C for 3 minutes and 45 cycles of (95°C for 15 seconds, 60°C for 1 minute). Amplicons were purified with a Monarch PCR Cleanup Kit (New England Biolabs T1030), quantified using a Qubit Broad Range dsDNA Assay (ThermoFisher), and prepared into 25µL aliquots of 20ng/µL adapter-tagged amplicon. A sample for each condition (solution, emulsion, emulsion with 10mM GuSCN, and emulsion with 100mM GuSCN) was submitted for Illumina sequencing using the AmpliconEZ service (Azenta Biosciences).

9.3 Preliminary Mock Selection Demonstrated Insufficient Enrichment of Wild-Type Against Inactive Variant

Our preliminary mock selections attempted CSR amplification of entire polymerase coding sequences instead of barcodes (**Figure B2**). We generated a TF polymerase mutant with an inactivating mutation (TF-XX) and quantified the ability of TF-WT to enrich itself relative to TF-XX after a single round of CSR selection (at various GuSCN concentrations) using primers that bind to the T7 promoter and T7 terminator sites flanking the polymerase coding sequences. Our initial emulsification procedures used only vortexing and appeared to produce emulsions that were not stable under thermal cycling and allowed for leaky replication of the inactive variant (results of early mock selections; not shown). We changed our emulsification protocol to be more vigorous, using a Qiagen TissueLyser LT with a rubber syringe stopper added to aid emulsification, as described in previous publications by the Ellington Group[57,63].

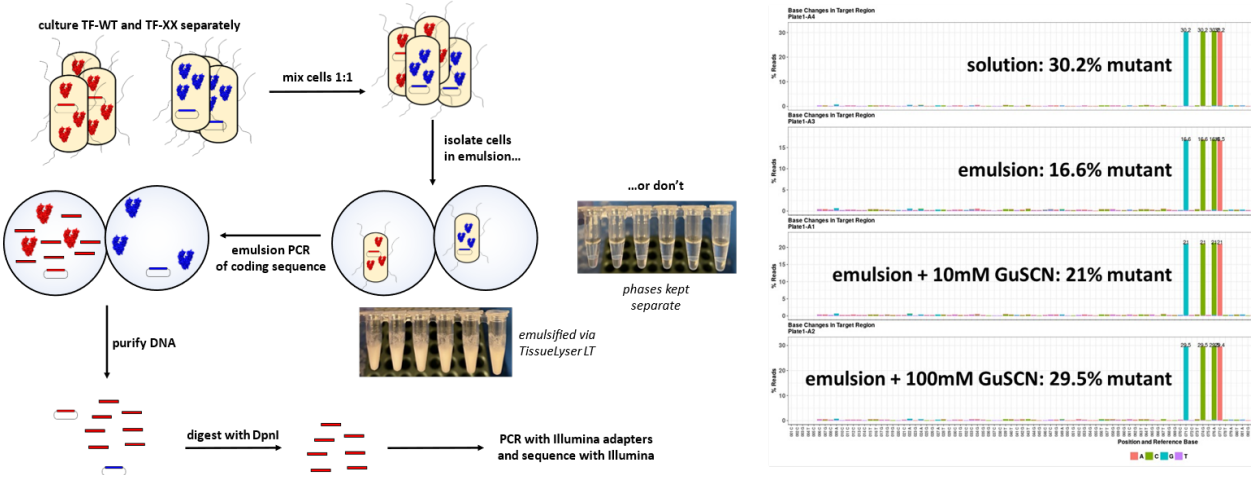

Figure B2. Mock CSR selection performed on TF-WT and TF-XX. *TF-XX is an inactive mutant in which an aspartic acid necessary for function (corresponding to Asp-610 in Taq polymerase)[90] has been changed to alanine. (LEFT) Cultures of TF-WT and TF-XX were induced to express polymerase, mixed 1:1 (cell ratio), and amplified via PCR in solution or in emulsion (CSR) with or without GuSCN. DNA was purified from pre- and post-amplification samples, digested with DpnI to remove genomic and plasmid DNA, amplified with primers tagged with Illumina adapters, and sequenced with Illumina. (RIGHT) Results of mock selection. Each library was sequenced with roughly 200,000 Illumina reads. Percentage of TF-XX reads is shown for each library; the vast majority of remaining reads were of TF-WT.*

After switching to the Tissuelyser LT for emulsification, we learned that TF-WT can slightly enrich itself relative to TF-XX in the emulsion condition relative to a no-emulsion (solution) control, but the

enrichment efficiency was poor relative to examples in the literature that attain selection efficiencies >100-fold[57]. Our mock selection also indicated that GuSCN lowered TF-WT enrichment, which may have been caused by lower TF-WT activity and/or by GuSCN-mediated lysis of *E. coli* before proper emulsification. Further validation of our emulsification protocol using EGFP-expressing cells (described below) suggested that cells withstood emulsification without lysis even in 100mM GuSCN, so we attribute the worsened mock selection enrichment in GuSCN to be caused by lower TF-WT activity. We therefore undertook several steps to attempt to improve CSR enrichment. Various factors that potentially contributed to the poor enrichment observed in these preliminary mock selections are discussed in **Table B2** along with the steps we took to address them before proceeding with the mock selection protocol discussed in the main results section.

Potential Issue	**Commentary / Troubleshooting Methods**
Poor polymerase expression	Polymerase expression had previously been validated in large-volume cultures for bulk purification of polymerase[44,64]. However, we switched to a codon-optimized coding sequence (TFO) to maximize polymerase expression.
Poor cell compartmentalization	We followed emulsification protocols described in a CSR paper from 2018[63] (which used the TissueLyser LT) but used the oil/surfactant mixture described in the original CSR paper from 2001[55] (which used vortexing for emulsification) because the reagents from the former are proprietary and difficult to procure. It is possible that the emulsification protocol could be optimized to accommodate the different oil phase. However, we checked our emulsions via fluorescence microscopy and found that emulsion compartments were within the desired size range and cells did not lyse during emulsification, so we assumed emulsification was not the cause of poor enrichment in preliminary mock selections.
Poor amplification efficiency	For preliminary mock selections, we used T7 primers to amplify the entire polymerase coding sequence. However, these primers were designed for Sanger sequencing to validate cloning steps, and were not validated for efficient PCR. Because they target the T7 promoter and terminator, their template sequences have strong secondary structure, and the amplicon is relatively long at roughly 2kbp. We ultimately circumvented both problems by switching to efficient, pre-screened CSR primers designed to amplify only short barcodes rather than entire coding sequences.

Contamination from plasmid DNA	This problem is minimized when amplification efficiency is high (see above) but also when plasmid DNA is removed from downstream use. To achieve this, we initially used DpnI (a restriction endonuclease specific to methylated DNA) to degrade plasmid and genomic DNA after preliminary mock selections. However, when switching to CSR primers that amplify only barcodes, we added recovery PCR tags to the CSR primers and targeted those tags for downstream sequencing preparation, which helped to prevent carryover of plasmid template DNA. We abandoned use of DpnI for the selections described in the main work, but we note that DpnI is not mutually exclusive with recovery PCR and both could be used to improve signal-to-noise ratios in future CSR-DMS selections.

Table B2. Potential causes of poor enrichment efficiency and steps to troubleshoot.

9.4 Emulsion Validation

9.4.1 Plasmid Construction

Enhanced green fluorescent protein (EGFP)[129] (GenBank: AAB02572.1) was codon-optimized[130] for expression in *E. coli* B, ordered as a gBlock dsDNA fragment (Integrated DNA Technologies) with tags for ligation-independent cloning flanking the coding sequence, cloned into 2B-T plasmid (Addgene plasmid #29666) via ligation-independent cloning[131], and transformed into T7 Express LysY/Iq cells (New England Biolabs C3013I) following the manufacturer protocol.

9.4.2 Culture and Expression

A colony of EGFP was inoculated into 2mL 2x YT broth with 100µg/mL carbenicillin in 14mL sterile round-bottom culture tubes. The culture was incubated overnight at 30°C, 200rpm. The following morning, 100µL of the culture was subcultured into 2mL fresh media and grown at 37°C, 250rpm until exponential phase was reached (OD600 = 0.4-0.6). The culture was induced with 0.4mM IPTG and allowed to express for 2 hours. Culture OD600 measurements were taken and equivalents of 0.5mL of culture at OD600=1.0 were transferred to new microcentrifuge tubes for further processing.

9.4.3 Emulsion Thermal Cycling

1.2mL of oil phase was prepared fresh for each condition: 54µL Span 80, 4.8µL Tween 80, 0.6µL Triton X-100, and 1140.6µL light mineral oil (all from Sigma Aldrich). Oil phase was aliquoted into 2mL tubes, to each of which a rubber stopper from a 1mL syringe was added, vortexed, and chilled on ice.

0.3mL of aqueous phase was prepared fresh for each condition and chilled on ice: 30µL 10x ThermoPol buffer, 7.8µL of (10mM each) dNTPs, 15µL 10µM AmpliconEZ 5950F primer, 15µL 10µM AmpliconEZ 6197R primer, 50µL 6x GuSCN, and 182.2µL water.

The previously aliquoted EGFP cells were pelleted at 1500g for 15 min. Supernatant was removed and cells were resuspended in 1mL tris-buffered saline (TBS). Cells were pelleted and resuspended in fresh TBS as above once more, then pelleted and resuspended in 0.3mL of ice-cold aqueous phase. The cell-aqueous phase mixtures were then added to the 1.2mL oil phase aliquots and emulsified on a Qiagen TissueLyser LT at 42 Hz for 4 min at 4°C. Following emulsification, 100µL of each emulsion was transferred into a PCR tube. Emulsions were placed onto a Bio-Rad T100 thermal cycler and incubated as follows: 95°C for 1 minute, 20 cycles of (95°C for 10 seconds, 68°C for 30 seconds), 68°C for 8 minutes.

9.4.4 Emulsion Microscopy

2µL samples of emulsions were taken before and after thermal cycling, diluted to 100µL with light mineral oil, and gently mixed via pipette. The diluted emulsions were then imaged on a Leica DMIL LED microscope using a 40x objective, phase contrast, and either brightfield or GFP-channel fluorescence.

9.5 Microscopy Validates Emulsion Stability and Compartmentalization of Cells

To determine whether our emulsification procedure had any issues that could cause poor enrichment in a selection, we processed EGFP-expressing cells under emulsification and thermal cycling procedures similar to those used in a selection, then examined the resulting emulsions under a microscope (**Figure B3**). The emulsions appeared to broadly possess the desired characteristics demonstrated in previous

studies[63], including aqueous droplets of roughly 1-10μm in diameter (some distribution is expected), stability under thermal cycling, and <20% of droplets containing a cell. Intact EGFP-expressing cells were visible through the microscope eyepiece at all tested GuSCN concentrations before thermal cycling (and absent after thermal cycling), but were too small, faint, and easily photobleached to easily photograph or conduct image processing, so are not shown here.

These microscopy results seemed to imply that emulsification of the phases and compartmentalization of the cells were both functioning as desired, and that some other defect in the mock selection with T7 primers was responsible for the poor enrichment observed. With that tentative conclusion drawn, we decided to focus on re-designing the CSR primers to amplify a short barcode instead of the entire polymerase gene. We hypothesized that amplification efficiency could significantly improve with this (roughly) 10-fold decrease in amplicon length, especially in a PCR regime where primers and polymerase concentrations are poorly controlled, and that careful screening of CSR primer candidates *in vitro* for sensitivity, specificity, and efficiency (none of which were design considerations for the T7 primers) could yield a primer pair that would exhibit the same characteristics in a CSR experiment and thereby improve CSR yields and enrichment.

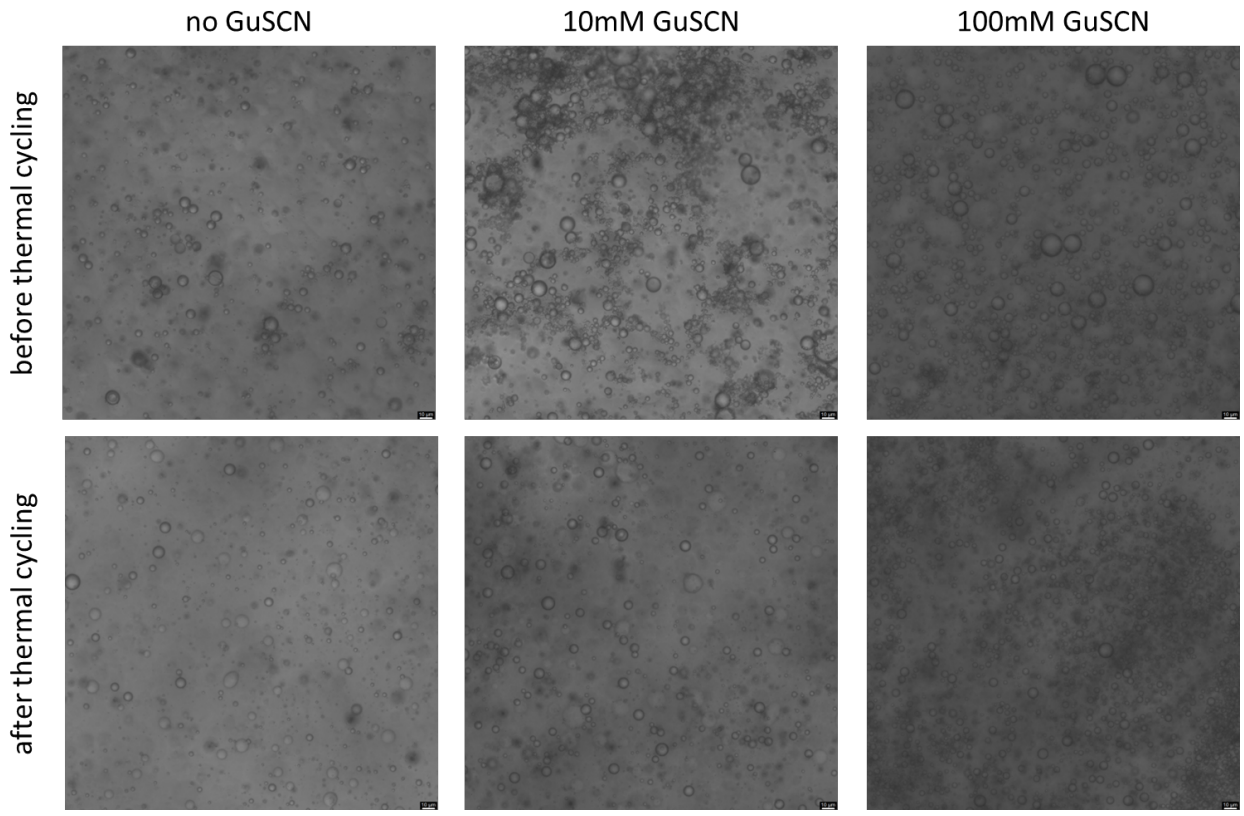

Figure B3. Brightfield images of emulsions before and after thermal cycling. *Emulsions were imaged using a 40x objective. All emulsions showed distinct aqueous compartments within the oil phase medium. Aqueous compartments appeared roughly 1-10µm in diameter (scale bar is 10µm) and persisted through thermal cycling, as desired, regardless of GuSCN concentration.*

9.6 Molecular Dynamics Simulations

A homology model of TF-WT was simulated via *in lucem* molecular mechanics[132,133] (*il*mm) for 40 nanoseconds at 335 K (61.85°C, roughly polymerase extension temperature) or 373 K (99.85°C, roughly PCR denaturation step temperature) solvated in explicit water molecules.

The homology model of TF-WT was constructed by uploading the TF-WT amino acid sequence to the RaptorX web server[97]. The server returned a homology model based on 1TAQ (*Taq* polymerase), which shares 83.5% sequence identity with TF-WT. The model was cleaned through the use of a script ("clean_ilmm_pdb.pl") that removes all non-"ATOM" lines from the file to leave only atomic coordinates, naively assigns "HIE" tautomers to histidine residues (to be re-assigned later), renames non-disulfide-bonded "CYS" residues to "CYH" (TF-WT has no disulfide bonds), ensures all other residues

have canonical names, removes hydrogen atoms, assigns a chain ID as "A" if one is missing, and assigns the C-terminal oxygen as "OT".

Following file cleaning, the model was prepared using the "mmpl" (molecular mechanics parameter library) workbook. This workbook creates an XML library listing each residue and inter-residue bond. Histidine tautomers were predicted by uploading the model to the H++ web server[134] with a salinity of 0.01, pH 8.8, and other options set to defaults and manually checking the resulting structure in UCSF Chimera[99]. All histidines were set to "HIE" tautomers (protonated at the epsilon nitrogen), except His^{112}, His^{121}, His^{151}, His^{243}, and His^{269}, which were set to "HID" tautomers (protonated at the delta nitrogen).

Following library generation, each design was minimized using the *il*mm "minimization" workbook. This workbook populates the PDB file with hydrogens and minimizes them for 500 steps of steepest-descent minimization. It then performs 1000 steps of minimization and finally checks to ensure that no D-amino acids have been created. At first, the workbook consistently added a hydrogen to Lys^{371} to erroneously create a D-amino acid, but the dihedral angles of this residue were minimized using the "wiggle" function in Foldit Standalone[135] before restarting *il*mm preparation, which resulted in Lys^{371} correctly forming an L-amino acid.

Following minimization, each design was prepared for simulation at 335 or 373 K using the "prep" workbook. This workbook solvates the protein in a box of explicit water molecules (with a 10 Å cutoff for water molecule proximity to the model) (water boxes are pre-equilibrated for given temperatures, densities, and pressures). It then minimizes the solvated protein by minimizing all water molecules for 1000 steps, running dynamics simulations of the water for 500 2-femtosecond timesteps, minimizes the water again for 500 steps, and finally minimizes the protein for 500 steps.

Following solvation, starting structures were checked in UCSF Chimera[99] to ensure that the protein looked normal. When the prepped "start.pdb" file was aligned with the original model in Chimera,

Chimera reported an RMSD between all atom pairs of 0.447 and 0.435 Å, respectively, for the 335 K and 373 K starting structures. Each structure was simulated via *il*mm for 40 nanoseconds (with 2-femtosecond step sizes, for a total of 20 million steps) using the Mox supercomputer at the University of Washington.

We used scripts from *il*mm to analyze MD simulations of our structures. For each simulation, we used the *rmsd* module to visualize structure RMSD over time and RMSF by residue, and the *dssp* module to visualize protein secondary structure by residue over time.

9.7 Molecular Dynamics Simulation Results

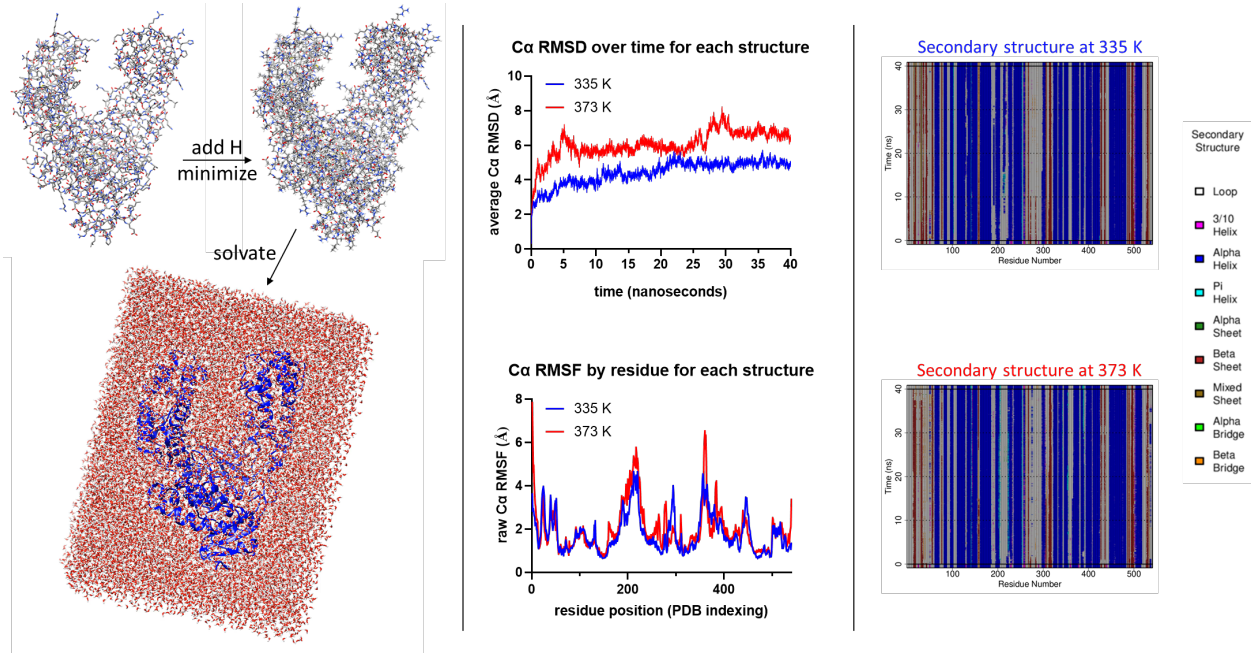

Figure B4. Molecular dynamics setup and preliminary results for TF-WT. *(LEFT) Preparatory steps before simulating a protein in MD. Hydrogen atoms are added to the polymerase model and minimized, then potential energy of all atoms is minimized. Protein is then solvated in explicit water for specific temperatures via a series of minimization and dynamics steps. (CENTER) Cα root-mean-square deviation (RMSD) relative to starting structure for 40ns of simulation. The 373 K simulation displays higher RMSD than the 335 K simulation, demonstrating a correlation between RMSD and temperatures known to inhibit activity. Cα root-mean-square fluctuation (RMSF) relative to starting structure (averaged across 40ns simulation) reveals flexible regions of the protein. (RIGHT) Secondary structure of protein residues throughout 40ns simulations. TF-WT does not lose significant secondary structure at either temperature.*

To provide a means of comparison to CSR-DMS data, we simulated TF-WT with explicitly modeled solvent at various temperatures using the *in lucem* Molecular Mechanics (*il*mm) package developed by

the Daggett Lab, which has been extensively validated[136]. Simulations in pure water at 335 K (61.85°C, typical temperature for thermostable polymerase activity) or 373 K (99.85°C, typical PCR denaturation step temperature) reveal certain regions of the polymerase that are flexible at high temperatures, especially 373 K (**Figure B4**). These regions include the N-terminus (part of the "palm" domain), residues 200-220 of the "thumb" domain, and a short alpha-helical segment (residues 355-365) of the "fingers" domain, all of which play a role in polymerase catalytic activity. These residues may play a role in heat-induced loss of activity and will be compared to CSR-DMS data on heat-sensitive residues.

9.8 Use of TF-WT in Molecular Assays for SARS-CoV-2

While most non-essential research was curtailed early in the pandemic, the Lutz Group developed an RT-LAMP assay and device for detection of SARS-CoV-2 RNA, in which we use TF-WT to amplify three distinct regions of the pathogen genome as a safeguard against diagnostic-escape mutants. A significant portion of our research over the course of the COVID-19 pandemic was devoted to polymerase production for use in our assay, stress-testing in-house devices to run the assay, and production of SARS-CoV-2 RNA to test the assay. Our lab has prepared two articles on this work[44,64]. Furthermore, as part of an effort to shorten the reaction time and evaluate the assay's robustness to lysis agents that might be used for direct amplification, we ran the RT-LAMP assay with various concentrations of GuHCl and found that TF-WT retains activity in GuHCl up to 100mM and may even have enhanced activity relative to zero GuHCl (**Figure B5**). These results bode well for TF-WT's use in direct diagnostics for RNA viruses.

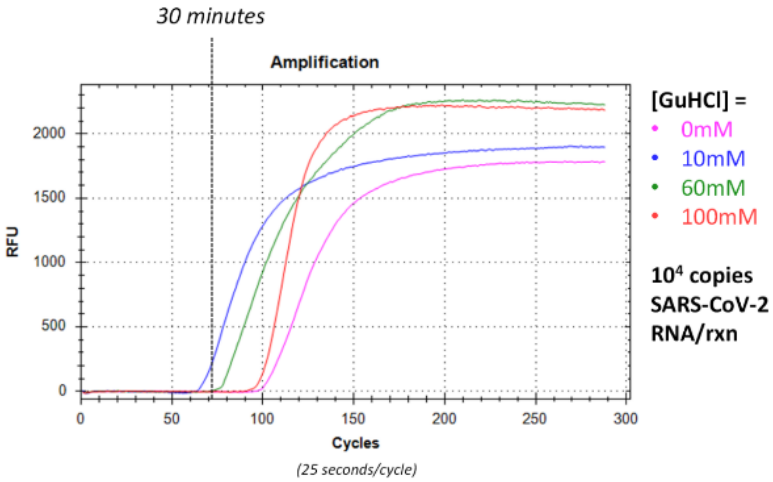

Figure B5. RT-LAMP assay for SARS-CoV-2 RNA using TF-WT polymerase. *Reactions were run using lyophilized reactions containing TF-WT. TF-WT retains activity in 0-100mM concentrations of GuHCl and may be enhanced at low concentrations. We have seen this effect before with dsDNA targets and hypothesized that low-concentration GuHCl helps to lower the melting temperature of dsDNA, but the reproduction of this effect with an RNA target suggests that GuHCl may directly increase TF-WT activity. Another possibility is that GuHCl may weaken RNA secondary structures.*

10 References

(1) Saiki, R. K.; Scharf, S.; Faloona, F.; Mullis, K. B.; Horn, G. T.; Erlich, H. A.; Arnheim, N. Enzymatic Amplification of β-Globin Genomic Sequences and Restriction Site Analysis for Diagnosis of Sickle Cell Anemia. *Science (80-.).* **1985**, *230* (4732), 1350–1354. https://doi.org/10.1126/SCIENCE.2999980.

(2) Mullis, K. B.; Faloona, F. A. Specific Synthesis of DNA in Vitro via a Polymerase-Catalyzed Chain Reaction. *Methods Enzymol.* **1987**, *155* (C), 335–350. https://doi.org/10.1016/0076-6879(87)55023-6.

(3) Saiki, R. K.; Gelfand, D. H.; Stoffel, S.; Scharf, S. J.; Higuchi, R.; Horn, G. T.; Mullis, K. B.; Erlich, H. A. Primer-Directed Enzymatic Amplification of DNA with a Thermostable DNA Polymerase. *Science (80-.).* **1988**, *239* (4839), 487–491. https://doi.org/10.1126/SCIENCE.2448875.

(4) Notomi, T.; Okayama, H.; Masubuchi, H.; Yonekawa, T.; Watanabe, K.; Amino, N.; Hase, T. Loop-Mediated Isothermal Amplification of DNA. *Nucleic Acids Res.* **2000**, *28* (12), E63.

(5) Piepenburg, O.; Williams, C. H.; Stemple, D. L.; Armes, N. A. DNA Detection Using Recombination Proteins. *PLoS Biol.* **2006**, *4* (7), e204. https://doi.org/10.1371/journal.pbio.0040204.

(6) New England BioLabs. Bst 3.0 DNA polymerase https://www.neb.com/products/m0374-bst-3-0-dna-polymerase.

(7) Hull, I. T.; Kline, E. C.; Gulati, G. K.; Kotnik, J. H.; Panpradist, N.; Shah, K. G.; Wang, Q.; Frenkel, L.; Lai, J.; Stekler, J.; Lutz, B. R. Isothermal Amplification with a Target-Mimicking Internal Control and Quantitative Lateral Flow Readout for Rapid HIV Viral Load Testing in Low-Resource Settings. *Anal. Chem.* **2022**, *94* (2), 1011–1021. https://doi.org/10.1021/ACS.ANALCHEM.1C03960.

(8) Hull, I. T.; Kline, E. C.; Gulati, G. K.; Kotnik, J. H.; Panpradist, N.; Shah, K. G.; Wang, Q.; Frenkel, L.; Lai, J.; Stekler, J.; Lutz, B. R. Addition to "Isothermal Amplification with a Target-Mimicking Internal Control and Quantitative Lateral Flow Readout for Rapid HIV Viral Load Testing in Low-Resource Settings." *Anal. Chem.* **2022**, *94* (15), 6071–6071. https://doi.org/10.1021/ACS.ANALCHEM.2C01256.

(9) Niemz, A.; Ferguson, T. M.; Boyle, D. S. Point-of-Care Nucleic Acid Testing for Infectious Diseases. *Trends Biotechnol.* **2011**, *29* (5), 240–250. https://doi.org/10.1016/j.tibtech.2011.01.007.

(10) Obande, G. A.; Singh, K. K. B. Current and Future Perspectives on Isothermal Nucleic Acid Amplification Technologies for Diagnosing Infections. *Infect. Drug Resist.* **2020**, *13*, 483. https://doi.org/10.2147/IDR.S217571.

(11) Jansson, L.; Hedman, J. Challenging the Proposed Causes of the PCR Plateau Phase. *Biomol. Detect. Quantif.* **2019**, *17*, 100082. https://doi.org/10.1016/J.BDQ.2019.100082.

(12) Lillis, L.; Lehman, D.; Singhal, M. C.; Cantera, J.; Singleton, J.; Labarre, P.; Toyama, A.; Piepenburg, O.; Parker, M.; Wood, R.; Overbaugh, J.; Boyle, D. S. Non-Instrumented Incubation of a Recombinase Polymerase Amplification Assay for the Rapid and Sensitive Detection of Proviral HIV-1 DNA. *PLoS One* **2014**, *9* (9), e108189. https://doi.org/10.1371/journal.pone.0108189.

(13) Lillis, L.; Siverson, J.; Lee, A.; Cantera, J.; Parker, M.; Piepenburg, O.; Lehman, D. A.; Boyle, D. S. Factors Influencing Recombinase Polymerase Amplification (RPA) Assay Outcomes at Point of Care. **2016**, *30* (2). https://doi.org/10.1016/j.mcp.2016.01.009.

(14) World Health Organization. *Consolidated Guidelines on the Use of Antiretroviral Drugs for Treating and Preventing HIV Infection: Recommendations for a Public Health Approach*, 2nd ed.; World Health Organization: Geneva, 2016.

(15) Centers for Disease Control and Prevention. HIV Treatment as Prevention https://www.cdc.gov/hiv/risk/art/index.html (accessed Aug 23, 2021).

(16) Institute for Health Metrics and Evaluation. GBD Results Tool http://ghdx.healthdata.org/gbd-results-tool (accessed Aug 20, 2021).

(17) Mazzola, L. T.; Pérez-Casas, C. *HIV/AIDS Diagnostics Technology Landscape, 5th Edition*; Geneva, Switzerland, 2015.

(18) UNAIDS. *Ending AIDS: Progress towards the 90–90–90 Targets*; 2017.

(19) UNAIDS. *UNAIDS DATA 2017*; 2017.

(20) Drain, P. K.; Dorward, J.; Bender, A.; Lillis, L.; Marinucci, F.; Sacks, J.; Bershteyn, A.; Boyle, D. S.; Posner, J. D.; Garrett, N. Point-of-Care HIV Viral Load Testing: An Essential Tool for a Sustainable Global HIV/AIDS Response. *Clin. Microbiol. Rev.* **2019**, *32* (3), e00097-18. https://doi.org/10.1128/CMR.00097-18.

(21) Crannell, Z. A.; Rohrman, B.; Richards-Kortum, R. Quantification of HIV-1 DNA Using Real-Time Recombinase Polymerase Amplification. *Anal. Chem.* **2014**, *86* (12), 5615–5619. https://doi.org/10.1021/ac5011298.

(22) Boyle, D. S.; Lehman, D. A.; Lillis, L.; Peterson, D.; Singhal, M.; Armes, N.; Parker, M.; Piepenburg, O.; Overbaugh, J. Rapid Detection of HIV-1 Proviral DNA for Early Infant Diagnosis Using Recombinase Polymerase Amplification. *MBio* **2013**, *4* (2), e00135-13.

https://doi.org/10.1128/mBio.00135-13.

(23) Nycz, C. M.; Dean, C. H.; Haaland, P. D.; Spargo, C. A.; Walker, G. T. Quantitative Reverse Transcription Strand Displacement Amplification: Quantitation of Nucleic Acids Using an Isothermal Amplification Technique. *Anal. Biochem.* **1998**, *259* (2), 226–234. https://doi.org/10.1006/ABIO.1998.2641.

(24) Piatak, M.; Saag, M.; Yang, L.; Clark, S.; Kappes, J.; Luk, K.; Hahn, B.; Shaw, G.; Lifson, J. High Levels of HIV-1 in Plasma during All Stages of Infection Determined by Competitive PCR. *Science (80-.).* **1993**, *259* (5102), 1749–1754. https://doi.org/10.1126/science.8096089.

(25) Los Alamos National Laboratory. HIV Sequence Database https://www.hiv.lanl.gov/content/sequence/HIV/mainpage.html (accessed May 8, 2018).

(26) Mathworks. MATLAB R2019a. The Mathworks, Inc.: Natick, Massachusetts 2019.

(27) d'Agostino, R. B. Tests for Normal Distribution. In *Goodness-Of-Fit Techniques*; d'Agostino, R. B., Stephens, M. A., Eds.; Marcel Dekker: New York, NY, 1986.

(28) Schneider, C. A.; Rasband, W. S.; Eliceiri, K. W. NIH Image to ImageJ: 25 Years of Image Analysis. *Nat. Methods* **2012**, *9* (7), 675. https://doi.org/10.1038/NMETH.2089.

(29) Moody, C.; Newell, H.; Viljoen, H. A Mathematical Model of Recombinase Polymerase Amplification under Continuously Stirred Conditions. *Biochem. Eng. J.* **2016**, *112*, 193–201. https://doi.org/10.1016/J.BEJ.2016.04.017.

(30) Arezi, B.; Xing, W.; Sorge, J. A.; Hogrefe, H. H. Amplification Efficiency of Thermostable DNA Polymerases. *Anal. Biochem.* **2003**, *321* (2), 226–235. https://doi.org/10.1016/S0003-2697(03)00465-2.

(31) Park, C.; Ngo, H.; Lavitt, L. R.; Karuri, V.; Bhatt, S.; Lubell-Doughtie, P.; Shankar, A. H.; Ndwiga, L.; Osoti, V.; Wambua, J. K.; Bejon, P.; Ochola-Oyier, L. I.; Chilver, M.; Stocks, N.; Lyon, V.; Lutz, B. R.; Thompson, M.; Mariakakis, A.; Patel, S. The Design and Evaluation of a Mobile System for Rapid Diagnostic Test Interpretation. *Proc. ACM Interactive, Mobile, Wearable Ubiquitous Technol.* **2021**, *5* (1), 1–26.

(32) Mathieu-Daudé, F.; Welsh, J.; Vogt, T.; McClelland, M. DNA Rehybridization During PCR: The 'C o t Effect' and Its Consequences. *Nucleic Acids Res.* **1996**, *24* (11), 2080–2086. https://doi.org/10.1093/NAR/24.11.2080.

(33) Tyagi, S.; Kramer, F. R. Molecular Beacons: Probes That Fluoresce upon Hybridization. *Nat. Biotechnol.* **1996**, *14* (3), 303–308. https://doi.org/10.1038/nbt0396-303.

(34) Lukhtanov, E. A.; Lokhov, S. G.; Gorn, V. V; Podyminogin, M. A.; Mahoney, W. Novel DNA Probes with Low Background and High Hybridization-Triggered Fluorescence. *Nucleic Acids Res.* **2007**, *35* (5), e30. https://doi.org/10.1093/nar/gkl1136.

(35) Wang, L.; Yang, C. J.; Medley, C. D.; Benner, S. A.; Tan, W. Locked Nucleic Acid Molecular Beacons. *J. Am. Chem. Soc.* **2005**, *127* (45), 15664–15665. https://doi.org/10.1021/JA052498G.

(36) Kersting, S.; Rausch, V.; Bier, F. F.; von Nickisch-Rosenegk, M. Rapid Detection of Plasmodium Falciparum with Isothermal Recombinase Polymerase Amplification and Lateral Flow Analysis. *Malar. J.* **2014**, *13* (1), 99. https://doi.org/10.1186/1475-2875-13-99.

(37) Rohrman, B.; Richards-Kortum, R. Inhibition of Recombinase Polymerase Amplification by Background DNA: A Lateral Flow-Based Method for Enriching Target DNA. *Anal. Chem.* **2015**, *87* (3), 1963–1967. https://doi.org/10.1021/ac504365v.

(38) Hemelaar, J.; Loganathan, S.; Elangovan, R.; Yun, J.; Dickson-Tetteh, L.; Kirtley, S.; WHO-UNAIDS Network for HIV Isolation and Characterization. Country Level Diversity of the HIV-1 Pandemic between 1990 and 2015. *J. Virol.* **2020**, *95* (2), e01580-20. https://doi.org/10.1128/JVI.01580-20.

(39) Davey, R. T.; Bhat, N.; Yoder, C.; Chun, T.-W.; Metcalf, J. A.; Dewar, R.; Natarajan, V.; Lempicki, R. A.; Adelsberger, J. W.; Miller, K. D.; Kovacs, J. A.; Polis, M. A.; Walker, R. E.; Falloon, J.; Masur, H.; Gee, D.; Baseler, M.; Dimitrov, D. S.; Fauci, A. S.; Lane, H. C. HIV-1 and T Cell Dynamics after Interruption of Highly Active Antiretroviral Therapy (HAART) in Patients with a History of Sustained Viral Suppression. *Proc. Natl. Acad. Sci.* **1999**, *96* (26), 15109–15114. https://doi.org/10.1073/PNAS.96.26.15109.

(40) Ritchie, A. V.; Ushiro-Lumb, I.; Edemaga, D.; Joshi, H. A.; De Ruiter, A.; Szumilin, E.; Jendrulek, I.; McGuire, M.; Goel, N.; Sharma, P. I.; Allain, J. P.; Lee, H. H. SAMBA HIV Semiquantitative Test, a New Point-of-Care Viral-Load-Monitoring Assay for Resource-Limited Settings. *J. Clin. Microbiol.* **2014**, *52* (9), 3377–3383. https://doi.org/10.1128/JCM.00593-14.

(41) Panpradist, N.; Beck, I. A.; Vrana, J.; Higa, N.; McIntyre, D.; Ruth, P. S.; So, I.; Kline, E. C.; Kanthula, R.; Wong-On-Wing, A.; Lim, J.; Ko, D.; Milne, R.; Rossouw, T.; Feucht, U. D.; Chung, M.; Jourdain, G.; Ngo-Giang-Huong, N.; Laomanit, L.; Soria, J.; Lai, J.; Klavins, E. D.; Frenkel, L. M.; Lutz, B. R. OLA-Simple: A Software-Guided HIV-1 Drug Resistance Test for Low-Resource Laboratories. *EBioMedicine* **2019**, *50*, 34–44. https://doi.org/10.1016/j.ebiom.2019.11.002.

(42) Panpradist, N.; Wang, Q.; Ruth, P. S.; Kotnik, J. H.; Oreskovic, A. K.; Miller, A.; Stewart, S. W. A.; Vrana, J.; Han, P. D.; Beck, I. A.; Starita,

L. M.; Frenkel, L. M.; Lutz, B. R. Simpler and Faster Covid-19 Testing: Strategies to Streamline SARS-CoV-2 Molecular Assays. *EBioMedicine* **2021**, *64*, 103236. https://doi.org/10.1016/J.EBIOM.2021.103236.

(43) Vrana, J. D.; Panpradist, N.; Higa, N.; Ko, D.; Ruth, P.; Kanthula, R.; Lai, J. J.; Yang, Y.; Sakr, S. R.; Chohan, B.; Chung, M. H.; Frenkel, L. M.; Lutz, B. R.; Klavins, E.; Beck, I. A.; Klavins Biosystems, E. Implementation of an Interactive Mobile Application to Pilot a Rapid Assay to Detect HIV Drug Resistance Mutations in Kenya. *medRxiv* **2021**, 2021.05.06.21256654. https://doi.org/10.1101/2021.05.06.21256654.

(44) Panpradist, N.; Kline, E.; Atkinson, R. G.; Roller, M.; Wang, Q.; Hull, I. T.; Kotnik, J. H.; Oreskovic, A. K.; Bennett, C.; Leon, D.; Lyon, V.; Gilligan-Steinberg, S. D.; Han, P. D.; Drain, P. K.; Starita, L. M.; Thompson, M. J.; Lutz, B. R. Harmony COVID-19: A Ready-to-Use Kit, Low-Cost Detector, and Smartphone App for Point-of-Care SARS-CoV-2 RNA Detection. *Sci. Adv.* **2021**, *7* (51), eabj1281. https://doi.org/10.1126/sciadv.abj1281.

(45) Rodriguez, N. M.; Linnes, J. C.; Fan, A.; Ellenson, C. K.; Pollock, N. R.; Klapperich, C. M. Paper-Based RNA Extraction, in Situ Isothermal Amplification, and Lateral Flow Detection for Low-Cost, Rapid Diagnosis of Influenza A (H1N1) from Clinical Specimens. *Anal. Chem.* **2015**, *87* (15), 7872–7879. https://doi.org/10.1021/ACS.ANALCHEM.5B01594.

(46) Phillips, E. A.; Moehling, T. J.; Ejendal, K. F. K.; Hoilett, O. S.; Byers, K. M.; Basing, L. A.; Jankowski, L. A.; Bennett, J. B.; Lin, L. K.; Stanciu, L. A.; Linnes, J. C. Microfluidic Rapid and Autonomous Analytical Device (MicroRAAD) to Detect HIV from Whole Blood Samples. *Lab Chip* **2019**, *19* (20), 3375–3386. https://doi.org/10.1039/C9LC00506D.

(47) Lillis, L.; Lehman, D. A.; Siverson, J. B.; Weis, J.; Cantera, J.; Parker, M.; Piepenburg, O.; Overbaugh, J.; Boyle, D. S. Cross-Subtype Detection of HIV-1 Using Reverse Transcription and Recombinase Polymerase Amplification. *J. Virol. Methods* **2016**, *230*, 28–35.

(48) Qian, J.; Boswell, S. A.; Chidley, C.; Lu, Z.; Pettit, M. E.; Gaudio, B. L.; Fajnzylber, J. M.; Ingram, R. T.; Ward, R. H.; Li, J. Z.; Springer, M. An Enhanced Isothermal Amplification Assay for Viral Detection. *Nat. Commun.* **2020**, *11* (1), 5920. https://doi.org/10.1038/s41467-020-19258-y.

(49) Piatak, M.; Luk, K. C.; Williams, B.; Lifson, J. D. Quantitative Competitive Polymerase Chain Reaction for Accurate Quantitation of HIV DNA and RNA Species. *Biotechniques* **1993**, *14* (1), 70–81.

(50) Wong, Y. P.; Othman, S.; Lau, Y. L.; Radu, S.; Chee, H. Y. Loop-Mediated Isothermal Amplification (LAMP): A Versatile Technique for Detection of Micro-Organisms. *J. Appl. Microbiol.* **2018**, *124* (3), 626–643. https://doi.org/10.1111/JAM.13647.

(51) Curtis, K. A.; Rudolph, D. L.; Owen, S. M. Rapid Detection of HIV-1 by Reverse-Transcription, Loop-Mediated Isothermal Amplification (RT-LAMP). *J. Virol. Methods* **2008**, *151* (2), 264–270. https://doi.org/10.1016/j.jviromet.2008.04.011.

(52) Mancuso, C. P.; Lu, Z. X.; Qian, J.; Boswell, S. A.; Springer, M. A Semi-Quantitative Isothermal Diagnostic Assay Utilizing Competitive Amplification. *Anal. Chem.* **2021**, *93* (27), 9541–9548.

(53) Pezza, J. A.; Kucera, R.; Sun, L.; New England BioLabs. Polymerase Fidelity: What is it, and what does it mean for your PCR? https://www.neb.com/tools-and-resources/feature-articles/polymerase-fidelity-what-is-it-and-what-does-it-mean-for-your-pcr (accessed Apr 28, 2022).

(54) Chen, T.; Romesberg, F. E. Directed Polymerase Evolution. *FEBS Letters*. January 21, 2014, pp 219–229. https://doi.org/10.1016/j.febslet.2013.10.040.

(55) Ghadessy, F. J.; Ong, J. L.; Holliger, P. Directed Evolution of Polymerase Function by Compartmentalized Self-Replication. *Proc. Natl. Acad. Sci. U. S. A.* **2001**, *98* (8), 4552–4557. https://doi.org/10.1073/pnas.071052198.

(56) Ellefson, J. W.; Gollihar, J.; Shroff, R.; Shivram, H.; Iyer, V. R.; Ellington, A. D. Synthetic Evolutionary Origin of a Proofreading Reverse Transcriptase. *Science* **2016**, *352* (6293), 1590–1593. https://doi.org/10.1126/science.aaf5409.

(57) Milligan, J. N.; Shroff, R.; Garry, D. J.; Ellington, A. D. Evolution of a Thermophilic Strand-Displacing Polymerase Using High-Temperature Isothermal Compartmentalized Self-Replication. *Biochemistry* **2018**, *57* (31), 4607–4619. https://doi.org/10.1021/acs.biochem.8b00200.

(58) Arezi, B.; McKinney, N.; Hansen, C.; Cayouette, M.; Fox, J.; Chen, K.; Lapira, J.; Hamilton, S.; Hogrefe, H. Compartmentalized Self-Replication under Fast PCR Cycling Conditions Yields Taq DNA Polymerase Mutants with Increased DNA-Binding Affinity and Blood Resistance. *Front. Microbiol.* **2014**, *5*, 408. https://doi.org/10.3389/fmicb.2014.00408.

(59) Araya, C. L.; Fowler, D. M. Deep Mutational Scanning: Assessing Protein Function on a Massive Scale. *Trends in Biotechnology*. September 2011, pp 435–442. https://doi.org/10.1016/j.tibtech.2011.04.003.

(60) Fowler, D. M.; Fields, S. Deep Mutational Scanning: A New Style of Protein Science. *Nat. Methods* **2014**, *11* (8), 801–807. https://doi.org/10.1038/nmeth.3027.

(61) Nikoomanzar, A.; Vallejo, D.; Chaput, J. C. Elucidating the Determinants of Polymerase Specificity by Microfluidic-Based Deep Mutational Scanning. *ACS Synth. Biol.* **2019**, *8* (6), 1421–1429. https://doi.org/10.1021/acssynbio.9b00104.

(62) Nikoomanzar, A.; Vallejo, D.; Yik, E. J.; Chaput, J. C. Programmed Allelic Mutagenesis of a DNA Polymerase with Single Amino Acid Resolution. *ACS Synth. Biol.* **2020**, *9* (7), 1873–1881. https://doi.org/10.1021/ACSSYNBIO.0C00236/ASSET/IMAGES/LARGE/SB0C00236_0006.JPEG.

(63) Abil, Z.; Ellington, A. D. Compartmentalized Self-Replication for Evolution of a DNA Polymerase. *Curr. Protoc. Chem. Biol.* **2018**, *10* (1), 1–17. https://doi.org/10.1002/cpch.34.

(64) Kline, E. C.; Panpradist, N.; Hull, I. T.; Wang, Q.; Oreskovic, A. K.; Han, P. D.; Starita, L. M.; Lutz, B. R. Multiplex Target-Redundant RT-LAMP for Robust Detection of SARS-CoV-2 Using Fluorescent Universal Displacement Probes. *Microbiol. Spectr.* **2022**, *10* (4). https://doi.org/10.1128/spectrum.01583-21.

(65) Dineva, M. A.; Mahilum-Tapay, L.; Lee, H. Sample Preparation: A Challenge in the Development of Point-of-Care Nucleic Acid-Based Assays for Resource-Limited Settings. *Analyst* **2007**, *132* (12), 1193. https://doi.org/10.1039/b705672a.

(66) Walker, F. M.; Hsieh, K. Advances in Directly Amplifying Nucleic Acids from Complex Samples. *Biosensors*. NLM (Medline) September 30, 2019. https://doi.org/10.3390/bios9040117.

(67) Hayashida, K.; Kajino, K.; Hachaambwa, L.; Namangala, B.; Sugimoto, C. Direct Blood Dry LAMP: A Rapid, Stable, and Easy Diagnostic Tool for Human African Trypanosomiasis. *PLoS Negl. Trop. Dis.* **2015**, *9* (3), e0003578. https://doi.org/10.1371/journal.pntd.0003578.

(68) Daher, R. K.; Stewart, G.; Boissinot, M.; Bergeron, M. G. Recombinase Polymerase Amplification for Diagnostic Applications. *Clin. Chem.* **2016**, *62* (7), 947–958. https://doi.org/10.1373/clinchem.2015.245829.

(69) Poltronieri, P.; Sun, B.; Mallardo, M. RNA Viruses: RNA Roles in Pathogenesis, Coreplication and Viral Load. *Curr. Genomics* **2015**, *16* (5), 327–335. https://doi.org/10.2174/1389202916666150707160613.

(70) Hasselmann, D. O.; Rappl, G.; Tilgen, W.; Reinhold, U. Stability of Endogenous and Added RNA in Blood Specimens, Serum, and Plasma. *Clin. Chem.* **2001**, *47* (8), 1488–1489.

(71) Horak, D.; Rittich, B.; Safar, J.; Spanova, A.; Lenfeld, J.; Benes, M. J. Properties of RNase A Immobilized on Magnetic Poly(2-Hydroxyethyl Methacrylate) Microspheres. *Biotechnol. Prog.* **2001**, *17* (3), 447–452. https://doi.org/10.1021/bp0100171.

(72) Brisco, M. J.; Morley, A. A. Quantification of RNA Integrity and Its Use for Measurement of Transcript Number. *Nucleic Acids Res.* **2012**, *40* (18), e144–e144. https://doi.org/10.1093/nar/gks588.

(73) Boom, R.; Sol, C. J.; Salimans, M. M.; Jansen, C. L.; Wertheim-van Dillen, P. M.; van der Noordaa, J. Rapid and Simple Method for Purification of Nucleic Acids. *J. Clin. Microbiol.* **1990**, *28* (3), 495–503.

(74) Bennion, B. J.; Daggett, V. The Molecular Basis for the Chemical Denaturation of Proteins by Urea. *Proc. Natl. Acad. Sci. U. S. A.* **2003**, *100* (9), 5142–5147. https://doi.org/10.1073/pnas.0930122100.

(75) Zou, Q.; Bennion, B. J.; Daggett, V.; Murphy, K. P. The Molecular Mechanism of Stabilization of Proteins by TMAO and Its Ability to Counteract the Effects of Urea. *J. Am. Chem. Soc.* **2002**, *124* (7), 1192–1202. https://doi.org/10.1021/ja004206b.

(76) Salvi, G.; De Los Rios, P.; Vendruscolo, M. Effective Interactions between Chaotropic Agents and Proteins. *Proteins Struct. Funct. Bioinforma.* **2005**, *61* (3), 492–499. https://doi.org/10.1002/prot.20626.

(77) Pitcher, D. G.; Saunders, N. A.; Owen, R. J. Rapid Extraction of Bacterial Genomic DNA with Guanidium Thiocyanate. *Lett. Appl. Microbiol.* **1989**, *8* (4), 151–156. https://doi.org/10.1111/j.1472-765X.1989.tb00262.x.

(78) Chirgwin, J. M.; Przybyla, A. E.; MacDonald, R. J.; Rutter, W. J. Isolation of Biologically Active Ribonucleic Acid from Sources Enriched in Ribonuclease. *Biochemistry* **1979**, *18* (24), 5294–5299. https://doi.org/10.1021/bi00591a005.

(79) Mccord, B.; Pionzio, A.; Thompson, R. *Analysis of the Effect of a Variety of PCR Inhibitors on the Amplification of DNA Using Real Time PCR, Melt Curves and STR Analysis*; 2015.

(80) Cox, R. A. The Use of Guanidinium Chloride in the Isolation of Nucleic Acids. *Methods Enzymol.* **1968**, *12* (PART B), 120–129. https://doi.org/10.1016/0076-6879(67)12123-X.

(81) Sela, M.; Anfinsen, C. B.; Harrington, W. F. The Correlation of Ribonuclease Activity with Specific Aspects of Tertiary Structure. *BBA - Biochim. Biophys. Acta* **1957**, *26* (3), 502–512. https://doi.org/10.1016/0006-3002(57)90096-3.

(82) Goto, M.; Honda, E.; Ogura, A.; Nomoto, A.; Hanaki, K.-I. Colorimetric Detection of Loop-Mediated Isothermal Amplification Reaction by Using Hydroxy Naphthol Blue. *Biotechniques* **2009**, *46* (3), 167–172. https://doi.org/10.2144/000113072.

(83) Seyrig, G.; Stedtfeld, R. D.; Tourlousse, D. M.; Ahmad, F.; Towery, K.; Cupples, A. M.; Tiedje, J. M.; Hashsham, S. A. Selection of Fluorescent DNA Dyes for Real-Time LAMP with Portable and Simple Optics. *J. Microbiol. Methods* **2015**, *119*, 223–227. https://doi.org/10.1016/j.mimet.2015.11.004.

(84) Kusumawati, A.; Tampubolon, I. D.; Hendarta, N. Y.; Salasia, S. I. O.; Wanahari, T. A.; Mappakaya, B. A.; Hartati, S. Use of Reverse

Transcription Loop-Mediated Isothermal Amplification Combined with Lateral Flow Dipstick for an Easy and Rapid Detection of Jembrana Disease Virus. *VirusDisease* **2015**, *26* (3), 189–195. https://doi.org/10.1007/s13337-015-0277-5.

(85) Toley, B. J.; Covelli, I.; Belousov, Y.; Ramachandran, S.; Kline, E.; Scarr, N.; Vermeulen, N.; Mahoney, W.; Lutz, B. R.; Yager, P. Isothermal Strand Displacement Amplification (ISDA): A Rapid and Sensitive Method of Nucleic Acid Amplification for Point-of-Care Diagnosis. *Analyst* **2015**, *140* (22), 7540–7549. https://doi.org/10.1039/C5AN01632K.

(86) Manning, M.; Colón, W. Structural Basis of Protein Kinetic Stability: Resistance to Sodium Dodecyl Sulfate Suggests a Central Role for Rigidity and a Bias toward β-Sheet Structure. *Biochemistry* **2004**, *43* (35), 11248–11254. https://doi.org/10.1021/bi0491898.

(87) Kurzban, G. P.; Bayer, E. A.; Wilchek, M.; Horowitz, P. M. The Quaternary Structure of Streptavidin in Urea. *J. Biol. Chem.* **1991**, *266* (22), 14470–14477.

(88) Das, M.; Dasgupta, D. Enhancement of Transcriptional Activity of T7 RNA Polymerase by Guanidine Hydrochloride. *FEBS Lett.* **1998**, *427* (3), 337–340. https://doi.org/10.1016/S0014-5793(98)00458-X.

(89) Ye, J.; Coulouris, G.; Zaretskaya, I.; Cutcutache, I.; Rozen, S.; Madden, T. L. Primer-BLAST: A Tool to Design Target-Specific Primers for Polymerase Chain Reaction. *BMC Bioinformatics* **2012**, *13*, 134. https://doi.org/10.1186/1471-2105-13-134.

(90) Patel, P. H.; Loeb, L. A. DNA Polymerase Active Site Is Highly Mutable: Evolutionary Consequences. *Proc. Natl. Acad. Sci. U. S. A.* **2000**, *97* (10), 5095–5100. https://doi.org/10.1073/pnas.97.10.5095.

(91) Geissmann, Q. OpenCFU, a New Free and Open-Source Software to Count Cell Colonies and Other Circular Objects. *PLoS One* **2013**, *8* (2). https://doi.org/10.1371/JOURNAL.PONE.0054072.

(92) Li, H. Aligning Sequence Reads, Clone Sequences and Assembly Contigs with BWA-MEM. *arXiv* **2013**, 1–3.

(93) Yeh, C. L. C.; Amorosi, C. J.; Showman, S.; Dunham, M. J. PacRAT: A Program to Improve Barcode-Variant Mapping from PacBio Long Reads Using Multiple Sequence Alignment. *Bioinformatics* **2022**, *38* (10), 2927–2929. https://doi.org/10.1093/BIOINFORMATICS/BTAC165.

(94) Zhang, J.; Kobert, K.; Flouri, T.; Stamatakis, A. PEAR: A Fast and Accurate Illumina Paired-End ReAd MergeR. *Bioinformatics* **2014**, *30* (5), 614–620. https://doi.org/10.1093/BIOINFORMATICS/BTT593.

(95) Rubin, A. F.; Gelman, H.; Lucas, N.; Bajjalieh, S. M.; Papenfuss, A. T.; Speed, T. P.; Fowler, D. M. A Statistical Framework for Analyzing Deep Mutational Scanning Data. *Genome Biol.* **2017**, *18* (1), 1–15. https://doi.org/10.1186/S13059-017-1272-5/FIGURES/7.

(96) Chander, Y.; Koelbl, J.; Puckett, J.; Moser, M. J.; Klingele, A. J.; Liles, M. R.; Carrias, A.; Mead, D. A.; Schoenfeld, T. W. A Novel Thermostable Polymerase for RNA and DNA Loop-Mediated Isothermal Amplification (LAMP). *Front. Microbiol.* **2014**, *5*, 395. https://doi.org/10.3389/fmicb.2014.00395.

(97) Källberg, M.; Wang, H.; Wang, S.; Peng, J.; Wang, Z.; Lu, H.; Xu, J. Template-Based Protein Structure Modeling Using the RaptorX Web Server. *Nat. Protoc. 2012 78* **2012**, *7* (8), 1511–1522. https://doi.org/10.1038/nprot.2012.085.

(98) Kim, Y.; Eom, S. H.; Wang, J.; Lee, D. S.; Suh, S. W.; Steitz, T. A. Crystal Structure of Thermus Aquaticus DNA Polymerase. *Nat. 1995 3766541* **1995**, *376* (6541), 612–616. https://doi.org/10.1038/376612a0.

(99) Pettersen, E. F.; Goddard, T. D.; Huang, C. C.; Couch, G. S.; Greenblatt, D. M.; Meng, E. C.; Ferrin, T. E. UCSF Chimera - A Visualization System for Exploratory Research and Analysis. *J. Comput. Chem.* **2004**, *25* (13), 1605–1612. https://doi.org/10.1002/jcc.20084.

(100) Fowler, D. M.; Stephany, J. J.; Fields, S. Measuring the Activity of Protein Variants on a Large Scale Using Deep Mutational Scanning. *Nature Protocols*. Nature Publishing Group 2014, pp 2267–2284. https://doi.org/10.1038/nprot.2014.153.

(101) Steitz, T. A. DNA Polymerases: Structural Diversity and Common Mechanisms. *J. Biol. Chem.* **1999**, *274* (25), 17395–17398. https://doi.org/10.1074/JBC.274.25.17395.

(102) Betz, K.; Malyshev, D. A.; Lavergne, T.; Welte, W.; Diederichs, K.; Dwyer, T. J.; Ordoukhanian, P.; Romesberg, F. E.; Marx, A. KlenTaq Polymerase Replicates Unnatural Base Pairs by Inclusing a Watson-Crick Geometry. *Nat. Chem. Biol.* **2012**, *8* (7), 612–614. https://doi.org/10.1038/nchembio.966.

(103) Pace, C. N.; Scholtz, J. M. A Helix Propensity Scale Based on Experimental Studies of Peptides and Proteins. *Biophys. J.* **1998**, *75* (1), 422–427. https://doi.org/10.1016/S0006-3495(98)77529-0.

(104) Mason, P. E.; Brady, J. W.; Neilson, G. W.; Dempsey, C. E. The Interaction of Guanidinium Ions with a Model Peptide. *Biophys. J.* **2007**, *93* (1). https://doi.org/10.1529/biophysj.107.108290.

(105) Camilloni, C.; Guerini Rocco, A.; Eberini, I.; Gianazza, E.; Broglia, R. A.; Tiana, G. Urea and Guanidinium Chloride Denature Protein L in Different Ways in Molecular Dynamics Simulations. *Biophys. J.* **2008**, *94* (12), 4654–4661. https://doi.org/10.1529/biophysj.107.125799.

(106) England, J. L.; Pande, V. S.; Haran, G. Chemical Denaturants Inhibit the Onset of Dewetting. *J. Am. Chem. Soc.* **2008**, *130* (36), 11854–11855. https://doi.org/10.1021/ja803972g.

(107) Paik, I.; Bhadra, S.; Ellington, A. D. Charge Engineering Improves the Performance of Bst DNA Polymerase Fusions. *ACS Synth. Biol.* **2022**, *11* (4), 1488–1496. https://doi.org/10.1021/ACSSYNBIO.1C00559/ASSET/IMAGES/LARGE/SB1C00559_0006.JPEG.

(108) Bender, A. T.; Sullivan, B. P.; Lillis, L.; Posner, J. D. Enzymatic and Chemical-Based Methods to Inactivate Endogenous Blood Ribonucleases for Nucleic Acid Diagnostics. *J. Mol. Diagnostics* **2020**, *22* (8), 1030–1040. https://doi.org/10.1016/J.JMOLDX.2020.04.211.

(109) Meyer, A. J.; Ellefson, J. W.; Ellington, A. D. Library Generation by Gene Shuffling. *Curr. Protoc. Mol. Biol.* **2014**, *105* (SUPPL.105). https://doi.org/10.1002/0471142727.MB1512S105.

(110) Peach, M.; Marsh, N.; MacPhee, D. J. Protein Solubilization: Attend to the Choice of Lysis Buffer. *Methods Mol. Biol.* **2012**, *869*, 37–47. https://doi.org/10.1007/978-1-61779-821-4_4/FIGURES/2.

(111) Baranauskas, A.; Paliksa, S.; Alzbutas, G.; Vaitkevicius, M.; Lubiene, J.; Letukiene, V.; Burinskas, S.; Sasnauskas, G.; Skirgaila, R. Generation and Characterization of New Highly Thermostable and Processive M-MuLV Reverse Transcriptase Variants. *Protein Eng. Des. Sel.* **2012**, *25* (10), 657–668. https://doi.org/10.1093/PROTEIN/GZS034.

(112) Heller, R. C.; Chung, S.; Crissy, K.; Dumas, K.; Schuster, D.; Schoenfeld, T. W. Engineering of a Thermostable Viral Polymerase Using Metagenome-Derived Diversity for Highly Sensitive and Specific RT-PCR. *Nucleic Acids Res.* **2019**, *47* (7), 3619. https://doi.org/10.1093/NAR/GKZ104.

(113) Walker, G. T.; Fraiser, M. S.; Schram, J. L.; Little, M. C.; Nadeau, J. G.; Malinowski, D. P. Strand Displacement Amplification--an Isothermal, in Vitro DNA Amplification Technique. *Nucleic Acids Res.* **1992**, *20* (7), 1691–1696.

(114) Vester, B.; Wengel, J. LNA (Locked Nucleic Acid): High-Affinity Targeting of Complementary RNA and DNA. *Biochemistry* **2004**, *43* (42), 13233–13241. https://doi.org/10.1021/bi0485732.

(115) D'Abbadie, M.; Hofreiter, M.; Vaisman, A.; Loakes, D.; Gasparutto, D.; Cadet, J.; Woodgate, R.; Pääbo, S.; Holliger, P. Molecular Breeding of Polymerases for Amplification of Ancient DNA. *Nat. Biotechnol. 2007 258* **2007**, *25* (8), 939–943. https://doi.org/10.1038/nbt1321.

(116) Sale, J. E.; Lehmann, A. R.; Woodgate, R. Y-Family DNA Polymerases and Their Role in Tolerance of Cellular DNA Damage. *Nat. Rev. Mol. Cell Biol. 2012 133* **2012**, *13* (3), 141–152. https://doi.org/10.1038/nrm3289.

(117) Yang, W. An Overview of Y-Family DNA Polymerases and a Case Study of Human DNA Polymerase π. *Biochemistry* **2014**, *53* (17), 2793–2803. https://doi.org/10.1021/BI500019S/ASSET/IMAGES/LARGE/BI-2014-00019S_0003.JPEG.

(118) Vincent, M.; Xu, Y.; Kong, H. Helicase-Dependent Isothermal DNA Amplification. *EMBO Rep.* **2004**, *5* (8), 795. https://doi.org/10.1038/SJ.EMBOR.7400200.

(119) Martin, L. L.; Unrau, P. J.; Müller, U. F. RNA Synthesis by in Vitro Selected Ribozymes for Recreating an RNA World. *Life* **2015**, *5* (1), 247. https://doi.org/10.3390/LIFE5010247.

(120) Pasloske, B. L.; Walkerpeach, C. R.; Obermoeller, R. D.; Winkler, M.; DuBois, D. B. Armored RNA Technology for Production of Ribonuclease-Resistant Viral RNA Controls and Standards. *J. Clin. Microbiol.* **1998**, *36* (12), 3594.

(121) Crannell, Z. A.; Rohrman, B.; Richards-Kortum, R. Equipment-Free Incubation of Recombinase Polymerase Amplification Reactions Using Body Heat. *PLoS One* **2014**, *9* (11). https://doi.org/10.1371/journal.pone.0112146.

(122) Reboud, J.; Bourquin, Y.; Wilson, R.; Pall, G. S.; Jiwaji, M.; Pitt, A. R.; Graham, A.; Waters, A. P.; Cooper, J. M. Shaping Acoustic Fields as a Toolset for Microfluidic Manipulations in Diagnostic Technologies. *Proc. Natl. Acad. Sci. U. S. A.* **2012**, *109* (38), 15162–15167. https://doi.org/10.1073/PNAS.1206055109/-/DCSUPPLEMENTAL.

(123) Catarino, S. O.; Silva, L. R.; Mendes, P. M.; Miranda, J. M.; Lanceros-Mendez, S.; Minas, G. Piezoelectric Actuators for Acoustic Mixing in Microfluidic Devices—Numerical Prediction and Experimental Validation of Heat and Mass Transport. *Sensors Actuators B Chem.* **2014**, *205*, 206–214. https://doi.org/10.1016/J.SNB.2014.08.030.

(124) Osborn, J. L.; Lutz, B.; Fu, E.; Kauffman, P.; Stevens, D. Y.; Yager, P. Microfluidics without Pumps: Reinventing the T-Sensor and H-Filter in Paper Networks. *Lab Chip* **2010**, *10* (20), 2659–2665. https://doi.org/10.1039/C004821F.

(125) Rezk, A. R.; Qi, A.; Friend, J. R.; Li, W. H.; Yeo, L. Y. Uniform Mixing in Paper-Based Microfluidic Systems Using Surface Acoustic Waves. *Lab Chip* **2012**, *12* (4), 773–779. https://doi.org/10.1039/C2LC21065G.

(126) Schrader, C.; Schielke, A.; Ellerbroek, L.; Johne, R. PCR Inhibitors - Occurrence, Properties and Removal. *J. Appl. Microbiol.* **2012**, *113* (5), 1014–1026. https://doi.org/10.1111/j.1365-2672.2012.05384.x.

(127) Hemelaar, J.; Elangovan, R.; Yun, J.; Dickson-Tetteh, L.; Fleminger, I.; Kirtley, S.; Williams, B.; Gouws-Williams, E.; Ghys, P. D.; Abimiku,

A. G.; Agwale, S.; Archibald, C.; Avidor, B.; Barbás, M. G.; Barre-Sinoussi, F.; Barugahare, B.; Belabbes, E. H.; Bertagnolio, S.; Birx, D.; Bobkov, A. F.; Brandful, J.; Bredell, H.; Brennan, C. A.; Brooks, J.; Bruckova, M.; Buonaguro, L.; Buonaguro, F.; Buttò, S.; Buve, A.; Campbell, M.; Carr, J.; Carrera, A.; Carrillo, M. G.; Celum, C.; Chaplin, B.; Charles, M.; Chatzidimitriou, D.; Chen, Z.; Chijiwa, K.; Cooper, D.; Cunningham, P.; Dagnra, A.; de Gascun, C. F.; Del Amo, J.; Delgado, E.; Dietrich, U.; Dwyer, D.; Ellenberger, D.; Ensoli, B.; Essex, M.; Gao, F.; Fleury, H.; Fonjungo, P. N.; Foulongne, V.; Gadkari, D. A.; García, F.; Garsia, R.; Gershy-Damet, G. M.; Glynn, J. R.; Goodall, R.; Grossman, Z.; Lindenmeyer-Guimarães, M.; Hahn, B.; Hamers, R. L.; Hamouda, O.; Handema, R.; He, X.; Herbeck, J.; Ho, D. D.; Holguin, A.; Hosseinipour, M.; Hunt, G.; Ito, M.; Bel Hadj Kacem, M. A.; Kahle, E.; Kaleebu, P. K.; Kalish, M.; Kamarulzaman, A.; Kang, C.; Kanki, P.; Karamov, E.; Karasi, J. C.; Kayitenkore, K.; Kelleher, T.; Kitayaporn, D.; Kostrikis, L. G.; Kucherer, C.; Lara, C.; Leitner, T.; Liitsola, K.; Lingappa, J.; Linka, M.; Lorenzana de Rivera, I.; Lukashov, V.; Maayan, S.; Mayr, L.; McCutchan, F.; Meda, N.; Menu, E.; Mhalu, F.; Mloka, D.; Mokili, J. L.; Montes, B.; Mor, O.; Morgado, M.; Mosha, F.; Moussi, A.; Mullins, J.; Najera, R.; Nasr, M.; Ndembi, N.; Neilson, J. R.; Nerurkar, V. R.; Neuhann, F.; Nolte, C.; Novitsky, V.; Nyambi, P.; Ofner, M.; Paladin, F. J.; Papa, A.; Pape, J.; Parkin, N.; Parry, C.; Peeters, M.; Pelletier, A.; Pérez-Álvarez, L.; Pillay, D.; Pinto, A.; Quang, T. D.; Rademeyer, C.; Raikanikoda, F.; Rayfield, M. A.; Reynes, J. M.; Rinke de Wit, T.; Robbins, K. E.; Rolland, M.; Rousseau, C.; Salazar-Gonzales, J.; Salem, H.; Salminen, M.; Salomon, H.; Sandstrom, P.; Santiago, M. L.; Sarr, A. D.; Schroeder, B.; Segondy, M.; Selhorst, P.; Sempala, S.; Servais, J.; Shaik, A.; Shao, Y.; Slim, A.; Soares, M. A.; Songok, E.; Stewart, D.; Stokes, J.; Subbarao, S.; Sutthent, R.; Takehisa, J.; Tanuri, A.; Tee, K. K.; Thapa, K.; Thomson, M.; Tran, T.; Urassa, W.; Ushijima, H.; van de Perre, P.; van der Groen, G.; van Laethem, K.; van Oosterhout, J.; van Sighem, A.; van Wijngaerden, E.; Vandamme, A. M.; Vercauteren, J.; Vidal, N.; Wallace, L.; Williamson, C.; Wolday, D.; Xu, J.; Yang, C.; Zhang, L.; Zhang, R. Global and Regional Molecular Epidemiology of HIV-1, 1990–2015: A Systematic Review, Global Survey, and Trend Analysis. *Lancet Infect. Dis.* **2019**, *19* (2), 143–155. https://doi.org/10.1016/S1473-3099(18)30647-9.

(128) Mikel, P.; Vasickova, P.; Tesarik, R.; Malenovska, H.; Kulich, P.; Vesely, T.; Kralik, P. Preparation of MS2 Phage-Like Particles and Their Use As Potential Process Control Viruses for Detection and Quantification of Enteric RNA Viruses in Different Matrices. *Front. Microbiol.* **2016**, *7*, 1911. https://doi.org/10.3389/FMICB.2016.01911.

(129) Cormack, B. P.; Valdivia, R. H.; Falkow, S. FACS-Optimized Mutants of the Green Fluorescent Protein (GFP). *Gene* **1996**, *173* (1), 33–38. https://doi.org/10.1016/0378-1119(95)00685-0.

(130) Integrated DNA Technologies. Codon Optimization Tool https://www.idtdna.com/CodonOpt (accessed Aug 7, 2020).

(131) Addgene. Ligation Independent Cloning https://www.addgene.org/protocols/lic/ (accessed Jan 30, 2023).

(132) Beck, D. A. C.; Daggett, V. Methods for Molecular Dynamics Simulations of Protein Folding/Unfolding in Solution. *Methods* **2004**, *34* (1), 112–120. https://doi.org/10.1016/j.ymeth.2004.03.008.

(133) Beck, D. A. C.; McCully, M. E.; Alonso, D. O. V.; Daggett, V. In Lucem Molecular Mechanics (Ilmm). University of Washington: Seattle 2020.

(134) Gordon, J. C.; Myers, J. B.; Folta, T.; Shoja, V.; Heath, L. S.; Onufriev, A. H++: A Server for Estimating PKas and Adding Missing Hydrogens to Macromolecules. *Nucleic Acids Res.* **2005**, *33* (Web Server issue), W368. https://doi.org/10.1093/NAR/GKI464.

(135) Cooper, S.; Khatib, F.; Treuille, A.; Barbero, J.; Lee, J.; Beenen, M.; Leaver-Fay, A.; Baker, D.; Popović, Z.; Players, F. Predicting Protein Structures with a Multiplayer Online Game. *Nature* **2010**, *466* (7307), 756–760. https://doi.org/10.1038/nature09304.

(136) Childers, M. C.; Daggett, V. Validating Molecular Dynamics Simulations against Experimental Observables in Light of Underlying Conformational Ensembles. *J. Phys. Chem. B* **2018**, *122* (26), 6673–6689. https://doi.org/10.1021/acs.jpcb.8b02144.